FACULDADE DE ENGENHARIA DA UNIVERSIDADE DO PORTO

# Security-Constrained Optimal Power Flow (SCOPF)

**Diogo André Costa Reis**

Mestrado em Engenharia Eletrotécnica e de Computadores

Supervisor: Prof. Tiago André Soares

July 23, 2026

# Resumo

A crescente integração de Fontes de Energia Renováveis (RESs) variáveis e a proliferação dos Recursos Energéticos Distribuídos (DERs) em geral transformaram profundamente a dinâmica operacional dos sistemas de energia elétrica. Consequentemente, o *Security-Constrained Optimal Power Flow* (SCOPF) determinístico tradicional, a principal ferramenta operacional para garantir a segurança da rede $N-1$, está a tornar-se cada vez mais inadequado, uma vez que não consegue ter explicitamente em conta a incerteza introduzida pela produção variável das RESs, pelo comportamento dos DERs e por uma maior procura, fatores que dão origem a erros de previsão estocásticos.

Embora as formulações do SCOPF com Restrições de Probabilidade (CC-SCOPF) ofereçam uma alternativa probabilística, os modelos completos de Corrente Alternada (AC) continuam a ser computacionalmente intratáveis para aplicações à escala das empresas de serviços públicos devido à sua natureza inerentemente não linear e não convexa, bem como ao rápido crescimento da dimensão do problema associado a horizontes de vários períodos e representações de incerteza. Estes desafios computacionais dão origem a um "trilema" persistente na otimização de sistemas de energia: a dificuldade de alcançar simultaneamente precisão na modelação física, eficiência computacional e escalabilidade do sistema em grande escala.

Esta dissertação propõe uma nova metodologia AC-SCOPF multipériodo baseada na Programação Não Linear (NLP), concebida para conciliar os requisitos concorrentes deste trilema sem sacrificar a fidelidade da física da corrente alternada. Em vez de recorrer a linearizações simplificadas em Corrente Contínua (DC) ou a formulações de Programação Mista Inteira (MIP) computacionalmente dispendiosas, o modelo proposto utiliza estrategicamente técnicas específicas de relaxamento de restrições, combinadas com variáveis de folga ponderadas por penalização. Esta reformulação matemática garante que as matrizes de *Karush-Kuhn-Tucker* (KKT) permaneçam bem condicionadas, melhorando assim a solubilidade numérica para solucionadores de NLP baseados em gradientes, ao mesmo tempo que preserva as equações exatas de equilíbrio de potência ativa e reativa. O modelo proposto tem em conta vários tipos de recursos controláveis, tais como os Sistemas de Armazenamento de Energia (ESSs) e a flexibilidade do lado da procura. Para lidar com a incerteza estocástica, evitam-se as variáveis binárias tradicionalmente utilizadas nas formulações de Otimização com Restrições de Probabilidade (CCO) e introduz-se um novo indicador de violação racional continuamente diferenciável, permitindo a incorporação de restrições de segurança probabilísticas, ao mesmo tempo que se preserva a estrutura de programação não linear do problema. Implementada em Python e resolvida utilizando o IPOPT, a metodologia é validada em redes de referência IEEE padronizadas com até 300 barramentos. Os resultados numéricos demonstram que a abordagem de NLP proposta alcança uma redução de até 97,7 % no tempo de computação em comparação com formulações convencionais de Programação Quadrática Mista-Inteira (MIQP), ao mesmo tempo que atinge uma diferença de otimização insignificante de 0,0058 %. Além disso, simulações em condições de operação de baixa inércia mostram que a formulação adota inerentemente ações de segurança preventivas que contribuem para reduzir os custos

de geração e o corte de energia renovável, garantindo simultaneamente uma segurança operacional robusta em condições de contingência.

Em geral, a metodologia proposta fornece um modelo de otimização não linear viável para a operação de sistemas elétricos com restrições de segurança em condições de incerteza, mantendo a representação completa da rede AC e acomodando altos níveis de integração de energia renovável.

# Abstract

The increasing integration of variable Renewable Energy Sources (RES) and the proliferation of Distributed Energy Resources (DERs) in general, have fundamentally transformed the operational dynamics of electrical power systems. Consequently, the traditional deterministic Security-Constrained Optimal Power Flow (SCOPF), the primary operational tool for enforcing $N-1$ grid security, is increasingly inadequate because it cannot explicitly account for the uncertainty introduced by variable RES production, DER behavior, and increasingly active demand, all of which give rise to stochastic forecast errors.

While Chance-Constrained SCOPF (CC-SCOPF) formulations offer a robust probabilistic alternative, full Alternating Current (AC) models remain computationally intractable for utility-scale applications due to their inherent nonlinear and non-convex nature, as well as the rapid growth in problem size associated with multi-period horizons and uncertainty representations. These computational challenges give rise to a persistent "trilemma" in power system optimization: the difficulty to simultaneously achieve physical modeling accuracy, computational efficiency, and large-scale system scalability.

This dissertation proposes a novel Multi-Period AC-SCOPF methodology based on NonLinear Programming (NLP) designed to reconcile the competing requirements of this trilemma without sacrificing the fidelity of AC physics. Rather than relying on simplified Direct Current (DC) linearizations or computationally expensive Mixed-Integer Programming (MIP) formulations, the proposed framework strategically utilizes targeted constraint relaxation techniques coupled with penalty-weighted slack variables. This mathematical reformulation ensures that the Karush-Kuhn-Tucker (KKT) matrices remain well-conditioned, thereby improving numerical solvability for gradient-based NLP solvers while preserving the exact active and reactive power balance equations. The proposed framework considers several types of controllable resources, such as Energy Storage Systems (ESSs) and demand-side flexibility. To address stochastic uncertainty, binary variables traditionally employed in Chance-Constrained Optimization (CCO) formulations are avoided, and a novel continuously differentiable rational violation indicator is introduced, enabling the incorporation of probabilistic security constraints while preserving the problem's nonlinear programming structure. Implemented in Python and solved using IPOPT, the methodology is validated on standardized IEEE benchmark networks up to 300 buses. The numerical results demonstrate that the proposed NLP approach achieves up to 97.7% reduction in computational time compared to conventional Mixed-Integer Quadratic Programming (MIQP) formulations, while achieving a negligible optimality gap of 0.0058%. Moreover, simulations under low-inertia operating conditions show that the formulation inherently adopts preventive security actions contributing to lower generation costs and renewable energy curtailment while ensuring robust operational security under contingency conditions.

Overall, the proposed methodology provides a tractable nonlinear optimization framework for security-constrained power system operation under uncertainty, while maintaining full AC network representation and accommodating high levels of renewable energy integration.

# UN Sustainable Development Goals

The United Nations Sustainable Development Goals (SDG) provide a global framework to achieve a better and more sustainable future for all. It includes 17 goals to address the world's most pressing challenges, including poverty, inequality, climate change, environmental degradation, peace, and justice.

The work developed in this dissertation is directly aligned with several United Nations SDGs, in particular:

- **SDG 7:** Ensure access to affordable, reliable, sustainable and modern energy for all.
  - Target 7.1: reliable energy access;
  - Target 7.2: renewable energy integration;
  - Target 7.3: energy efficiency.
- **SDG 8:** Promote sustained, inclusive and sustainable economic growth, full and productive employment and decent work for all.
  - Target 8.2: technological innovation.
- **SDG 13:** Take urgent action to combat climate change and its impacts.
  - Target 13.1: climate resilience;
  - Target 13.2: integration of climate action into planning and policy.

From the perspective of SDG 7, the proposed Security-Constrained Optimal Power Flow (SCOPF) framework successfully facilitates the integration of variable Renewable Energy Sources (RES), demonstrating the secure operation of the studied system with high renewable penetration levels, while preserving system security. Furthermore, the model actively manages flexibility-providing resources, ensuring that these preventively ensure security reserves to guarantee reliable service delivery in post-contingency states.

In the context of SDG 8, the development of this optimization tool supports technological upgrading and innovation within the electricity sector. The proposed framework successfully extracts maximum efficiency from existing infrastructure, avoiding severe thermal congestion and preventing voltage collapse without requiring immediate physical grid reinforcement.

Finally, regarding SDG 13, the framework provides a critical tool for rapid decarbonization by securing the grid against the chaotic variability of large-scale Renewable Energy Sources (RES). Validated on massive networks up to 300 buses, the tool proves the system can survive the severe operational strains of climate-induced weather shifts and sudden drops in solar generation. By safely managing multiple $N-1$ contingencies during these volatile periods, the framework directly enhances the grid's climate resilience, ensuring that the urgent transition to clean energy doesn't come at the cost of blackouts during extreme weather events.

Table 1 summarizes the contributions of this thesis to the UN SDG goals.

Table 1: Thesis contribution to the United Nations Sustainable Development Goals.

| **SDG** | **Target** | **Contribution** | **Performance Indicators and Metrics** |
|---|---|---|---|
| 7 | 7.1 | The multi-period SCOPF formulation improves secure grid operation under the $N-1$ criterion, reducing the risk of load shedding and ensuring access to reliable energy. | Successfully solved critical $N-1$ contingency scenarios across systems up to 300 buses. |
| | 7.2 | The model integrates new sources of operational flexibility, enabling optimal dispatch that maximizes renewable utilization while maintaining system security. | Achieved approximately 66% renewable integration while maintaining system security and limiting renewable energy curtailment to negligible levels. |
| | 7.3 | The proposed Chance-Constrained Optimization (CCO) framework optimizes power routing to minimize transmission losses while securely managing volatile solar generation to diminish renewable curtailment. It also replaces inefficient overgeneration practices with precise, preventive $N-1$ reserve calculation, lowering the grid's overall operational energy intensity. | Maintained very low curtailment values, while also achieving lower power system losses compared to its probabilistic counterpart. |
| 8 | 8.2 | The proposed framework constitutes an innovation in grid optimization tools, supporting sustainable economic growth. | Developed an efficient framework capable of replacing computationally heavy discrete variables with continuous surrogate functions with only a 0.0058% difference in optimal cost. It also achieved a 97.7% reduction in computation time (down to 5.13 s for 10 scenarios). Scaled successfully to the IEEE 300-bus network, handling over 1.9 million variables and 1.5 million constraints. |
| 13 | 13.1 | The proposed approach improves grid security by improving the system's capacity to handle contingencies and renewable variability. | Maintained structural robustness during the severe "solar ramp" hour (09:00–10:00 h) under low-inertia conditions, ensuring lines did not reach emergency overload limits across diverse contingency realizations. |
| | 13.2 | The developed tool integrates renewable resources, energy storage systems, and $N-1$ security criteria, supporting decarbonization-oriented system operational planning. | Validated across five progressively complex IEEE networks (5, 9, 30, 118, and 300 buses) under high renewable penetration scenarios. |

In summary, the developed framework in this dissertation bridges the gap between complex power systems engineering and global sustainability objectives. By transforming the traditional grid into an agile, highly optimized system, the proposed tools move past purely theoretical models to deliver concrete solutions for real-world grid challenges. Whether by enhancing day-to-day operational efficiency (SDG 7), dramatically slashing optimization computation times to foster industry innovation (SDG 8), or guaranteeing structural robustness against the compounding threats of weather variability and unexpected line outages (SDG 13), this work proves that rapid decarbonization is both technically viable and securely manageable. Ultimately, the methodologies and metrics validated herein provide utility operators with a reliable mathematical foundation to accelerate the global transition toward a clean, resilient, and climate-defensive energy future.

# Acknowledgements

First and foremost, I would like to express my sincere gratitude to my supervisor, Tiago Soares, as well as to all the teachers who guided me throughout this challenging journey. As I often like to say, teachers are like farmers, they cultivate each generation not only as professionals but also as individuals. Through their teaching, care, and belief in their students, they help shape the people we become. For that, I am deeply grateful to all my teachers. Each of whom contributed to my journey in one way or another...

I would also like to thank Micael Simões for all his support throughout this project. He helped me understand how computers and, more specifically, the Python interpreter "thinks" which ultimately enabled me to develop a more efficient algorithm. He also patiently endured my daily stream of questions and messages, for which I am especially thankful.

I would like to give a special shout-out to my dear friends for helping me stay sane throughout this academic journey. In particular, I would like to thank Bárbara Costa and Diogo Pereira for all the teamwork we shared and for the many laughs along the way.

A very special acknowledgment goes to Margarida Tiago, with whom I shared countless memorable moments and laughter. She believed in me as much as I believed in her and showed me that not everything in life is simply black and white.

Finally, I would like to thank my family for their unwavering support, especially my brother, who has been both a role model and an inspiration to me since I was young. I have always believed that as long as I grew up to be even a little like you, I would become a good person. Thank you for setting such an example and for always being there for me.
P.S: Vai guardar as galinhas Peixoto!

Diogo Reis

*"I just never thought I couldn't."*

Lightning McQueen

# Contents

# List of Figures

# List of Tables

# List of Acronyms

| | |
|---|---|
| **AC** | Alternating Current |
| **AC-OPF** | Alternating Current Optimal Power Flow |
| **ADMM** | Alternating Direction Method of Multipliers |
| **BD** | Benders Decomposition |
| **CCO** | Chance-Constrained Optimization |
| **CC-OPF** | Chance-Constrained Optimal Power Flow |
| **CC-SCOPF** | Chance-Constrained Security-Constrained Optimal Power Flow |
| **DC** | Direct Current |
| **DC-OPF** | Direct Current Optimal Power Flow |
| **DRL** | Deep Reinforcement Learning |
| **ED** | Economic Dispatch |
| **ESS** | Energy Storage System |
| **IPFC** | Interline Power Flow Controller |
| **ISO** | Independent System Operator |
| **KKT** | Karush–Kuhn–Tucker |
| **LP** | Linear Programming |
| **MILP** | Mixed-Integer Linear Programming |
| **ML** | Machine Learning |
| **MP-AC-SCOPF** | Multi-Period AC Security-Constrained Optimal Power Flow |
| **MIQP** | Mixed-Integer Quadratic Programming |
| **NLP** | Nonlinear Programming |
| **OPF** | Optimal Power Flow |
| **OLTC** | On-Load Tap Changer |
| **OTDF** | Outage Transfer Distribution Factor |

| | |
|---|---|
| **PR** | Power Router |
| **pSCOPF** | Probabilistic Security-Constrained Optimal Power Flow |
| **PTDF** | Power Transfer Distribution Factor |
| **RES** | Renewable Energy Source |
| **SAA** | Sample Average Approximation |
| **SCOPF** | Security-Constrained Optimal Power Flow |
| **SCUC** | Security-Constrained Unit Commitment |
| **SDP** | Semidefinite Programming |
| **SLA** | Sequential Linear Approximation |
| **SoC** | State-of-charge |
| **SOCP** | Second-Order Cone Programming |
| **QP** | Quadratic Programming |
| **SQP** | Sequential Quadratic Programming |
| **TOAT** | Taguchi Orthogonal Array Testing |
| **TSO** | Transmission System Operator |
| **VSC** | Voltage Source Converter |
| **WCC** | Weighted Chance Constraints |

# Nomenclature

## Sets

| | |
|---|---|
| $K$ | Set of contingencies |
| $N$ | Set of nodes/buses |
| $G$ | Set of generators |
| $G^R$ | Set of renewable generators |
| $B$ | Set of branches |
| $L$ | Set of loads |
| $F^l$ | Set of flexible loads |
| $Cb$ | Set of capacitor banks |
| $R$ | Set of reactors |
| $\Omega_o$ | Set of operational scenarios |
| $T$ | Set of periods/instants |
| $E$ | Set of energy storage systems |

## Optimization Variables

| | |
|---|---|
| $P^g_{i,k,o,t}$ | Active power generation at bus $i$ in contingency $k$ |
| $Q^g_{i,k,o,t}$ | Reactive power generation at bus $i$ in contingency $k$ |
| $e_{i,k,o,t}$ | Real part of voltage at bus $i$ in contingency $k$ |
| $f_{i,k,o,t}$ | Imaginary part of voltage at bus $i$ in contingency $k$ |
| $P_{ij,k,o,t}$ | Active power flow of branch $ij$ in contingency $k$ |
| $Q_{ij,k,o,t}$ | Reactive power flow of branch $ij$ in contingency $k$ |
| $S_{ij,k,o,t}$ | Apparent power flow of branch $ij$ in contingency $k$ |
| $e^{Sl,up}_{i,k,o,t}$ | Slack variable, real part of voltage at bus $i$ in upward direction |
| $f^{Sl,up}_{i,k,o,t}$ | Slack variable, imaginary part of voltage at bus $i$ in upward direction |
| $e^{Sl,dn}_{i,k,o,t}$ | Slack variable, real part of voltage at bus $i$ in downward direction |
| $f^{Sl,dn}_{i,k,o,t}$ | Slack variable, imaginary part of voltage at bus $i$ in downward direction |
| $S^{Sl}_{ij,k,o,t}$ | Slack variable associated with the apparent power flow in branch $ij$ |
| $P^{ch}_{e,k,o,t}$ | Active power charging of energy storage system $e$ |
| $P^{dch}_{e,k,o,t}$ | Active power discharging of energy storage system $e$ |
| $\mathrm{SoC}_{e,k,o,t}$ | State-of-Charge of ESS $e$ |

## Parameters

| | |
|---|---|
| $P_i^c$ | Active power consumption at bus $i$ |
| $Q_i^c$ | Reactive power consumption at bus $i$ |
| $P_i^{g,\min}$ | Minimum active power generation at bus $i$ |
| $P_i^{g,\max}$ | Maximum active power generation at bus $i$ |
| $Q_i^{g,\min}$ | Minimum reactive power generation at bus $i$ |
| $Q_i^{g,\max}$ | Maximum reactive power generation at bus $i$ |
| $V_i^{\min}$ | Minimum voltage magnitude at bus $i$ |
| $V_i^{\max}$ | Maximum voltage magnitude at bus $i$ |
| $\Delta P_g^{\max}$ | Maximum ramp variation of active power for generator $g$ |
| $\Delta V_i^{\max}$ | Maximum allowed voltage deviation for bus $i$ |
| $\Delta V_i^{\min}$ | Minimum allowed voltage deviation for bus $i$ |
| $S_{ij}^{\max}$ | Maximum apparent power flow of branch $ij$ |
| $g_{ij}$ | Conductance of branch $ij$ |
| $b_{ij}$ | Susceptance of branch $ij$ |
| $b_{ij}^{Sh}$ | Shunt susceptance of branch $ij$ |
| $c_{g,t}$ | €/MWh cost of generator $g$ at the time instant $t$ |
| $c^V$ | Penalty associated with the use of voltage slack variables |
| $c^S$ | Penalty associated with the use of power flow slack variables |
| $c^{\text{Load, curt}}$ | Cost of active and reactive load curtailment |
| $c^{\text{RES, curt}}$ | Cost of renewable generation curtailment |
| $P_{l,k,o,t}^{\text{curt,up}}$ | Upward curtailed active power of load $l$ in contingency $k$ |
| $Q_{l,k,o,t}^{\text{curt,up}}$ | Upward curtailed reactive power of load $l$ in contingency $k$ |
| $P_{l,k,o,t}^{\text{curt,down}}$ | Downward curtailed active power of load $l$ in contingency $k$ |
| $Q_{l,k,o,t}^{\text{curt,down}}$ | Downward curtailed reactive power of load $l$ in contingency $k$ |
| $c^{\text{ESS}}$ | Penalty associated with the slack variable representing the ESS charging–discharging complementarity violation. |
| $\text{SoC}_e^{\min}$ | Minimum State-of-Charge of ESS $e$ |
| $\text{SoC}_e^{\max}$ | Maximum State-of-Charge of ESS $e$ |
| $\eta_e^{ch}$ | charging efficiency of ESS $e$ |
| $\eta_e^{dch}$ | discharging efficiency of ESS $e$ |

# Chapter 1

# Introduction

This chapter presents the research context, motivation, and objectives of this dissertation. It first discusses the ongoing transformation of modern power systems, driven by the increasing integration of Renewable Energy Sources (RESs), Energy Storage Systems (ESSs), and other emerging flexibility-providing resources, and highlights the associated challenges for secure and economically efficient grid operation. The chapter then defines the central research problem by examining the trade-offs among modeling accuracy, computational efficiency, and scalability in Security-Constrained Optimal Power Flow (SCOPF) approaches. It subsequently describes the objectives and methodological approach adopted in this work, with particular emphasis on the development of a stochastic Multi-Period AC Security-Constrained Optimal Power Flow (MP-AC-SCOPF) framework based on Nonlinear Programming (NLP) techniques. Finally, the chapter provides an overview of the dissertation structure and summarizes the contents of the remaining chapters.

## 1.1 Context and Motivation

The secure and cost-effective operation of modern electric power systems is a fundamental requirement for contemporary society, supporting economic activity, social welfare, and human development. At the core of this operational task lies a complex optimization problem: determining how system operators can dispatch available resources to meet time-varying demand while respecting the physical, thermal, and voltage limits of the transmission network. Although decades of research have led to increasingly sophisticated mathematical optimization tools, this task has become significantly more challenging due to the ongoing decarbonization of the energy sector and the large-scale integration of new types of flexibility-providing resources.

The European power system is currently undergoing a profound transformation. The progressive replacement of conventional synchronous generation by variable RESs, particularly wind and solar photovoltaic generation, has changed the dynamic and operational characteristics of the grid. In addition to reducing the contribution of synchronous inertia, the increasing integration of weather-dependent generation introduces greater variability and uncertainty into system operation. Figure 1.1 illustrates the evolution of the RES share at the EU-27 level.

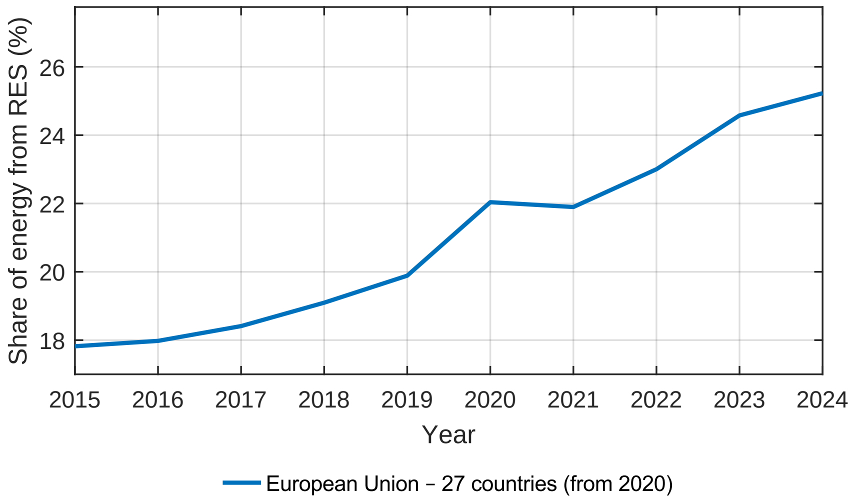


Figure 1.1: Share of energy from RESs at the EU-27 level between 2015 and 2024 [1].

Unlike conventional dispatchable generators, RESs are only partially controllable and depend on meteorological conditions, leading to forecast errors and deviations between scheduled and actual power injections. As a result, system operators require additional sources of flexibility to maintain the balance between generation and demand while preserving network security. In this context, ESSs have emerged as a key enabling technology. Their fast response capability allows them to provide frequency support, energy shifting, reserve services, and congestion relief. Figure 1.2 shows the installed ESS capacity at the EU-27 level between 2019 and 2023.

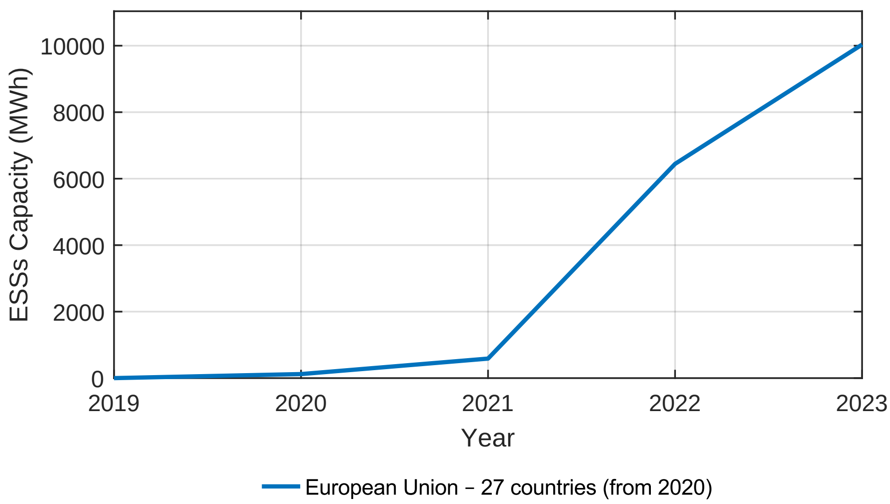


Figure 1.2: ESS installed capacity at the EU-27 level between 2019 and 2023 [2].

While ESSs can help relieve operational constraints, they also introduce additional decision variables and intertemporal dependencies, increasing network management complexity. Consequently, the combined large-scale deployment of RESs, ESSs, and other flexible resources has made power system operation increasingly stochastic, dynamic, and computationally demanding. These developments place increasing pressure on Transmission System Operators (TSOs), which are responsible for maintaining secure system operation under both normal and contingency conditions. In particular, transmission networks must be operated in accordance with security criteria such as the $N-1$ criterion, which requires the system to remain within operational limits following the outage of a single relevant network element, such as a transmission line, transformer, or generator. Under high levels of uncertainty and variable renewable generation, satisfying these security requirements may require costly corrective actions, including generation redispatch, renewable curtailment, balancing-service procurement, or other congestion-management measures. Figure 1.3 shows the annual congestion-management costs in the Iberian control region between 2015 and 2022, while Figure 1.4 provides a monthly breakdown for the same period.

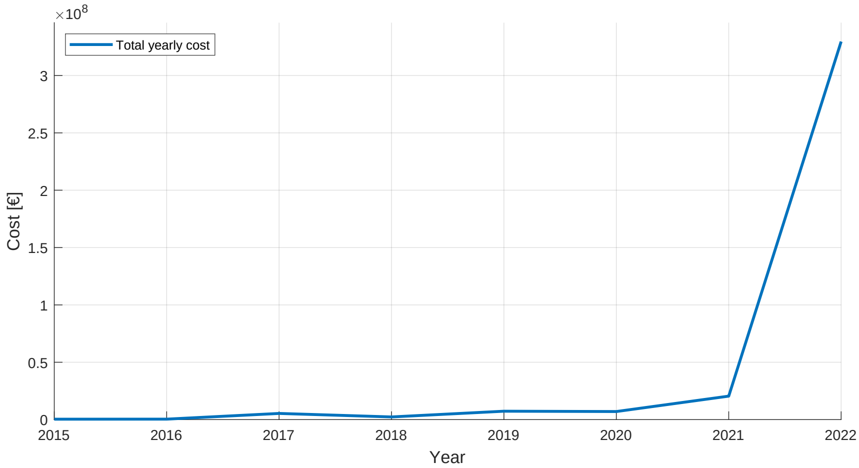


Figure 1.3: Annual congestion management costs in the Iberian control region [3].

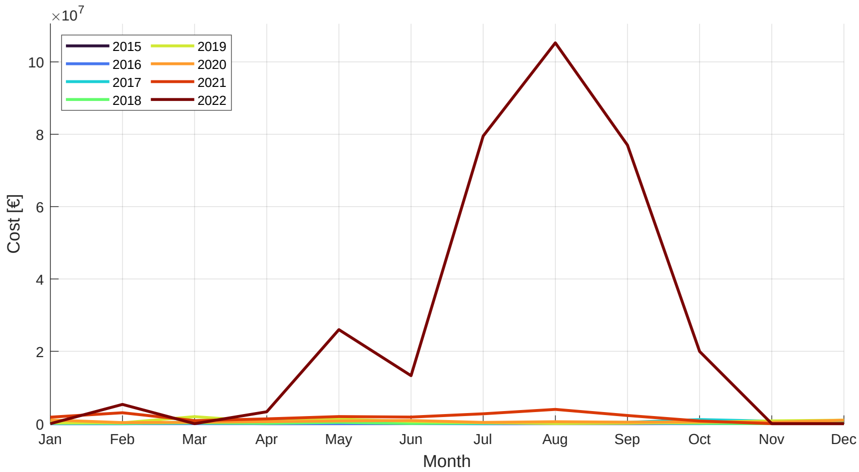


Figure 1.4: Monthly congestion-management costs in the Iberian control region [3].

The monthly detail presented in Figure 1.4 further indicates that congestion management costs were particularly high during specific summer months. While congestion costs are influenced by multiple technical and market factors, the observed trend illustrates the growing operational relevance of network constraints in systems with increasing shares of variable renewable generation. As renewable generation expands, power injections tend to become more dependent on the geographical distribution of wind and solar resources, which are not always located close to major consumption centers. This can increase the need to transport large volumes of power over long transmission corridors, thereby raising the likelihood of congestion. During such operating conditions, renewable production may exceed the transmission capacity available to deliver energy from generation-rich areas to load centers. To preserve network security TSOs must therefore rely on remedial actions such as redispatch, RES curtailment, or the procurement of balancing and congestion-management services. These actions are essential for secure operation, but they may also increase operational costs and reduce the efficient utilization of renewable generation.

Addressing this operational paradigm requires advanced decision-support tools that can explicitly represent uncertainty, network security constraints, and emerging flexibility-providing resources. Traditional deterministic Optimal Power Flow (OPF) and SCOPF formulations remain valuable for operational planning, but they typically rely on forecasted operating points, reserve margins, or predefined contingencies rather than explicitly modeling the uncertainty associated with renewable generation and demand. At the same time, incorporating uncertainty into multi-period Alternating Current (AC) optimization problems substantially increases computational complexity. The combination of non-convex AC power-flow equations, intertemporal resource constraints, contingency modeling, and uncertainty representations limits the scalability of many stochastic formulations proposed in the literature. Consequently, developing optimization models that preserve physical network fidelity while remaining computationally tractable for operational use remains an open research challenge.

Therefore, there is a clear need for optimization frameworks that simultaneously: (i) preserve AC network modeling accuracy, (ii) explicitly incorporate uncertainty in renewable generation and demand, (iii) account for the temporal coupling of flexibility resources, and (iv) remain computationally scalable for large-scale, multi-period system operation. This thesis addresses this gap by developing a stochastic MP-AC-SCOPF formulation designed to improve both modeling accuracy and computational efficiency under realistic grid conditions.

## 1.2 The Optimization “Trilemma” and Problem Definition

One of the main optimization frameworks used to support secure transmission system operation is the SCOPF. Executed primarily during day-ahead and intra-day operational planning, the SCOPF balances pre-contingency preventive actions with post-contingency corrective actions to ensure that the electrical network remains within operational limits following predefined outages. However, formulating a full AC-based SCOPF involves solving a nonlinear, non-convex, large-scale optimization problem. When this model is expanded to incorporate probabilistic uncertainty and inter-temporal constraints, the dimensionality and computational burden of the problem increase rapidly. Researchers and system operators are thus continuously confronted by these objectives, forcing severe compromises across three competing axes:

1. **Modeling accuracy:** The accurate modeling of electrical grids requires full AC equations to represent reactive power, network losses, and voltage magnitudes. Simplified Direct Current (DC) models neglect these aspects, which may limit their accuracy in highly loaded or voltage-constrained networks.

2. **Computational efficiency:** The mathematical model must converge rapidly to be viable for intra-day market clearing and near real-time operational adjustments.

3. **System scalability:** The algorithm must successfully scale to handle networks comprising hundreds of buses, lines, and contingency scenarios without excessive memory consumption or solver performance degradation.

This trade-off can be conceptualized as an optimization "trilemma", as illustrated in Figure 1.5.

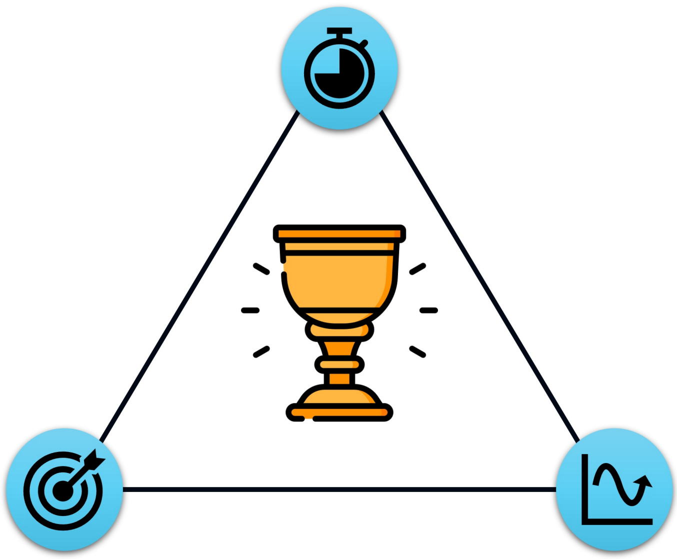

Figure 1.5: The optimization trilemma: balancing modeling accuracy, computational efficiency, and system scalability.

This dissertation focuses on this trade-off by addressing the challenge of formulating a stochastic, multi-period AC-based SCOPF model that can explicitly represent renewable generation and demand uncertainty, $N-1$ security constraints, and the temporal coupling introduced by flexibility resources, while remaining computationally tractable for large-scale transmission systems. The central research problem is therefore not only to improve the physical accuracy of SCOPF formulations, but also to develop a solution approach that can preserve this accuracy without compromising computational efficiency and scalability.

## 1.3 Objectives and Methodological Approach

To address the operational challenges discussed in the previous section, this dissertation develops a stochastic MP-AC-SCOPF formulation based on continuous NLP. The main objective is to contribute to the development of optimization tools capable of balancing three key requirements of modern power-system operation: physical modeling accuracy, computational tractability, and scalability to large-scale networks.

### 1.3.1 Core Research Objectives

The specific theoretical and modeling objectives of this dissertation are defined as follows:

- **Formulate a tractable nonlinear AC framework:** Design an AC-based SCOPF formulation that preserves the full nonlinear power-flow physics of the transmission network while improving numerical robustness through a structured constraint-relaxation strategy based on penalty-weighted slack variables and rectangular voltage modeling.

- **Integrate risk-bounded probabilistic margins:** Extend the proposed continuous optimization framework to handle stochastic uncertainty through a chance-constrained layer, substituting discrete violation indicators with smooth continuous approximations compatible with gradient-based algorithms.

- **Characterize multi-period flexibility dynamics:** Model the complex intertemporal behavior of emerging flexibility resources, including ESSs State-of-charge (SoC) tracking, time-shiftable demand patterns, and renewable generation variability, within a unified, optimization environment.

### 1.3.2 Implementation and Validation Tasks

To realize the mathematical models and verify their practical viability, the following software development and algorithmic validation tasks are executed:

- **Modular software implementation:** Construct a functional, modular Python-based SCOPF package capable of natively compiling and executing the complete mathematical formulation alongside its associated network asset profiles.

- **Comparative performance benchmarking:** Evaluate the solution quality and computational efficiency of the proposed continuous NLP approach by conducting direct comparative assessments against alternative, exact Mixed-Integer Quadratic Programming (MIQP) baselines.

- **Scalability verification:** Assess the numerical stability and algorithmic scaling of the proposed optimization engines using standardized transmission network test systems of increasing dimensionality, up to a 300-bus configuration.

The achievement of these objectives and completion of these tasks provide several practical benefits for modern transmission system operations:

- **Enhanced security assessment:** The proposed stochastic MP-AC-SCOPF framework supports preventive security management by jointly considering renewable generation uncertainty, temporal operating constraints, and $N-1$ contingencies within a physically detailed AC network model.
- **Improved utilization of flexibility resources:** The multi-period formulation explicitly represents the temporal coupling of flexibility-providing resources, including the state-of-charge dynamics of ESSs and the scheduling constraints of time-shiftable loads. This enables a more coordinated use of flexibility to accommodate variable renewable generation and reduce operational costs.
- **Improved diagnosis of operational stress:** The use of penalty-weighted slack variables provides information on the magnitude and location of constraint violations when the system is infeasible or severely stressed. This can support the identification of network bottlenecks, operational vulnerabilities, and potential reinforcement needs.

Overall, these categorized components define the methodological foundation of the dissertation and establish a clear link between the real-world operational challenges of modern power systems and the specific optimization tasks executed in this work.

## 1.4 Related Projects and Publications

The work developed in the scope of this dissertation partially concerns the objectives and results of the following research project:

- ATE – Aliança para a Transição Energética (Agenda Mobilizadora para a Inovação Empresarial), PRR Project No. 56, financed by Component 5 – Capitalisation and Business Innovation of the Portuguese Recovery and Resilience Plan (PRR), under the NextGenerationEU programme.

The developed work has resulted in the writing of 3 scientific papers for journal conference publication. The following should be referred to:

- Diogo Pereira, Diogo Reis, Micael Simões and Tiago Soares. "Nonlinear Programming-Based Multi-Period Approach for Security Constrained Optimal Power Flow". In: Smart Grids and Sustainable Energy 11.2 (2026), p. 41. ISSN: 2731-8087. DOI: 10.1007/s40866-026-00355-8 [4];
- Security-Constrained Multi-Period Optimal Power Flow with Stochastic Uncertainty Modelled through Chance Constraints, submitted for publication in the MEDPOWER conference proceedings;

- Stochastic Multi-Period Security-Constrained Optimal Power Flow via Approximated Chance Constraints, submitted for publication in the Wind and Solar conference proceedings.

## 1.5 Dissertation Structure

The remainder of this dissertation is organized as follows:

1. **Chapter 2 – State-of-the-Art:** Reviews the OPF and SCOPF problems, with particular emphasis on existing solution methodologies, including mathematical decomposition techniques, convex relaxations, and uncertainty-aware formulations such as stochastic and chance-constrained optimization.

2. **Chapter 3 – Methodology:** Presents the mathematical formulation of the proposed NLP-based MP-AC-SCOPF framework, including the rectangular voltage representation and slack-variable reformulations, the modeling of ESSs and flexible loads, and the continuous chance-constrained violation indicator.

3. **Chapter 4 – Case Studies and Results:** Evaluates the computational performance and operational relevance of the proposed framework using standardized IEEE benchmark systems, with particular focus on high-RES integration, resource utilization, and scalability.

4. **Chapter 5 – Conclusions and Future Work:** Summarizes the main findings and contributions of the dissertation, discusses its current limitations, and identifies possible directions for future research.

This chapter established the context, motivation, and objectives of the dissertation, highlighting the need for optimization tools capable of addressing uncertainty, network security, and temporal flexibility in modern power-system operation. Building on this motivation, the next chapter reviews the state-of-the-art in OPF and SCOPF methodologies, with particular emphasis on deterministic, stochastic, and chance-constrained formulations, as well as existing approaches for improving tractability and scalability.

# Chapter 2

# Literature Review

This chapter reviews the theoretical foundations, mathematical formulations, and solution methodologies underlying the OPF and SCOPF problems in modern power systems. It provides a comprehensive synthesis of the state-of-the-art, evaluating how different optimization paradigms balance modeling accuracy, computational tractability, and security guarantees under uncertainty. The chapter first establishes OPF as the fundamental building block for secure operations, analyzing the non-convex Alternating Current Optimal Power Flow (AC-OPF) formulation, the linearized Direct Current Optimal Power Flow (DC-OPF) approximation, the traditional $N-1$ security criterion, and the principles of Chance-Constrained Optimal Power Flow (CC-OPF). It then transitions to a detailed evaluation of classical and contemporary solution methodologies for the SCOPF problem, comparing nonlinear programming, linear programming, mathematical decomposition schemes, convexification strategies, metaheuristics, and data-driven machine learning approaches. Next, the chapter focuses specifically on the Chance-Constrained Security-Constrained Optimal Power Flow (CC-SCOPF) framework, detailing analytical reformulations, data-driven randomized approaches, and advanced AC-based risk extensions used to manage continuous renewable generation and load uncertainty. This is followed by a dedicated examination of relaxation techniques, encompassing engineering-focused slack variables, theoretical convex relaxations (spanning semidefinite programming to higher-order moment hierarchies), and targeted discrete or staged linearizations. Finally, the chapter synthesizes these developments within the context of an operational optimization "trilemma" and highlights the critical research gaps that motivate the robust framework developed in this dissertation.

## 2.1 OPF: The Foundation for Secure Power System Operation

The OPF problem is a fundamental steady-state optimization model in power system operation. Its objective is to determine economically or technically optimal control actions while satisfying the physical and operational constraints of the network. In practical applications, OPF provides the basis for more advanced operation-oriented formulations, including SCOPF and Security-Constrained Unit Commitment (SCUC) [5]. These formulations are commonly embedded in day-ahead market clearing, operational planning, and real-time dispatch tools used by Independent System Operators (ISOs) and TSOs, where they support energy scheduling, reserve allocation, congestion management, and the procurement of ancillary services [5].

From a modeling perspective, OPF can be viewed as a core building block within a hierarchy of power system decision problems. At the short-term operational level, SCUC extends the OPF framework by introducing unit commitment decisions, generator operating constraints, reserve requirements, and intertemporal coupling. In parallel, SCOPF extends OPF by enforcing security constraints under a predefined set of credible contingencies, typically according to the $N-1$ security criterion [5, 6].

Further extensions, such as probabilistic SCOPF and CC-OPF, incorporate stochastic representations of uncertain quantities, including loads, renewable generation, and component outages. These formulations allow operators to explicitly account for uncertainty and control the risk of constraint violations under variable operating conditions [6, 7]. Independent of the uncertainty modeling approach adopted, the network representation used in OPF, particularly the choice between AC and DC formulations, strongly influences the trade-off between physical accuracy, computational tractability, and the level of operational detail that can be represented in subsequent security-constrained and probabilistic models [5, 6].

### 2.1.1 The AC-OPF Formulation

The full AC-OPF formulation retains the nonlinear AC power flow equations and therefore provides the most detailed steady-state representation of power-system operation. In contrast to simplified formulations, AC-OPF explicitly models active and reactive power injections, voltage magnitudes, and voltage phase angles at each bus. These quantities are essential for accurately assessing thermal loading, voltage profiles, reactive power limits, and network losses [5]. This level of modeling detail is particularly relevant in modern power systems, where increasing shares of converter-interfaced renewable generation and changing patterns of reactive power support make voltage and reactive-power management central aspects of secure operation [5].

Mathematically, AC-OPF is a nonlinear and non-convex optimization problem. When discrete controls such as transformer tap positions, capacitor banks, or shunt switching are explicitly represented, the formulation may become a mixed-integer nonlinear program [5]. Interior-point methods and other NLP algorithms are widely used to solve continuous AC-OPF formulations and can obtain high-quality local solutions for realistic system sizes. However, due to the non-convexity of the AC power flow equations, global optimality cannot generally be guaranteed. In addition, convergence and computational performance may deteriorate as the network size increases, when multi-period couplings are introduced, or when the formulation is embedded within SCOPF or SCUC frameworks [5]. These difficulties become more pronounced in stochastic and chance-constrained settings, where uncertainty must be represented in addition to the underlying non-convex AC network model [7]. The resulting formulations must simultaneously capture the physical behavior of the grid, the uncertainty associated with renewable generation and demand, and the operational limits required to ensure secure operation.

Despite these limitations, AC-OPF remains the natural starting point for security-constrained analysis whenever voltage security, reactive power limits, or detailed post-contingency operating points are relevant. For this reason, many AC-based SCOPF and SCUC formulations build directly on the AC-OPF structure, either by solving the full nonlinear formulation or by adopting approximations, relaxations, and decomposition strategies to improve computational tractability.

### 2.1.2 The DC-OPF Approximation

A widely used approach to reduce the computational complexity of OPF is the DC-OPF approximation. This formulation linearizes the power flow equations by assuming a lossless network, voltage magnitudes close to 1 p.u., and small voltage-angle differences between connected buses [7]. Under these assumptions, active power flows can be expressed as linear functions of nodal power injections, commonly through Power Transfer Distribution Factors (PTDFs). The resulting optimization problem can be formulated as a linear program, which is significantly easier to solve than the full nonlinear AC-OPF. This makes DC-OPF particularly attractive for large-scale and time-sensitive applications, including market clearing, real-time dispatch, and large-scale SCUC problems with many network and contingency constraints [5, 6].

In practice, DC-OPF is widely adopted as the core network model in deterministic and probabilistic SCOPF studies. In these formulations, uncertainty may be represented through scenario generation, data clustering, or chance constraints applied to active-power line flows [6, 7]. For example, probabilistic SCOPF approaches based on data clustering solve multiple DC-OPF or linearized AC-OPF problems at representative operating points, thereby approximating the impact of load, renewable generation, and contingency uncertainties on system cost and reliability indices [6]. Similarly, in the unit commitment context, standard SCUC formulations often rely on DC network models to preserve tractability, while enforcing transmission security through linearized network constraints, contingency screening, and reserve requirements [5].

Despite its computational advantages, DC-OPF sacrifices important physical detail. In particular, it neglects reactive power flows and voltage magnitude constraints, which limits its suitability for studies where voltage security, reactive power management, or detailed post-contingency assessment are relevant [5]. These simplifications may become especially restrictive in highly loaded systems or in networks with high levels of converter-interfaced renewable generation, where voltage constraints can significantly influence feasible and secure operating points [5, 6]. Therefore, DC-OPF is best understood as a computationally efficient approximation that is well suited for large-scale screening, market-clearing, and active-power dispatch studies, whereas AC-OPF remains necessary when accurate voltage, reactive power, losses, and detailed security representations are required.

### 2.1.3 The N-1 Criterion and the Need for SCOPF

To ensure a high level of operational security, system operators rely on the $N-1$ security criterion. This criterion requires the power system to remain in a secure operating state, i.e., within all relevant operational limits, following the loss of a single component, such as a generator, transformer, or transmission line [8]. In practice, this requirement is often interpreted in a static steady-state sense: for each postulated contingency, the system must be able to accommodate the resulting redistribution of power flows without violating thermal or voltage limits.

SCOPF extends the OPF framework by incorporating this security requirement directly into the optimization problem. Its objective is to determine an operating point that is not only economically efficient under normal operating conditions, but also secure with respect to a predefined set of credible contingencies. AC-SCOPF formulations typically combine preventive pre-contingency decisions with corrective post-contingency control actions, ensuring that feasible post-contingency operating points exist and satisfy the relevant network and device constraints [9].

However, the classical $N-1$ criterion is primarily contingency-oriented. It is designed to assess the system response to discrete equipment outages, but it does not explicitly represent the continuous variability and forecast uncertainty associated with renewable generation and load. As renewable penetration increases, a dispatch solution that is secure for a single forecasted operating point may still be exposed to constraint violations under plausible forecast errors [8, 9]. This limitation has motivated extensions of the SCOPF framework that combine contingency security with uncertainty-aware decision-making. Among these extensions, stochastic MP-AC-SCOPF formulations incorporate temporal coupling and uncertainty scenarios, allowing the coordinated scheduling of flexible resources over multiple time periods. Chance-constrained AC-SCOPF approaches, in turn, enforce security constraints with a prescribed confidence level, thereby limiting the probability of constraint violations under uncertain renewable generation and load conditions [9]. In this broader perspective, the deterministic $N-1$ criterion remains a cornerstone of secure system operation. However, it must increasingly be complemented by stochastic or probabilistic tools capable of representing continuous uncertainty, temporal coupling, and flexibility from resources such as ESSs, demand response, and renewable generation.

### 2.1.4 Chance-Constrained OPF

Forecast uncertainty in modern power systems arises from multiple sources, including weather-dependent renewable generation, load variability, and increasingly short scheduling and trading intervals. When these fluctuations are significant, deterministic dispatch decisions based on point forecasts may result in real-time overloads, voltage-limit violations, or the need for costly corrective actions [6, 7]. These challenges become particularly relevant when the operating point must also remain secure under a set of credible contingencies, as in SCOPF and SCUC, or when the system is operated close to its physical limits.

Probabilistic variants of OPF have therefore been proposed to explicitly account for uncertainty in operational decision-making. Among these approaches, Chance-Constrained Optimization (CCO) has received significant attention due to its intuitive reliability interpretation. In CC-OPF, operational constraints are not required to hold for all possible realizations of uncertainty, since this would generally lead to overly conservative or cost-prohibitive solutions [7, 8]. Instead, the operator specifies an acceptable violation probability, denoted by $\varepsilon$, and requires each constraint, or a set of constraints, to be satisfied with probability at least $(1-\varepsilon)$ [7].

For an individual operational constraint, this can be expressed as:

$$\mathbb{P}\left(f_i(x,\xi) \leq b_i\right) \geq 1-\varepsilon_i \tag{2.1}$$

where $x$ denotes the decision variables, $\xi$ represents the uncertain parameters, $f_i(x,\xi)$ is the constraint function, $b_i$ is the corresponding limit, and $\varepsilon_i$ is the maximum admissible probability of violation. This formulation allows system operators to explicitly tune the trade-off between economic efficiency and operational risk. As a result, chance-constrained formulations have been applied both at the OPF level and within security-constrained problems such as chance-constrained SCOPF and SCUC [5, 7].

The main challenge in CC-OPF lies in mathematical tractability. In general, probability terms are difficult to evaluate directly, and chance constraints may define non-convex feasible regions, particularly when combined with nonlinear AC network models [7]. When uncertainty follows a known distribution, such as a Gaussian distribution, individual linear chance constraints can be reformulated analytically using quantile functions. This leads to deterministic equivalents that are often linear or convex, making them suitable for efficient solution in DC-OPF or convexified OPF settings [7]. However, these reformulations rely on strong assumptions regarding the probability distribution of the uncertain variables, which may limit their accuracy in practical applications.

Several solution strategies have been proposed to address these tractability challenges. Analytical reformulations convert chance constraints into deterministic equivalents under specific assumptions, such as Gaussian uncertainty and affine uncertainty propagation. Scenario-based and Sample Average Approximation (SAA) methods approximate probabilistic constraints using finite samples, providing greater modeling flexibility at the cost of increased computational burden. Distributionally robust and data-driven methods seek to reduce dependence on exact probability distributions by calibrating safety margins or ambiguity sets from data [7]. These approaches provide the methodological basis for CC-SCOPF, where uncertainty must be handled together with contingency constraints and, in AC formulations, nonlinear network equations. In this context, CC-OPF acts as a bridge between deterministic OPF-based formulations and fully probabilistic risk-based operation, allowing uncertainty to be incorporated explicitly while maintaining a tunable balance between reliability, cost, and computational tractability.

## 2.2 Solution Methodologies for SCOPF

The computational complexity of SCOPF has motivated extensive research into efficient solution methodologies. While classical deterministic SCOPF formulations remain central to secure power system operation, their practical application becomes increasingly challenging when full AC network models, large contingency sets, uncertainty representations, and multi-period flexibility resources are considered simultaneously.

To address these challenges, the literature has proposed a wide range of methodological approaches, including nonlinear programming, linear approximations, decomposition techniques, convexification methods, metaheuristics, and, more recently, machine learning-assisted strategies. This section reviews these approaches and discusses their relevance for improving the tractability, scalability, and applicability of SCOPF in modern power systems.

### 2.2.1 Nonlinear Programming

A direct way to retain the full nonlinear network representation is to solve AC-based SCOPF formulations using NLP techniques. The main advantage of these approaches is that they explicitly model voltage magnitudes, phase angles, reactive power flows, network losses, and other nonconvex relationships that are neglected or approximated in simplified models.

A major research direction concerns the extension of nonlinear formulations to stochastic and multi-period operational planning. Several works propose stochastic MP-AC-SCOPF frameworks that combine renewable generation uncertainty with intertemporal flexibility from ESSs and flexible loads [9, 10]. By jointly considering time coupling, scenario uncertainty, and contingency security, these formulations provide a detailed representation of modern power-system operation. However, the simultaneous inclusion of multiple time periods, uncertainty scenarios, and contingencies substantially increases the size and complexity of the optimization problem. This limits their applicability to large transmission networks and time-sensitive operational settings. Similarly, [11] investigates the use of Interline Power Flow Controllers (IPFCs) within a preventive SCOPF framework, enabling optimal mode selection and parameter adjustment to enhance power-flow controllability and system security. Although the study demonstrates operational benefits, the formulation remains deterministic and therefore does not explicitly consider renewable generation uncertainty or stochastic load behavior. In addition, relevant implementation details, including the NLP solver used, are not fully reported. This limits reproducibility and makes computational performance difficult to assess.

Given the computational burden of nonlinear SCOPF formulations, several studies have focused on improving scalability without fundamentally changing the underlying AC network model. For example, [12] proposes an iterative contingency-filtering methodology that evaluates post-contingency violations at intermediate optimal base-case solutions. By discarding low-impact contingencies and prioritizing the most critical violations, the approach reduces the number of evaluations required while maintaining an acceptable level of security assessment accuracy.

Extending nonlinear optimization toward operational planning, [13] introduces a framework referred to as multi-period corrective SCOPF. The method co-optimizes preventive and corrective actions for dispatchable generators, storage systems, and flexible loads within a rolling-horizon setting. The formulation captures time-coupled operational constraints through a multi-period look-ahead model and employs a quadratic penalty mechanism to discourage deviations from day-ahead schedules, thereby reducing myopic short-term decisions and redispatch costs. A closed-loop architecture iteratively updates the set of critical contingencies between optimization and security-checking stages, progressively improving system security. Nevertheless, because the approach relies on solving a centralized, non-convex NLP, computational requirements remain substantial, limiting scalability to very small systems. Moreover, key penalty parameters are tuned empirically through trial-and-error procedures, highlighting the need for more systematic parameter-calibration methods.

In summary, NLP-based SCOPF approaches provide a detailed representation of nonlinear power system physics and are well suited for modeling voltage constraints, reactive power limits, controllable devices, and stochastic multi-period operation. However, their computational burden, sensitivity to initialization, and limited global optimality guarantees remain important barriers to large-scale or real-time application. These limitations motivate continued research into formulations and solution strategies that preserve the accuracy of AC modeling while improving numerical robustness, scalability, and operational applicability.

### 2.2.2 Linear Programming

To alleviate the computational burden associated with nonlinear formulations, several studies have adopted Linear Programming (LP)-based approaches for SCOPF. These methods prioritize scalability, computational speed, and suitability for near real-time applications, often at the expense of full physical modeling accuracy.

Linear SCOPF formulations commonly rely on DC approximations, since the resulting optimization problems are computationally tractable and can be integrated into distributed or large-scale solution frameworks. For example, [14] proposes a fully distributed agent-based DC-SCOPF framework in which geographically dispersed network components operate as intelligent agents. Through iterative information exchange with neighboring agents, the system collaboratively solves the linearized optimization problem. While this decentralized structure improves scalability and parallel execution, the reliance on DC modeling prevents the representation of voltage-magnitude variations and reactive power flows. In addition, convergence performance remains sensitive to algorithm-tuning parameters.

To overcome the limitations of purely DC-based models while maintaining computational tractability, recent works have proposed sequential linear programming methodologies that approximate the full AC power flow equations. For instance, [15] proposes a tractable linearization-based approach to solve the highly complex stochastic MP-AC-SCOPF problem. Instead of relying on a standard DC approximation, this methodology achieves tractability by sequentially solving a limited number of varying linear approximations of the full AC problem. This is executed across a three-stage process that iteratively updates state-dependent active and reactive power losses, filters constraints, and adaptively tightens critical voltage and thermal limits. This approach not only accommodates renewable energy stochasticity alongside time-coupling flexibility from ESSs and flexible loads, but it also enforces voltage and reactive power bounds that DC models typically ignore. Extensive numerical experiments on large test systems demonstrate that this sequential linear methodology can eliminate constraint violations and is up to 95.8% faster than exact NLP solvers (such as IPOPT), all while maintaining a highly accurate solution with a sub-optimality gap of less than 1%. However, because the approach relies on sequential approximations and heuristic constraint tightening, it lacks a theoretical guarantee of convergence to a fully feasible solution under all operating conditions. Furthermore, the piecewise linearization of apparent power flows increases the total number of constraints by up to 37% compared to the exact NLP formulation. This structural expansion ultimately imposes a scalability ceiling. The authors note that modeling larger networks with extensive temporal and stochastic dimensions continues to face compilation bottlenecks, highlighting the need for advanced decomposition techniques or high-performance computing architectures to scale further.

Sensitivity-based formulations constitute another important class of computationally efficient SCOPF methods. For instance, [16] develops an LP-based formulation using PTDFs, Outage Transfer Distribution Factors (OTDFs), and Power Router (PR) sensitivity factors. The resulting model achieves high computational efficiency. However, its dependence on linear sensitivity coefficients inherently limits its accuracy when compared with full AC formulations. Extending this concept, [17] introduces a sensitivity-based SCOPF framework for near real-time redispatch in renewable-dominated systems. The formulation exploits linear sensitivities derived from the system Jacobian matrix, enabling a compact optimization problem solved through a Sequential Linear Approximation (SLA) algorithm combined with an adaptive trust-region strategy. The approach achieves strong computational performance, typically converging within three iterations, while incorporating time-coupled storage units and flexible loads through a power flow verification stage. However, because feasibility relies on linear approximations, post-contingency violations may occur, preventing strict guarantees of full AC feasibility. Moreover, solution quality remains sensitive to initialization, and validation is limited to a medium-scale 60-bus Nordic test system.

As power systems evolve toward hybrid transmission infrastructures, linear methodologies have also been extended to integrated AC–DC networks. In [18], the SCOPF problem for multi-terminal Voltage Source Converter (VSC)-based AC–DC networks is addressed through piecewise-linear approximations of operational costs and losses. This enables efficient corrective rescheduling of generators and converters using droop-control mechanisms. Nevertheless, the additional modeling requirements introduced by hybrid grids may expose scalability limitations when the network size and number of control variables increase substantially.

Linear optimization has also been used to improve computational tractability under uncertainty. In [19], an uncertainty-aware AC-SCOPF framework is proposed in which an affinely adjustable robust SCOPF approximation is used to identify post-contingency voltage and branch-current constraints that remain inactive under all uncertainty realizations and corrective control actions. These constraints can then be safely removed from the subsequent nonlinear problem. Tested on networks with up to 2 737 buses, the method demonstrates significant scalability benefits, reducing problem size by up to 82% and execution time by up to 95%, while preserving nonlinear voltage and thermal-limit verification. Despite these advantages, the framework depends on an accurately calibrated starting point obtained from sequential linear programming. Poor initialization may therefore degrade sensitivity estimation and reduce the effectiveness of constraint screening. Furthermore, the formulation is restricted to a single-period operating horizon. The numerical studies also consider only a small subset of highly loaded contingencies, leaving performance for larger contingency sets insufficiently explored.

In summary, LP formulations represent a pragmatic compromise between modeling fidelity and scalability. Although they generally sacrifice detailed representation of voltage and reactive power, their speed and numerical robustness make them attractive for operational planning, market-oriented applications, and real-time security assessment. Consequently, linear approaches often serve as a foundational layer upon which hybrid, decomposition-based, or nonlinear refinement strategies are built to reconcile computational performance with physical accuracy.

### 2.2.3 Decomposition Methodologies

Mathematical decomposition methodologies have been widely investigated as a means of addressing the computational complexity of large-scale SCOPF formulations. Their main advantage lies in the possibility of exploiting the structure of the problem, for example by separating base-case and contingency scenarios, decoupling time periods, or distributing computations across network regions. The reviewed decomposition approaches can be grouped into three main categories: Benders Decomposition (BD)-based methods, Alternating Direction Method of Multipliers (ADMM), and hybrid or filtering-based strategies.

Among these approaches, BD and its generalized variants have received particular attention. In [20], a SCOPF framework combining preventive and corrective controls is developed using Sequential Quadratic Programming (SQP) within a BD scheme. The formulation accounts for system constraints and generator ramp-rate limits, thereby enabling the coordination of pre- and post-contingency control actions. However, the validation is limited to relatively small test systems, namely the IEEE 9-bus system and a modified Jawa Bali 25-bus system, leaving its scalability to large transmission networks uncertain. Moreover, detailed computational indicators, such as execution times or convergence behavior, are not reported in the case studies.

Similarly, [21] proposes a SCOPF framework for coordinating multiple microgrids through an incentive-based mechanism. The method employs a scenario-decomposition strategy that combines Taguchi Orthogonal Array Testing (TOAT) with BD to manage uncertainties in renewable generation and load demand. The study highlights the potential of corrective control to reduce generator cycling. However, it does not provide a long-term quantitative assessment of this benefit. A more scalable application of BD is presented in [22], which proposes a multi-period secure stochastic AC OPF using a generalized BD strategy. The formulation decomposes the large-scale day-ahead scheduling problem by assigning intertemporal and active power coupling variables to a linear master problem, while post-contingency operating conditions are solved as nonlinear AC-OPF subproblems. Subproblem feasibility is promoted through active and reactive power slack variables, allowing the method to retain the nonlinear AC network representation without convex relaxation. To improve convergence, the authors introduce a bundle trust-region stabilization mechanism and exploit parallel multicore computation, achieving significant computational gains, including a 94.8% reduction in execution time and a decrease in the number of iterations from 25 to 13 on a Colombian 96-bus system. Nevertheless, scalability remains partially limited by the sequential nature of the master problem and the synchronization overhead between parallel subproblems, in line with the limitations predicted by Amdahl's Law[1].

A second research direction involves distributed optimization methods, particularly ADMM-based approaches. In [23], spatial decomposition is used to coordinate transmission and distribution system operation while preserving detailed power-flow modeling and consistency in resource sharing. By distributing computations across network partitions, the approach improves parallel execution and reduces the dependence on a centralized hierarchical structure. However, the absence of detailed computational performance indicators, such as convergence rates, iteration counts, or execution times, limits a rigorous comparison with classical decomposition approaches.

A third group of methods combines decomposition with additional algorithmic strategies, such as Lagrangian relaxation, branch-and-bound, contingency filtering, or sequential optimization. The work presented in [24] integrates Lagrangian duality, branch-and-bound techniques, generalized BD, and ADMM to address the SCOPF problem. Although such approaches can improve solution quality and provide stronger optimality guarantees, the resulting computational burden remains significant. This may restrict their applicability to large-scale or real-time operational settings, particularly when discrete control actions are explicitly represented. Other hybrid methodologies aim to reduce computational effort by limiting the number of contingencies that must be explicitly optimized. For instance, [25] proposes an iterative constraint-modification strategy that avoids solving a full optimization problem for every contingency. The method combines parallel power-flow analysis with contingency-filtering rules to identify the most relevant constraints. While this strategy improves computational efficiency, its reliance on interior-point methods may introduce sensitivity to initialization, and the identification of critical contingencies depends on heuristic ranking metrics based on network characteristics.

Building on these scalability-oriented ideas, [26] proposes a two-stage methodology for solving multi-period SCOPF problems in large transmission systems under strict execution-time requirements. The framework separates the optimization into a Mixed-Integer Linear Programming (MILP) "DC module", responsible for discrete operational decisions such as switching states and downtime-dependent startup costs, followed by a nonlinear continuous "AC module", which restores a more detailed physical network representation. Scalability to systems exceeding 2 000

[1]Principle used in parallel computing to estimate the theoretical maximum speedup achievable when only part of a task can be parallelized.

buses is achieved through analytical derivative evaluation, vectorized formulations, and a forward–backward sequential optimization procedure. However, meeting stringent computational deadlines requires structural simplifications. In particular, reserve allocation is removed from the main optimization loop and handled through an offline greedy post-processing stage, while contingency modeling retains only simplified energy balance constraints.

Overall, the literature on decomposition methodologies reveals a trade-off between modeling fidelity, computational scalability, and practical implementability. BD-based techniques provide a clear separation between master decisions and contingency subproblems, but may suffer from convergence and synchronization limitations. Distributed approaches such as ADMM enable greater parallelization, but their efficiency and convergence properties can be problem-dependent and are not always fully documented. Hybrid and filtering-based methods can further reduce computational effort, but often rely on simplifications, heuristics, or post-processing steps that may affect solution accuracy. These observations highlight the need for solution frameworks capable of preserving detailed modeling, accommodating uncertainty and intertemporal operational constraints, and achieving scalable computational performance for realistic power system applications.

### 2.2.4 Convexification-Based Methodologies

Convexification-based methodologies provide an alternative strategy for improving the tractability of SCOPF formulations. Rather than solving the original non-convex AC-based problem directly, these approaches reformulate, relax, or approximate the nonlinear constraints so that the resulting problem can be addressed using convex optimization techniques. This can improve numerical robustness and, in some cases, provide stronger theoretical guarantees.

The method proposed in [27] uses a Taylor-series expansion to obtain a signomial representation of nonlinear terms, followed by a sequence of transformations that convert non-convex signomial expressions into a convex form. This enables the use of convex optimization tools and can improve solver reliability. Nevertheless, the approach introduces additional modeling complexity and approximation errors. Related convexification ideas have also been applied to multi-energy systems. In [28], an adaptive convex-relaxation framework is developed for the coordinated operation of transportation and power distribution networks under $N-1$ contingencies. Adaptive relaxations are used to handle non-convexities, while contingency filtering discards scenarios that are unlikely to become binding in the optimal solution. Numerical results indicate that this combined strategy can produce reliable and computationally efficient preventive actions across both networks. However, the reliance on static traffic modeling and simplified outage representations limits its applicability to dynamic and time-varying operating conditions.

Convex reformulations have also been explored in the context of stability-constrained optimal operation. In [29], a convex framework is proposed for the small-signal stability-constrained OPF problem. Instead of relying on direct eigenvalue analysis, the stability constraints are expressed through a Lyapunov-based bilinear matrix inequality, which is then relaxed into a Semidefinite Programming (SDP) formulation. This stability relaxation is combined with convex approximations of the power flow equations, and a penalization mechanism is introduced to recover feasible operating points that satisfy the stability requirements. Numerical experiments on benchmark systems show that the method can identify stability-compliant solutions with modest cost increases and improved scalability relative to traditional approaches. Nevertheless, the semidefinite relaxation introduces conservativeness, since the resulting formulation provides sufficient rather than necessary conditions for the original stability constraints. Moreover, the computational burden of large-scale semidefinite programs remains a significant challenge for very large systems.

Overall, convexification techniques offer an attractive pathway for improving tractability, solver reliability, and theoretical interpretability in SCOPF-related problems. However, their practical effectiveness depends strongly on the tightness of the adopted relaxation or approximation, the operating region considered, and the level of physical detail that must be preserved. Consequently, while convexification methods are valuable for reducing computational complexity, they may introduce approximation errors, conservativeness, or formulation overhead that limit their direct applicability to large-scale, uncertainty-aware, MP-AC-SCOPF formulations.

### 2.2.5 Metaheuristic Methodologies

In response to the non-convexity and combinatorial complexity of SCOPF, several studies have explored metaheuristic algorithms as alternative solution strategies. These methods search for near-optimal solutions through population-based, probabilistic, or adaptive exploration mechanisms, making them flexible tools for handling nonlinearities and discrete control variables. However, this flexibility is generally obtained at the expense of stronger optimality guarantees and predictable computational performance.

The study in [30] introduces a cross-entropy-based optimization tool for SCOPF. The method employs adaptive probability density updates to guide the search process while maintaining nonlinear constraints and integer variables. This allows the algorithm to address complex SCOPF formulations without requiring extensive simplification of the feasible region. Nevertheless, as with many stochastic search methods, computational performance and solution quality may depend on parameter tuning and the number of samples used during the search process. Similarly, [31] proposes a mixed-integer genetic algorithm tailored for non-convex OPF problems. The algorithm simultaneously handles continuous and discrete control variables, such as generator dispatch and transformer tap positions, while accounting for security constraints, bus voltage limits, and valve point effects. Its population-based structure improves the exploration of non-convex search spaces, but it can also result in significant computational times, particularly for large-scale systems or extensive contingency sets. To explicitly address renewable uncertainty, [6] proposes a probabilistic SCOPF framework based on multi-objective particle swarm optimization. The approach analyzes the trade-off between expected operating cost and system-security indicators, while using $k$-means clustering to reduce the dimensionality of uncertainty data associated with renewable generation and load. By combining probabilistic assessment, clustering, and LP-based evaluations, the method improves the tractability of uncertainty-aware security assessment. However, the reliance on metaheuristic search may still limit reproducibility and computational predictability when applied to larger systems or time-sensitive operational settings.

Taken together, these studies show that metaheuristic approaches provide considerable modeling flexibility and can be effective for addressing non-convex, discrete, and multi-objective aspects of SCOPF. They are particularly useful when classical optimization methods struggle with non-smooth objective functions, integer controls, or highly nonlinear feasible regions. However, their stochastic nature, sensitivity to algorithmic parameters, lack of strong optimality guarantees, and reliance on iterative sampling make them less predictable than deterministic decomposition, LP, or NLP-based approaches. These limitations have motivated increasing interest in hybrid and data-driven optimization frameworks, where metaheuristics or machine learning techniques are used to guide, accelerate, or complement mathematical optimization methods.

### 2.2.6 Machine Learning Methodologies

Recent research has increasingly explored the integration of Machine Learning (ML) techniques into SCOPF formulations to improve computational efficiency, accelerate decision-making, and support predictive security assessment. In most cases, these approaches are not intended to replace traditional optimization entirely. Instead, they act as hybrid or learning-augmented frameworks in which data-driven models complement physics-based optimization, for example by predicting operating points, identifying active constraints, or approximating corrective actions.

The work presented in [32] introduces a learning-augmented optimization framework based on a multi-input multi-output random forest model. The model is used to predict bus voltage magnitudes and phase angles, which are subsequently refined using physics-based current and power-injection equations to improve physical consistency. This hybrid design can reduce computational effort while retaining a degree of interpretability. However, its performance depends strongly on the representativeness of the training data, the selected input features, and the ability of the model to generalize unseen operating conditions. Extending this direction, [33] proposes a framework that combines primal-dual Deep Reinforcement Learning (DRL) methods with traditional SCOPF models. The learning agent is trained to identify preventive control actions through interaction with a simulated environment that includes power system dispatch and contingency evaluation. Although this hybridization improves the treatment of feasibility constraints compared with purely data-driven approaches, the learning-based component still faces difficulties in satisfying equality constraints exactly. In addition, the exclusion of infeasible cases during training may bias the model toward less challenging operating conditions and reduce robustness under stressed scenarios.

Compared with metaheuristic algorithms, ML-based frameworks can exploit historical data and learned correlations to reduce computational burden during inference, providing fast approximate decisions. However, their dependence on training data introduces vulnerability to load and RES variability, rare contingencies, and operating conditions not adequately represented in the dataset. Moreover, the limited interpretability of some ML models and the difficulty of guaranteeing constraint satisfaction remain important barriers to deployment in operational environments.

In summary, data-driven and hybrid ML approaches represent a promising direction for accelerating SCOPF computations and supporting security assessment. Their main potential lies in complementing physics-based optimization through prediction, screening, warm-starting, or policy approximation. Nevertheless, ensuring robustness, feasibility, interpretability, and generalization under unseen or stressed operating conditions remains an open research challenge. Future developments are likely to rely on physics-guided and optimization-informed learning paradigms that combine the adaptability of data-driven methods with the physical rigor and constraint awareness of traditional optimization.

### 2.2.7 Synthesis of SCOPF Solution Methodologies

The reviewed methodologies reveal a fundamental trade-off between modeling fidelity, computational efficiency, and scalability. Table 2.1 summarizes representative SCOPF studies, highlighting their main modeling assumptions, sources of uncertainty and flexibility, solution techniques, network formulations, and treatment of multi-period operation.

Table 2.1: Summary of representative SCOPF studies and modeling characteristics.

| Ref. | Uncertainty and Flexibility Sources | Optimization Technique | Formulation | Multi-Period |
|---|---|---|---|---|
| [6] | RES | Metaheuristic | DC | No |
| [9] | RES, flexible loads, ESSs | NLP | AC | Yes |
| [10] | RES, flexible loads, ESSs | NLP | AC | Yes |
| [11] | None | NLP | AC | No |
| [12] | None | NLP | AC | No |
| [13] | RES, flexible loads, ESS | NLP | AC | Yes |
| [14] | None | LP | DC | No |
| [15] | RES, flexible loads, ESSs | LP | Linearized AC | Yes |
| [16] | None | LP | Linearized AC | No |
| [17] | None | SLA | Linearized AC | Yes |
| [18] | None | LP | AC/DC | No |
| [19] | RES, flexible loads | Affinely Adjustable Robust Optimization | AC | No |
| [20] | None | BD | AC | No |
| [21] | RES, flexible loads | BD and TOAT | DC | No |
| [22] | RES, ESS | BD | AC | No |
| [23] | RES, flexible loads, ESSs | ADMM | AC | Yes |
| [24] | None | BD, Lagrangian duality, branch-and-bound and ADMM | Linearized AC | No |
| [25] | None | Decomposition method | AC | No |
| [26] | None | MILP/NLP | Decoupled DC then AC | Yes |
| [27] | None | Convexification | Convex AC | No |
| [28] | Traffic patterns, EV charging behavior | Convex relaxation | Convex AC | No |
| [29] | None | SDP-based convexification with Lyapunov stability relaxation | Convex AC | No |

Continued on next page

| Ref. | Uncertainty and Flexibility Sources | Optimization Technique | Formulation | Multi-Period |
|---|---|---|---|---|
| [30] | None | Metaheuristic | AC | No |
| [31] | None | Metaheuristic | AC | No |
| [32] | None | ML | AC | No |
| [33] | None | ML | AC | No |
| [34] | None | NLP (Han–Powell algorithm with penalty function) | AC | No |

Decomposition-based approaches improve tractability by partitioning the problem into smaller subproblems. However, their performance may deteriorate for highly non-convex formulations, and convergence behavior can become problem-dependent. On the other hand, NLP-based approaches preserve the full nonlinear AC network representation and can naturally accommodate temporal and stochastic couplings, but typically at a significantly higher computational cost. Methods based on LP prioritize computational speed and scalability by simplifying network physics. While this enables the efficient solution of large-scale systems, important aspects such as reactive power flows and voltage magnitudes are only partially represented or neglected altogether. Convexification techniques seek to improve tractability by transforming non-convex problems into convex approximations or relaxations. Although these approaches may provide stronger theoretical properties, the resulting approximations can introduce modeling errors, conservativeness, or additional formulation complexity. Alternative paradigms address these challenges from different perspectives. Metaheuristic algorithms offer considerable flexibility for handling non-convexities and discrete decision variables, but they generally lack strong optimality guarantees and rely on iterative search procedures that may require significant computation times. More recently, ML and hybrid data-driven approaches have emerged as promising tools for accelerating computation, supporting screening, or approximating control actions. Nevertheless, their performance depends on the quality and representativeness of the training data, and ensuring reliable constraint satisfaction under unseen operating conditions remains a significant challenge.

The main advantages and limitations of the reviewed methodologies are summarized in Table 2.2. None of the reviewed SCOPF methodological approaches simultaneously achieves the three desired properties of the operational optimization “trilemma”: detailed physical modeling, computational tractability, and scalability.

Table 2.2: Comparative overview of SCOPF methodological approaches.

| **Class** | **Main Strengths** | **Main Limitations** | **Key Focus / Trade-off** |
|---|---|---|---|
| Decomposition-based (Benders, ADMM) | Scalable. Enables parallel and modular solutions. | Iterative convergence; possible infeasibility under non-convexity. | Scalability vs. convergence robustness. |
| NLP | Preserves nonlinear AC physics. Handles temporal and stochastic couplings. | High computational cost, local optimality and sensitivity to initialization. | Physical fidelity vs. tractability. |
| LP | Fast and suitable for large or real-time systems. | DC simplifications and limited voltage/reactive modeling. | Efficiency vs. modeling accuracy. |
| Metaheuristics (GA, PSO, Cross-Entropy) | Handles discrete/non-convex variables. Flexible. | No optimality guarantee and is parameter-sensitive. | Global search vs. deterministic reliability. |
| Machine Learning / Hybrid | Fast inference, useful for screening, prediction, and warm-starting. | Data dependence, generalization issues and has possible constraint violations. | Computational speed vs. reliability. |
| Convexification | Improves tractability through convex approximations or relaxations. May provide bounds. | Approximation errors, conservativeness and formulation complexity. | Theoretical guarantees vs. modeling exactness. |

While the methodologies reviewed in this section address the computational challenges of deterministic and stochastic SCOPF from different perspectives, the explicit incorporation of probabilistic security requirements introduces additional modeling and reformulation challenges. In particular, extending CC-OPF to SCOPF requires uncertainty to be handled simultaneously with contingency constraints and, in AC formulations, nonlinear network equations. These aspects are discussed in Section 2.3.

## 2.3 Chance-Constrained SCOPF

Stochastic optimization provides a general framework for decision-making under uncertainty, in which uncertain parameters are explicitly represented through probabilistic models or scenario-based descriptions. In power system operation, these methods are widely used to improve the robustness of optimal dispatch scheduling decisions under uncertain operating conditions.

Among the different stochastic optimization approaches, chance-constrained formulations are particularly relevant because they impose probabilistic guarantees on constraint satisfaction. Instead of requiring constraints to hold for all possible uncertainty realizations, chance constraints allow a controlled probability of violation, thereby providing a compromise between robustness and operational efficiency. Within the broader field of stochastic optimization, chance-constrained methods have been extensively studied in the context of OPF. These ideas naturally extend to SCOPF, leading to the so-called CC-SCOPF framework.

The transition from deterministic SCOPF to CC-SCOPF introduces significant mathematical and computational challenges. A central difficulty is the reformulation of probabilistic constraints into deterministic equivalents or approximations that can be handled efficiently by standard optimization solvers. Depending on the uncertainty model and the network constraints considered, these reformulations may result in non-convex feasible regions. Moreover, the size and complexity of realistic power systems, with many buses, transmission elements, uncertain injections, and contingency cases, require algorithms that remain computationally scalable while preserving meaningful security guarantees [35].

### 2.3.1 Reformulation Strategies for Chance-Constrained SCOPF

The practical implementation of CC-SCOPF depends largely on how the probabilistic constraints are transformed into a form that can be solved efficiently. Different reformulation strategies have been proposed in the literature, ranging from analytical deterministic equivalents based on distributional assumptions to data-driven, randomized, AC-based, and risk-based methods.

These approaches differ in terms of tractability, conservativeness, reliance on uncertainty models, and ability to capture the nonlinear behavior of power systems. This subsection reviews the main methodological families used in CC-SCOPF, emphasizing their assumptions, advantages, and limitations.

#### 2.3.1.1 Analytical Reformulations

A common approach for implementing CC-SCOPF is based on the analytical reformulation of individual chance constraints [36]. In this framework, probabilistic limits are converted into deterministic constraints by introducing uncertainty margins. These margins effectively reduce the admissible operating range of transmission lines or generators, thereby providing a safety buffer against uncertainty realizations.

The general form of an individual chance constraint for a line flow or generator output can be written as:

$$\mathbb{P}\left[a\left(p_G\right)+b\left(p_G\right)\delta u \leq c\right] \geq 1-\varepsilon \tag{2.2}$$

where $a(p_G)$ represents a power flow or generator output under the forecasted operating point, $b(p_G)$ captures the sensitivity of the constraint to the uncertainty $\delta u$, and $c$ denotes the corresponding technical limit. The term $b(p_G)\delta u$ defines a scalar random variable with mean $\mu$ and variance $\sigma^2$.

Under suitable assumptions on the uncertainty distribution, the probabilistic constraint can be reformulated as the following deterministic constraint [36]:

$$a\left(p_G\right) \leq c-b\left(p_G\right)\mu-f_{\mathscr{P}}^{-1}(1-\varepsilon)\left\|b\left(p_G\right)\Sigma_W^{\frac{1}{2}}\right\|_2 \tag{2.3}$$

where $\Sigma_W$ is the covariance matrix of the uncertainty sources, and $f_{\mathscr{P}}^{-1}(1-\varepsilon)$ is a safety parameter determined by the assumed distribution family $\mathscr{P}$ [36]. This parameter defines the size of the uncertainty margin. Larger values lead to more conservative and secure dispatch decisions, but generally increase operating costs. The value of the safety parameter depends on the assumed uncertainty model, as summarized in Table 2.3. In this table, $\Phi$ denotes the cumulative distribution function of the standard normal distribution. The notation $t_{\nu,\sigma_T}$ denotes the cumulative distribution function of the Student's $t$ distribution with zero mean, $\nu$ degrees of freedom, and scale parameter $\sigma_T = (\nu-2)/\nu$ [36].

Table 2.3: Safety parameters for different uncertainty models [36].

| **Uncertainty model** | **Safety parameter** |
|---|---|
| Normal | $\Phi^{-1}(1-\varepsilon)$ |
| Student's $t$ | $t_{\nu,\sigma_T}^{-1}(1-\varepsilon)$ |
| Symmetric, unimodal | $f_S^{-1}(1-\varepsilon) = \begin{cases} \sqrt{\frac{2}{9\varepsilon}}, & 0 \le \varepsilon \le \frac{1}{6} \\ \sqrt{3(1-2\varepsilon)}, & \frac{1}{6} < \varepsilon < \frac{1}{2} \\ 0, & \frac{1}{2} \le \varepsilon \le 1 \end{cases}$ |
| Unimodal | $f_U^{-1}(1-\varepsilon) = \begin{cases} \sqrt{\frac{4}{9\varepsilon} - 1}, & 0 \le \varepsilon \le \frac{1}{6} \\ \sqrt{\frac{3(1-\varepsilon)}{1+3\varepsilon}}, & \frac{1}{6} < \varepsilon \le 1 \end{cases}$ |
| Mean and covariance | $f_C^{-1}(1-\varepsilon) = \sqrt{\frac{1-\varepsilon}{\varepsilon}}$ |

Analytical reformulations are attractive because they are scalable and transparent. Once the uncertainty margins are computed, the resulting optimization problem can often retain a structure similar to that of a conventional deterministic SCOPF. This makes the approach compatible with standard optimization solvers and avoids the dependence on specific random samples that characterizes sampling-based methods.

Early applications of CCO to power system operation focused mainly on its integration into OPF and SCOPF formulations. In particular, [37] apply CCO to the SCOPF problem by enforcing transmission line flow limits through individual chance constraints under uncertainty. The study incorporates wind power forecast uncertainty into day-ahead operational planning through a Probabilistic Security-Constrained Optimal Power Flow (pSCOPF) formulation and introduces a valuation framework comparing the financial implications of the *cost of security* and the *cost of uncertainty*. In this formulation, wind power forecast errors are modeled as Gaussian random variables, enabling the analytical reformulation of probabilistic constraints into deterministic equivalents. The resulting formulation preserves the linear structure and computational complexity of a standard deterministic OPF, allowing the problem to be solved efficiently using conventional optimization software. Despite these advantages, the methodology relies strongly on the Gaussian assumption, whereas real wind power forecast errors often exhibit non-Gaussian characteristics. Nevertheless, this work represents one of the earliest systematic efforts to embed probabilistic security constraints into contingency-constrained system operation. Later experiments by the same authors, reported in [35], showed that although power injections may be non-Gaussian, the resulting line flows can be close to Gaussian. This behavior is mainly attributed to the aggregation of multiple uncertainty sources and the approximately linear mapping introduced by the DC power flow model. These results support the use of Gaussian approximations as a practical reference model in large-scale systems.

#### 2.3.1.2 Data-Driven and Randomized Approaches

Although analytical reformulations are computationally efficient, they rely on explicit distributional assumptions. To reduce this dependence, alternative methods based on data-driven calibration have been proposed. For example, [7] introduce a data-driven tuning procedure that decouples the optimization model from the underlying uncertainty distribution. The method iteratively refines a lightweight analytical approximation using sample-based feedback. The model uses a bisection search to tune a safety parameter $s$ until the observed empirical violation probability $\varepsilon_{\text{obs}}$ matches the desired violation probability $\varepsilon_{\text{des}}$. The algorithm first solves the CC-OPF to obtain a candidate dispatch. This dispatch is then evaluated using 10 000 samples to estimate $\varepsilon_{\text{obs}}$. The safety parameter $s$ is adjusted based on whether the resulting solution is overly risky or overly conservative. Because the method does not require the uncertainty to belong to a predefined family of distributions, it is robust against model mismatch. In tests on the IEEE 24-bus system, the method achieved the desired reliability for both individual and joint constraints within approximately 10 to 15 iterations.

Another line of work relies on randomized optimization. Building on previous CCO formulations, [38] propose a probabilistically robust framework for chance-constrained power system optimization problems. This approach uses concepts from scenario-based and randomized optimization to approximate chance constraints while requiring significantly fewer uncertainty realizations than classical scenario approaches. At the same time, it maintains comparable probabilistic feasibility guarantees. As a result, it provides a computationally tractable alternative for applying CCO to large-scale power system problems. The study shows that explicitly accounting for wind forecast uncertainty prevents constraint violations even under worst-case realizations. However, the framework assumes that the available redispatch capacity is known *a priori* rather than co-optimized with generation scheduling. This assumption limits the operational flexibility of the formulation, particularly in applications where corrective actions should be optimized jointly with the base dispatch, such as SCOPF.

#### 2.3.1.3 AC and Risk-Based Extensions

Despite their computational advantages, DC-based formulations neglect important nonlinear characteristics of AC networks. This limitation has motivated the development of chance-constrained formulations based on the full AC power flow model. One such approach is the *inner–outer approximation* proposed by [8]. This method reformulates the nonlinear probabilistic constraints into two parametric NLP problems, corresponding to inner and outer approximations of the feasible region. The main idea is to approximate the discontinuous indicator function associated with the chance constraint using a smooth function, thereby enabling the use of gradient-based nonlinear optimization methods. This type of formulation improves physical modeling accuracy by retaining the nonlinear AC network equations. However, this improvement comes at a significant computational cost when compared with DC-based or analytically reformulated models. Therefore, AC-based chance-constrained formulations are particularly relevant when voltage magnitudes, reactive power flows, and nonlinear network effects play a central role.

The work presented in [35] further extends the CC-SCOPF framework by incorporating optimized *corrective control* policies and a *risk-based assessment* of violation severity. In particular, it introduces Weighted Chance Constraints (WCC), which limit the expected severity of constraint violations rather than only their probability:

$$\mathbb{E}\left[f\left(y\left(\omega\right)\right)\right] \leq \overline{R} \tag{2.4}$$

where $f(y)$ is a convex weighting function, either linear or quadratic, that penalizes the magnitude of a violation $y$. Unlike classical chance constraints, which treat all violations equally, WCC distinguish between minor and severe violations by assigning larger penalties to larger deviations. The proposed formulation is solved using a sequential Second-Order Cone Programming (SOCP) approach and scales efficiently to systems with very large numbers of constraints, including the 2383-bus Polish grid. The use of WCC improves system resilience by reducing the occurrence of severe, high-risk overloads. However, some WCC, particularly those associated with wind power output limits, do not admit simple analytical expressions. Consequently, the corresponding risk measures must be computed numerically, for example, via Gaussian quadrature, thereby increasing the overall computational burden. Numerical results show that introducing corrective control under uncertainty can reduce the *cost of uncertainty* by 0.35% while maintaining a 99% security level, confirming that grid flexibility can directly reduce operating costs.

Overall, the reviewed approaches reveal a fundamental trade-off in CC-SCOPF design between computational scalability, physical modeling accuracy, and robustness to uncertainty. Analytical reformulations provide tractability and transparency, data-driven methods reduce dependence on predefined uncertainty distributions, randomized methods offer probabilistic feasibility guarantees with fewer samples than classical scenario approaches, and AC-based formulations improve physical fidelity at the expense of higher computational burden. The appropriate methodology, therefore, depends on the size of the system, the quality of available uncertainty information, the required reliability level, and the operational time scale of the application.

## 2.4 Relaxation Techniques

While convexification methods were previously discussed as one class of SCOPF solution methodology, this section adopts a broader view of relaxation, including not only convex relaxations but also feasibility-oriented slack variables, emergency actions, discrete-variable relaxation, and staged linear approximations.

Relaxation techniques play an important role in AC-OPF and SCOPF formulations, where non-convexity, contingency requirements, and strict operational limits can make the resulting optimization problems difficult to solve. In this context, the term *relaxation* can refer to different modeling strategies, depending on the objective of the formulation. Relaxations may be used to recover feasibility when the original problem is over-constrained, to obtain convex approximations with stronger optimality guarantees, or to simplify discrete or complex elements of the model.

The literature reviewed in this section illustrates these different purposes through representative approaches. These include emergency-action and slack-variable relaxations, algebraic convexifications, and targeted relaxations used to handle discrete variables or linear approximations in AC power flow optimization.

### 2.4.1 Emergency Action Relaxation and Slack Variable Approaches

In AC-SCOPF, infeasibility may arise when the system is unable to satisfy all base-case and post-contingency constraints simultaneously. To address this issue, [39] proposes two complementary relaxation frameworks. The first approach, based on the relaxation of control variables, expands the set of post-contingency control actions to include emergency measures such as load shedding. This provides operators with actionable and interpretable information on where and by how much load should be curtailed to restore feasibility. The second approach relaxes operational constraints directly by introducing slack variables. These variables soften the limits on thermal loading, voltage magnitudes, and generator ramping constraints. The comparative analysis shows that load-shedding relaxation generally yields more operationally meaningful solutions than the use of fictitious slack variables, since the latter do not correspond directly to physical control actions.

While this strategy is mathematically simple and computationally efficient, the resulting violations are less directly interpretable from an operational perspective. A related strategy is presented in [25], where slack variables are embedded in an iterative decomposition process. In this framework, slack variables accommodate constraint violations during intermediate iterations, while penalty terms guide the solution toward feasible operating regions as the constraints are progressively tightened based on contingency evaluation results.

### 2.4.2 Convex Relaxations: From SDP to Moment Hierarchies

A more theoretical perspective on relaxation techniques is provided in [40], where the authors analyze the relationships between three convex relaxations of the AC-OPF: the full SDP relaxation, the chordal or sparse SDP relaxation, and the SOCP relaxation. These relaxations are studied under both the bus-injection and branch-flow formulations. The full SDP relaxation is obtained by lifting the voltage variables into a matrix representation and relaxing the non-convex *rank-1* constraint on the lifted voltage matrix. The chordal SDP relaxation exploits network sparsity by enforcing positive semidefiniteness only on the maximal cliques of a chordal extension of the network graph, thereby reducing the computational burden. The SOCP relaxation further weakens the SDP formulation by imposing positive semidefiniteness only on $2 \times 2$ principal submatrices, or equivalently on edge-wise constraints. This makes the SOCP relaxation computationally attractive, but generally less tight. The results show that, for radial networks, all three relaxations are equivalent under strong assumptions. In such cases, the SOCP relaxation is often preferable because it offers the same level of exactness as the SDP-based approaches at a substantially lower computational cost. For meshed networks, however, the SDP and chordal SDP relaxations are strictly tighter than the SOCP relaxation. Among these, the chordal relaxation preserves the accuracy of the full SDP formulation while exploiting sparsity to improve computational performance.

Complementing conventional SDP-based approaches, [41] introduces a hierarchy of moment-based relaxations derived from the Lasserre framework. By systematically increasing the relaxation order, the method generates a sequence of SDP programs that provide progressively tighter approximations of the original non-convex OPF problem. In the limit, this hierarchy converges to the global optimum. Compared with standard first-order SDP relaxations, higher-order moment relaxations can solve cases in which the basic SDP relaxation is not exact. Numerical results show that low-order relaxations, often of second order, are sufficient to recover globally optimal solutions in challenging cases involving disconnected feasible regions, multiple local optima, or stringent line-flow constraints. Unlike approaches based on a single convex relaxation, moment relaxations provide a systematic hierarchy with provable convergence properties. However, their computational burden increases rapidly with the relaxation order due to the growth of the associated moment and localizing matrices. This limits their practical applicability to smaller systems or to implementations that exploit sparsity.

### 2.4.3 Linearization and Targeted Discrete Relaxation

Not all relaxation strategies rely on convexifying the power flow equations. In [23], the authors preserve the full nonlinear AC power flow equations in order to maintain modeling accuracy across both transmission and distribution networks. To keep the resulting NLP computationally manageable, the relaxation is applied only to selected discrete variables. In particular, the tap ratios of On-Load Tap Changer (OLTC) transformers are represented as continuous variables rather than integer-valued settings. This targeted relaxation allows the ADMM-based solver to detect voltage limit violations and coordinate shared resources while avoiding the modeling errors associated with DC or fully convexified formulations.

A complementary approach is proposed in [15], where the authors develop a multi-stage linearization strategy for stochastic MP-AC-SCOPF. Instead of relying on a single linear approximation, the method solves a sequence of linearized problems with progressively refined constraint limits. Early stages use relaxed voltage constraints to accelerate convergence, while later stages incorporate reactive power and voltage constraints more explicitly. In the final stage, only the constraints that were violated in previous iterations are tightened. This staged procedure reduces the approximation errors associated with single-step linearization while avoiding the computational expense of enforcing all potentially binding constraints from the beginning. The method therefore provides a practical compromise between the scalability of linear models and the accuracy required for AC-based security-constrained operation.

### 2.4.4 Synthesis: Relaxation as Strategic Design Choice

Taken as a whole, the reviewed contributions show that relaxation is not a single technique, but a family of modeling choices adapted to different computational and operational challenges. Slack-variable and emergency-action relaxations are primarily designed to recover feasibility and provide diagnostic or corrective information. Convex relaxations, such as SDP, chordal SDP, SOCP, and moment relaxations, aim to improve tractability and provide optimality guarantees or bounds. Linearization-based approaches seek scalability through staged approximations, while targeted discrete relaxations simplify selected components of the model without abandoning the nonlinear AC representation.

The appropriate relaxation strategy depends strongly on the application context. Real-time or near-real-time operation requires interpretable corrective actions and fast computation, making emergency-action or slack-variable approaches attractive. Offline planning studies may benefit from convex relaxations, and multi-operator settings can benefit from selective relaxations combined with decomposition methods. These methodologies highlight the fundamental trade-off between physical accuracy, computational tractability, scalability, and operational interpretability in OPF and SCOPF formulations. Convex relaxations improve solvability and provide valuable theoretical guarantees, but may simplify or omit relevant nonlinear system behavior. Conversely, full AC-based formulations retain greater physical fidelity but are usually harder to solve and may lack global optimality guarantees.

## 2.5 Summary and Research Gaps

This chapter has provided a comprehensive review of the theoretical foundations, mathematical formulations, and solution methodologies underlying the OPF and SCOPF problems. The extensive literature highlights a persistent optimization "trilemma" in power system operation, where methodologies must continuously trade off between three competing dimensions: physical modeling fidelity, computational tractability, and algorithmic scalability.

The critical synthesis of the state-of-the-art reveals several open challenges and research gaps in modern power system optimization:

- **The linearization gap:** While LP and DC approximations achieve the speed and robustness required for large-scale, real-time applications, they fail to capture voltage magnitudes, reactive power dynamics, and system losses. This limitation is increasingly problematic in modern grids characterized by declining inertia and shifting reactive power profiles.

- **The conservativeness of relaxations:** Convexification and relaxation techniques (such as SDP and SOCP) offer appealing theoretical bounds and global optimality guarantees. However, they frequently introduce severe modeling conservativeness or physical inexactness when applied to meshed, highly stressed, or multi-period networks.

- **The infeasibility vulnerability in stochastic settings:** Extending deterministic security criteria to chance-constrained frameworks (CC-SCOPF) allows operators to manage continuous renewable uncertainty. However, these formulations remain highly vulnerable to mathematical infeasibility when networks are operated near their physical limits, often lacking a clear mechanism to diagnose or gracefully handle constraint violations.

- **Tractability of multi-period AC physics:** NLP-based approaches naturally preserve full AC physics and accommodate temporal couplings from flexible resources like ESSs. Yet, their extreme computational burden and sensitivity to initialization have historically limited their practical deployment in security-constrained multi-period settings.

Building on these observations, it is evident that modern power systems require a framework capable of navigating the trade-offs of the optimization trilemma without sacrificing physical rigor or failing under stressed, over-constrained operational states. To address these limitations, Chapter 3 develops an NLP-based formulation that preserves the full AC representation of the power system, allowing nonlinear operational constraints and uncertainty effects to be modeled directly. To improve numerical robustness and eliminate the strict convergence failures typical of rigid feasibility boundaries, selected constraints are systematically reformulated through penalized slack variables in the objective function. This framework establishes the methodological basis for a scalable, robust architecture that successfully balances physical modeling accuracy, computational efficiency, and operational interpretability under uncertainty.

# Chapter 3

# Proposed Methodology

This chapter presents the methodological framework proposed in this thesis for the formulation of a stochastic multi-period SCOPF. Building upon the concepts and limitations identified in Chapter 2, it is proposed an optimization approach capable of simultaneously addressing operational security, uncertainty, and flexibility integration while preserving the full nonlinear AC network representation.

This chapter progressively develops the complete model. First, Section 3.2 introduces the probabilistic multi-period OPF formulation, including the modeling of generators, flexible loads, ESSs, and reactive power support devices. Next, Section 3.3 extends the formulation to a chance-constrained OPF, incorporating smooth violation indicators that enable probabilistic security assessment while preserving compatibility with gradient-based nonlinear solvers. Section 3.4 then extends the framework to a SCOPF formulation by explicitly accounting for contingency conditions. Finally, Section 3.5 details the Python software package developed to implement the proposed methodology, outlining its structure and workflow and demonstrating how the optimization models are formulated and executed.

## 3.1 Introduction

The family of optimization problems collectively referred to as OPF represents one of the most important and extensively studied topics in both power systems engineering and constrained nonlinear optimization. The concept was first introduced by [42] as an extension of the classical Economic Dispatch (ED) problem, with its defining contribution being the explicit inclusion of network power flow equations within the optimization framework. Since then, OPF has become indispensable for modern power system operation and planning, supporting day-ahead scheduling, congestion management, loss minimization, and other essential operational processes. SCOPF extends the OPF concept by explicitly incorporating security requirements into the optimization model. Instead of determining an operating point that is feasible only under normal conditions, SCOPF seeks a dispatch solution that remains secure under a predefined set of credible contingencies, typically following the $N-1$ security criterion.

This chapter presents the methodology adopted in this dissertation for formulating and solving a stochastic MP-AC-SCOPF problem. The proposed formulation preserves the nonlinear AC network representation while incorporating contingency constraints, uncertainty scenarios, and multi-period operational couplings associated with flexible resources. To improve numerical tractability and support feasibility recovery, selected operational constraints are reformulated through penalized slack variables.

## 3.2 Stochastic OPF

As discussed in Chapter 2, the OPF problem is the core steady-state model for managing power systems, while satisfying network constraints. However, traditional deterministic formulations assume perfect forecast, making them ill-suited for modern grids characterized by high renewable penetration. To account for the inherent unpredictability of these resources, a stochastic OPF approach is required to evaluate system behavior across a broad spectrum of uncertainty realizations, such as fluctuating wind and solar generation profiles.

The proposed stochastic framework expands the traditional deterministic formulation by explicitly representing operational uncertainty through a discrete set of scenarios, each weighted by its respective probability of occurrence. By transitioning from a single expected grid state to a multi-scenario framework, the optimization model introduces penalty-weighted slack variables into selected operational constraints and into the computation of scenario-specific optimization variables. In this context, these slack variables act as controlled relaxations of otherwise hard operational limits, allowing the optimization problem to remain solvable even when extreme, low-probability uncertainty scenarios render the network stressed or deterministically infeasible. To preserve operational realism, all slack variables are heavily penalized in the objective function. Consequently, the optimization simultaneously minimizes the primary operational target (e.g., expected operating costs or network congestion) and the magnitude of constraint violations across the considered uncertainty distribution, ensuring that violations occur only when no strictly feasible solution exists. The resulting slack values therefore provide a statistical measure of security margins, highlighting specific network nodes and lines where available control actions are insufficient to accommodate renewable generation uncertainty, and where additional flexibility or network reinforcement is required.

A core mathematical characteristic of the proposed framework is the systematic representation of voltage phasors in rectangular coordinates rather than traditional polar forms. By expressing the network states using real and imaginary voltage components, the nonlinear AC power flow equations and operational boundaries are cast entirely as quadratic polynomials. This algebraic choice eliminates trigonometric functions and avoids geometric singularities typically associated with voltage angles. Crucially, this quadratic formulation allows the underlying model to be highly compatible with the Quadratic Programming (QP) domain, ultimately facilitating its extension into the mixed-integer linear and quadratic variants (MIQP) presented later in this work, yielding superior numerical conditioning and computational performance.

Additionally, constraints involving absolute value expressions are reformulated to improve computational tractability within the probabilistic framework. Absolute value functions are non-differentiable at zero, introducing sharp gradient discontinuities that cause severe convergence issues for gradient-based NLP solvers when processing diverse uncertainty scenarios. Therefore, a standard relaxation technique is adopted, whereby each absolute value expression is replaced by an equivalent pair of inequality constraints. This reformulation removes non-differentiable elements from the model, significantly improving convergence stability with gradient-based NLP solvers such as IPOPT [43] when handling large-scale, uncertainty-mapped networks.

### 3.2.1 Objective Function

The objective function of the proposed stochastic OPF, representing the minimization of overall network operation costs, is given by:

$$
\begin{aligned}
\min \quad & \sum_{o \in \Omega_o} \sum_{t \in T} \omega_o \cdot \Bigg( \\
& \sum_{g \in G} c_{g,t} \cdot (P_{g,o,t}) \\
& + \sum_{l \in L} c^{\text{Load, curt}} \cdot \left( P^{\text{curt,down}}_{l,o,t} + P^{\text{curt,up}}_{l,o,t} + Q^{\text{curt,down}}_{l,o,t} + Q^{\text{curt,up}}_{l,o,t} \right) \\
& + \sum_{g \in G^R} c^{\text{RES, curt}} \cdot P^{\text{curt}}_{g,o,t} \\
& + \sum_{l \in F^l} c^F_t \cdot \left( P^{\text{flex,down}}_{l,o,t} + Q^{\text{flex,down}}_{l,o,t} \right) \\
& + \sum_{e \in E} c^{\text{ESS}} \cdot \left( P^{ch}_{e,o,t} \cdot P^{dch}_{e,o,t} \right) \\
& + \sum_{i \in N} c^V \cdot \left( e^{\text{Sl,up}}_{i,o,t} + e^{\text{Sl,dn}}_{i,o,t} + f^{\text{Sl,up}}_{i,o,t} + f^{\text{Sl,dn}}_{i,o,t} \right) \\
& + \sum_{ij \in B} c^S \cdot \left( S^{SI}_{ij,o,t} \right) \Bigg)
\end{aligned}
\tag{3.1}
$$

where,

- $\Omega_o$ represents the set of operational scenarios and $\omega_o$ the probability of each scenario;
- $T$ represents the set of time instants;
- $L$ indicates the set of loads, while, $F^l$ denotes the set of flexible loads ($F^l \subseteq L$);
- $c^{\text{Load, curt}}$ represents the cost associated with active and reactive load curtailment;
- $P^{\text{curt,up}}_{l,o,t}, Q^{\text{curt,up}}_{l,o,t}$ and $P^{\text{curt,down}}_{l,o,t}, Q^{\text{curt,down}}_{l,o,t}$ represent the active and reactive power adjustments for upward and downward flexibility provision (or demand response) of load $l$ in operational scenario $o$ and time instant $t$, respectively;
- $c^F_t$ corresponds to the cost associated with load flexibility;

- $P_{l,o,t}^{\text{flex,down}}$ and $Q_{l,o,t}^{\text{flex,down}}$ represent the downward flexibility of active and reactive power of load $l$ in operational scenario $o$ and time instant $t$, respectively;
- $G^R \subseteq G$ is the set of RES generators, while, $G$ is the set of all generators;
- $c_{g,t}$ represents the €/MWh cost of generator $g$ in the corresponding $t$ period;
- $P_{g,o,t}$ is the active power output of generator $g \in G$ in operational scenario $o \in \Omega_o$ and time instant $t \in T$;
- $c^{\text{RES, curt}}$ represents the cost of RES generation curtailment;
- $P_{g,o,t}^{\text{curt}}$ denotes curtailed active power from generator $g \in G^R$;
- $E$ represents the set of all ESSs;
- $c^{\text{ESS}}$ corresponds to the penalty associated with the slack affiliated with the charging-discharging complementarity violation of an ESS;
- $P_{e,o,t}^{ch}$ and $P_{e,o,t}^{dch}$ respectively represent the active power charged and discharged of ESS $e$ in scenario $o$ at the time instant $t$;
- $N$ refers to the set of nodes;
- $c^V$ refers to the penalty associated with the use of voltage slack variables;
- $e_{i,o,t}^{\text{Sl,up}}, f_{i,o,t}^{\text{Sl,up}}$ and $e_{i,o,t}^{\text{Sl,dn}}, f_{i,o,t}^{\text{Sl,dn}}$ represent the upward and downward slack variables associated with the real and imaginary voltage components at bus $i$;
- $B$ denotes the set of branches;
- $c^S$ denotes the penalty coefficient associated with the violation of power flow slack variables;
- $S_{ij,o,t}^{SI}$ represents the slack variable associated with the apparent power flow limits in branch $ij$.

The coefficients $c^{\text{ESS}}$, $c^V$ and $c^S$ are intentionally selected to be sufficiently large so that, whenever a feasible operating point exists, the optimization naturally drives the corresponding slack variables to zero.

When slack variables assume strictly positive values, they provide a quantitative measure of constraint violation. Rather than representing modeling artifacts, these values offer operational insight by identifying network locations where available control resources are insufficient to satisfy security requirements. To leverage this insight, these slack values are preserved in the optimization outputs rather than being discarded post-convergence. As demonstrated later in this work (see the results breakdown in Table 3.2), this transparency allows the system operator to interpret slack activation as an implicit request for additional flexibility, corrective actions, or network reinforcement.

### 3.2.2 Controllable Resources

#### 3.2.2.1 Generators

The physical capabilities of the available generators are strictly maintained. Constraints (3.2) and (3.3) enforce the upper and lower bounds on active and reactive power generation, respectively.

$$P_g^{\min} \leq P_{g,o,t} \leq P_g^{\max}, \quad \forall g \in G,\ \forall o \in \Omega_o,\ \forall t \in T \tag{3.2}$$

$$Q_g^{\min} \leq Q_{g,0,t} \leq Q_g^{\max}, \quad \forall g \in G,\ \forall o \in \Omega_o,\ \forall t \in T \tag{3.3}$$

in which,

- $P_g^{\min}$ and $P_g^{\max}$ define the minimum and maximum active power generation of generator $g$, while $Q_g^{\min}$ and $Q_g^{\max}$ represent its minimum and maximum reactive power generation, respectively;
- $P_{g,o,t}$ and $Q_{g,o,t}$ represent the active and reactive power generation output of generator $g$ in scenario $o$ at period $t$, respectively.

#### 3.2.2.2 Energy Storage Systems

In this formulation, the ESSs were assumed to exchange only active power (charging and discharging) while neglecting reactive power to simplify the model and maintain the unity power factor assumption.

Three alternative formulations are considered for modeling the operation of ESSs, which differ in how the charging and discharging exclusivity is enforced, namely:

- **EXACT** model: Enforces absolute operational exclusivity through a strict non-linear equality constraint.
- **RELAXED** model: Softens the exclusivity requirement using an inequality constraint with a small tolerance threshold and an objective function penalty.
- **SIMPLIFIED** model: Removes explicit exclusivity constraints entirely, relying solely on an objective function penalty to discourage simultaneous charging and discharging.

The **EXACT** model enforces constraint (3.4) to prevent simultaneous charging and discharging. While this formulation is the most physically accurate, it introduces significant difficulties for the NLP solver, increasing the computational burden and often impairing convergence.

$$P_{e,o,t}^{ch} \cdot P_{e,o,t}^{dch} = 0, \quad \forall e \in E,\ \forall o \in \Omega_o,\ \forall t \in T \tag{3.4}$$

To mitigate these issues, the **RELAXED** model replaces this hard constraint with a softened formulation, as given in constraint (3.5). In addition, a penalty term ($c^{\text{ESS}}$) is incorporated into the objective function, which is activated when the product $P^{ch}_{e,o,t} \cdot P^{dch}_{e,o,t}$ deviates from zero, thereby discouraging simultaneous charging and discharging while maintaining a larger feasible region.

$$P^{ch}_{e,o,t} \cdot P^{dch}_{e,o,t} \leq \varepsilon^{\text{ESS}} \quad \forall e \in E,\, \forall o \in \Omega_o,\, \forall t \in T \tag{3.5}$$

Finally, the **SIMPLIFIED** model removes both constraint (3.4) and (3.5). Instead, infeasible operating behavior is indirectly discouraged through a sufficiently large penalty parameter $c^{\text{ESS}}$ in the objective function, which penalizes simultaneous charging and discharging without explicitly enforcing exclusivity.

The temporal evolution of the state-of-charge for each ESS is modeled as follows:

$$\text{SoC}_{e,o,t} - \text{SoC}_{e,o,t-1} = \left( P^{ch}_{e,o,t}\, \eta^{ch}_{e} - \frac{P^{dch}_{e,o,t}}{\eta^{dch}_{e}} \right), \quad \forall e \in E,\, \forall o \in \Omega_o,\, \forall t \in T \tag{3.6}$$

in which,

- $\eta^{ch}_{e}$ and $\eta^{dch}_{e}$ refer to the efficiency of charging and discharging the ESS $e$, respectively;
- $\text{SoC}_{e,o,t}$ represents the State-of-Charge of ESS $e$.

For $t = 0$, the state-of-charge of the previous instant is defined as $\text{SoC}_{e,o,t-1} = \text{SoC}^{\text{init}}$, where the initial state-of-charge ($\text{SoC}^{\text{init}}$) is assumed to be 50% of the total energy capacity of ESS $e$, expressed in MWh. This value is selected to provide a neutral operational starting point, ensuring that the ESS has symmetric flexibility for both charging and discharging actions at the beginning of the scheduling horizon, thus preventing artificial constraints in the initial time steps. The operational limits of the ESS state-of-charge are enforced through constraint (3.7).

$$\text{SoC}^{\min}_{e} \;\leq\; \text{SoC}_{e,o,t} \;\leq\; \text{SoC}^{\max}_{e}, \quad \forall e \in E,\, \forall o \in \Omega_o,\, \forall t \in T \tag{3.7}$$

#### 3.2.2.3 Capacitor Banks and Reactors

Voltage regulation and reactive power support are essential components of secure transmission system operation. Since the proposed ESS formulation does not explicitly model reactive power exchange capabilities, local voltage control is instead provided through shunt compensation devices, namely capacitor banks and shunt reactors. These devices represent standard TSO-controlled assets used to manage voltage profiles and reactive power flows under both normal and contingency operating conditions.

Capacitor banks inject reactive power into the network, supporting voltage magnitudes under high-load conditions, whereas reactors absorb reactive power to mitigate overvoltage conditions typically associated with light-load operation. Their behavior is modeled through the following relationships:

$$Q_{c,o,t} = \left( Q^{\text{nom}}_{c} \cdot \frac{s_{c,o,t}}{N^{\text{steps}}_{c}} \right) \cdot V^{2}_{i,o,t}, \quad \forall c \in Cb,\, \forall i \in N,\, \forall o \in \Omega_o,\, \forall t \in T \tag{3.8}$$

$$Q_{r,o,t} = \left( Q_r^{\text{nom}} \cdot \frac{s_{r,o,t}}{N_r^{\text{steps}}} \right) \cdot V_{i,o,t}^2, \quad \forall r \in R,\, \forall i \in N,\, \forall o \in \Omega_o,\, \forall t \in T \tag{3.9}$$

where:

- $Cb$ and $R$ denote the sets of capacitor banks and reactors, respectively;
- $Q^{\text{nom}}$ represents the nominal reactive power rating (MVAr) of the respective device, $c$ or $r$;
- $s$ corresponds to the discrete switching position (step) of each device;
- $N^{\text{steps}}$ indicates the total number of available switching steps.

The quadratic dependence on the voltage magnitude reflects the physical behavior of shunt elements, whose reactive power injection or absorption varies proportionally with $V^2$. The discrete step variable models practical switching operation, allowing the optimization to emulate real-world tap or stage activation performed by system operators.

By explicitly incorporating capacitor banks and reactors, the formulation preserves adequate voltage controllability despite the absence of reactive power support from ESSs. This separation of functionalities reflects common operational practice, in which energy-oriented resources (e.g., storage and flexible loads) primarily manage active power balancing, while dedicated shunt devices ensure voltage security.

#### 3.2.2.4 Flexible Loads

Demand-side flexibility constitutes an increasingly relevant resource for transmission system operation, enabling corrective and preventive actions without relying exclusively on generation redispatch. In the proposed formulation, flexible loads are modeled as controllable active and reactive power adjustments that can either increase or decrease consumption within predefined operational limits. This representation allows the TSO to exploit aggregated demand flexibility as a security-enhancing resource within the SCOPF framework.

To ensure that the collective load flexibility across the entire fleet and all operational scenarios represents an aggregated temporal shift of energy rather than net portfolio-wide load creation or curtailment, a global energy neutrality condition is imposed through:

$$p_{up} - p_{down} = 0 \tag{3.10}$$

where,

$$p_{up} = \sum_{l \in F^l} \sum_{o \in \Omega_o} \sum_{t \in T} P_{l,o,t}^{\text{flex,up}}$$

and

$$p_{down} = \sum_{l \in F^l} \sum_{o \in \Omega_o} \sum_{t \in T} P_{l,o,t}^{\text{flex,down}}$$

This constraint is applied exclusively to the active flexibility component. From the perspective of a TSO, active power flexibility corresponds to energy shifting over time, which directly affects system energy balance, generation scheduling, and congestion management. Therefore, enforcing strict equality between the total upward and downward active flexibility guarantees that the flexible load portfolio, as a collective whole, functions as an energy-neutral resource across the evaluated scenario space over the optimization horizon.

In contrast, reactive power flexibility primarily provides local voltage support and does not represent energy consumption or production over time. Since reactive power does not accumulate as energy and is mainly used for instantaneous voltage regulation, enforcing an energy balance condition on reactive flexibility would not reflect its physical or operational role within transmission system operation.

### 3.2.3 Voltage and Power Flow Constraints

The voltage magnitude limits of each bus are usually enforced through:

$$V_i^{\min} \leq V_{i,o,t} \leq V_i^{\max}, \quad \forall i \in N,\ \forall o \in \Omega_o,\ \forall t \in T$$

in which, $V_{i,o,t}$ represents the voltage magnitude of bus $i$, scenario $o$ for the time instant $t$. $V_i^{\min}$ and $V_i^{\max}$ represent the minimum and maximum voltage magnitude of that same bus $i$.

However, in the proposed formulation, these limits are maintained using the rectangular representation of voltage phasors, in which the voltage is expressed in terms of the real and imaginary components:

$$(V_i^{\min})^2 \leq e_{i,o,t}^2 + f_{i,o,t}^2 \leq (V_i^{\max})^2, \quad \forall i \in N,\ \forall o \in \Omega_o,\ \forall t \in T \tag{3.11}$$

where,

- $e_{i,o,t}$ and $f_{i,o,t}$ refer to the real and imaginary components of voltage at bus $i$ in scenario $o$ for period $t$, respectively.

Through this voltage representation, both the voltage magnitudes and power levels ((3.14) and (3.15)) are expressed as quadratic polynomials. Additionally, this approach facilitates the direct integration of slack variables into the voltage magnitude constraints, as detailed in Constraint (3.16).

Power flow constraints on transmission lines are imposed by limiting the apparent power:

$$S_{ij,o,t}^2 \leq \left(S_{ij}^{\max}\right)^2, \quad \forall ij \in B,\ \forall o \in \Omega_o,\ \forall t \in T \tag{3.12}$$

in which,

- $S_{ij}^{\max}$ stands for maximum apparent power flow of the branch $ij$;

- $S_{ij,o,t}$ represents the apparent power flow of the branch $ij$ in secnario $o$ for the $t$ period.

And the apparent power flow is computed as the sum of the squares of the active and reactive power components:

$$S_{ij,o,t}^2 = P_{ij,o,t}^2 + Q_{ij,o,t}^2, \quad \forall ij \in B, \, \forall o \in \Omega_o, \, \forall t \in T \tag{3.13}$$

where $P_{ij,o,t}$ and $Q_{ij,o,t}$ respectively quantify the active and reactive power flow of the transmission line $ij \in B$ in scenario $o$ for the $t$ period. These are calculated using the following expressions based on the rectangular voltage coordinates:

$$\begin{aligned} P_{ij,o,t} = & \, g_{ij} \left( e_{i,o,t}^2 + f_{i,o,t}^2 \right) \\ & - g_{ij} \left( e_{i,o,t} \cdot e_{j,o,t} + f_{i,o,t} \cdot f_{j,o,t} \right) \\ & - b_{ij} \left( f_{i,o,t} \cdot e_{j,o,t} - e_{i,o,t} \cdot f_{j,o,t} \right), \\ & \forall ij \in B, \, \forall o \in \Omega_o, \, \forall t \in T \end{aligned} \tag{3.14}$$

$$\begin{aligned} Q_{ij,o,t} = & - \left( b_{ij} + b_{ij}^{Sh} \right) \left( e_{i,o,t}^2 + f_{i,o,t}^2 \right) \\ & + b_{ij} \left( e_{i,o,t} \cdot e_{j,o,t} + f_{i,o,t} \cdot f_{j,o,t} \right) \\ & - g_{ij} \left( f_{i,o,t} \cdot e_{j,o,t} - e_{i,o,t} \cdot f_{j,o,t} \right), \\ & \forall ij \in B, \, \forall o \in \Omega_o, \, \forall t \in T \end{aligned} \tag{3.15}$$

in which,

- $g_{ij}$ and $b_{ij}$ describe the conductance and susceptance of the branch $ij$, respectively;
- And $b_{ij}^{Sh}$ represents the shunt susceptance of the branch $ij$.

Under severe uncertainty or contingency scenarios, the standard operational boundaries governing voltage magnitudes and transmission line thermal capacities can become tightly binding, often leading to mathematical infeasibility in rigid deterministic formulations. To ensure computational robustness during these stressed grid states, these constraints are reformulated through the introduction of slack variables, which allow the optimization engine to quantify localized voltage deviations and branch overloads, respectively

$$\begin{aligned} (V_i^{\min})^2 - \left( e_{i,o,t}^{\mathrm{Sl,dn}^2} + f_{i,o,t}^{\mathrm{Sl,dn}^2} \right) \leq e_{i,o,t}^2 + f_{i,o,t}^2 \leq (V_i^{\max})^2 + \left( e_{i,o,t}^{\mathrm{Sl,up}^2} + f_{i,o,t}^{\mathrm{Sl,up}^2} \right), \\ \forall i \in N, \, \forall o \in \Omega_o, \, \forall t \in T \end{aligned} \tag{3.16}$$

$$S_{ij,o,t}^2 \leq \left( S_{ij}^{\max} \right)^2 + S_{ij,o,t}^{SI}, \quad \forall ij \in B, \, \forall o \in \Omega_o, \, \forall t \in T \tag{3.17}$$

in which,

- $e_{i,o,t}^{\mathrm{Sl,dn}}$, $e_{i,o,t}^{\mathrm{Sl,up}}$, $f_{i,o,t}^{\mathrm{Sl,dn}}$, and $f_{i,o,t}^{\mathrm{Sl,up}}$ represent the downward and upward voltage violation slack variables applied to the real and imaginary voltage components, respectively;

- $S^{\mathrm{SI}}_{ij,o,t}$ represents the slack variable used to accommodate violations of the transmission line apparent power flow limit.

### 3.2.4 Power Balance Constraints

The nodal active and reactive power balance equations ensure that generation matches demand and network injections. These are given by:

$$\begin{aligned} P^g_{i,o,t} - P^c_{i,o,t} = & \sum_{j \in N_i} g_{ij} \left(e^2_{i,o,t} + f^2_{i,o,t}\right) \\ & - \sum_{j \in N_i} g_{ij}(e_{i,o,t} \cdot e_{j,o,t} + f_{i,o,t} \cdot f_{j,o,t}) \\ & - \sum_{j \in N_i} b_{ij}(f_{i,o,t} \cdot e_{j,o,t} - f_{j,o,t} \cdot e_{i,o,t}), \\ & \forall i \in N,\ \forall o \in \Omega_o,\ \forall t \in T \end{aligned} \tag{3.18}$$

$$\begin{aligned} Q^g_{i,o,t} - Q^c_{i,o,t} = & - \sum_{j \in N_i} (b_{ij} + b^{Sh}_{ij}) \left(e^2_{i,o,t} + f^2_{i,o,t}\right) \\ & + \sum_{j \in N_i} b_{ij}(e_{i,o,t} \cdot e_{j,o,t} + f_{i,o,t} \cdot f_{j,o,t}) \\ & - \sum_{j \in N_i} g_{ij}(f_{i,o,t} \cdot e_{j,o,t} - f_{j,o,t} \cdot e_{i,o,t}), \\ & \forall i \in N,\ \forall o \in \Omega_o,\ \forall t \in T \end{aligned} \tag{3.19}$$

where $P^c_{i,o,t}$ and $Q^c_{i,o,t}$ respectively stand for the active and reactive power consumption at bus $i$ for scenario $o$ during the $t$ period, while $P^g_{i,o,t}$ and $Q^g_{i,o,t}$, respectively represent the active and reactive power generated at the same bus and period, for scenario $o$.

From a modeling perspective, the reformulation of constraints (3.16) and (3.17) using slack variables enables the explicit representation and quantification of voltage and line-flow limit violations. In both AC-OPF and SCOPF problems, the high dimensionality and the presence of conflicting contingency constraints can lead to ill-conditioned Karush–Kuhn–Tucker (KKT) systems. The slack variables, penalized in the objective function, transform these boundaries into soft limits, providing the mathematical solver with a better conditioned system. This approach prevents numerical stagnation and ensures that the solver can provide a meaningful "near-feasible" solution even under highly stressed network conditions that would otherwise result in local infeasibility. In addition, the introduced slack variables constitute a fundamental component for the implementation of both the CC-OPF and CC-SCOPF, as presented in Section 3.3.

### 3.2.5 Power Flows Reformulation

Considering the inclusion of voltage-magnitude slack variables, the active and reactive power flows, $P_{ij}$ and $Q_{ij}$, are now computed as follows:

$$\begin{aligned}P_{ij,o,t} = & \, g_{ij}\left(\tilde{e}_{i,o,t}^2 + \tilde{f}_{i,o,t}^2\right) \\ & - g_{ij}\left(\tilde{e}_{i,o,t} \cdot \tilde{e}_{j,o,t} + \tilde{f}_{i,o,t} \cdot \tilde{f}_{j,o,t}\right) \\ & - b_{ij}\left(\tilde{f}_{i,o,t} \cdot \tilde{e}_{j,o,t} - \tilde{e}_{i,o,t} \cdot \tilde{f}_{j,o,t}\right), \\ & \forall ij \in B,\ \forall o \in \Omega_o,\ \forall t \in T\end{aligned} \tag{3.20}$$

$$\begin{aligned}Q_{ij,o,t} = & - (b_{ij} + b_{ij}^{Sh})\left(\tilde{e}_{i,o,t}^2 + \tilde{f}_{i,o,t}^2\right) \\ & + b_{ij}\left(\tilde{e}_{i,o,t} \cdot \tilde{e}_{j,o,t} + \tilde{f}_{i,o,t} \cdot \tilde{f}_{j,o,t}\right) \\ & - g_{ij}\left(\tilde{f}_{i,o,t} \cdot \tilde{e}_{j,o,t} - \tilde{e}_{i,o,t} \cdot \tilde{f}_{j,o,t}\right), \\ & \forall ij \in B,\ \forall o \in \Omega_o,\ \forall t \in T\end{aligned} \tag{3.21}$$

where, $\tilde{e}_{i,o}$ and $\tilde{f}_{i,o}$ represent the real and imaginary components, respectively, of the voltage at bus $i$ under operational scenario $o$, adjusted by their corresponding slack variables:

$$\tilde{e}_{i,o,t} = e_{i,o,t} + e_{i,o,t}^{Sl,up} - e_{i,o,t}^{Sl,dn}, \quad \forall i \in N,\ \forall o \in \Omega_o,\ \forall t \in T \tag{3.22}$$

$$\tilde{f}_{i,o,t} = f_{i,o,t} + f_{i,o,t}^{Sl,up} - f_{i,o,t}^{Sl,dn}, \quad \forall i \in N,\ \forall o \in \Omega_o,\ \forall t \in T \tag{3.23}$$

The nodal active and reactive power balance equations are thus reformulated as:

$$\begin{aligned}P_{i,o,t}^{g} - P_{i,o,t}^{c} + \left(P_{e,o,t}^{ch} - P_{e,o,t}^{dch}\right) - \left(P_{l,o,t}^{\text{curt,up}} - P_{l,o,t}^{\text{curt,down}}\right) = & \\ \sum_{j \in N_i} g_{ij}\left(\tilde{e}_{i,o,t}^2 + \tilde{f}_{i,o,t}^2\right) & \\ - \sum_{j \in N_i} g_{ij}\left(\tilde{e}_{i,o,t} \cdot \tilde{e}_{j,o,t} + \tilde{f}_{i,o,t} \cdot \tilde{f}_{j,o,t}\right) & \\ - \sum_{j \in N_i} b_{ij}\left(\tilde{f}_{i,o,t} \cdot \tilde{e}_{j,o,t} - \tilde{f}_{j,o,t} \cdot \tilde{e}_{i,o,t}\right), & \\ \forall i \in N,\ \forall o \in \Omega_o,\ \forall t \in T &\end{aligned} \tag{3.24}$$

$$\begin{aligned}Q_{i,o,t}^{g} + Q_{c,o,t}^{\text{Cb}} - Q_{i,o,t}^{c} - \left(Q_{l,o,t}^{\text{curt,up}} - Q_{l,o,t}^{\text{curt,down}}\right) - Q_{r,o,t}^{\text{Reactor}} = & \\ - \sum_{j \in N_i} (b_{ij} + b_{ij}^{Sh})\left(\tilde{e}_{i,o,t}^2 + \tilde{f}_{i,o,t}^2\right) & \\ + \sum_{j \in N_i} b_{ij}\left(\tilde{e}_{i,o,t} \cdot \tilde{e}_{j,o,t} + \tilde{f}_{i,o,t} \cdot \tilde{f}_{j,o,t}\right) & \\ - \sum_{j \in N_i} g_{ij}\left(\tilde{f}_{i,o,t} \cdot \tilde{e}_{j,o,t} - \tilde{f}_{j,o,t} \cdot \tilde{e}_{i,o,t}\right), & \\ \forall i \in N,\ \forall o \in \Omega_o,\ \forall t \in T &\end{aligned} \tag{3.25}$$

## 3.3 CC-OPF

Power system operation under uncertainty requires ensuring that security limits are satisfied not deterministically, but with a prescribed level of confidence. CC-OPF formulations address this requirement by allowing a controlled probability of constraint violations while maintaining operational feasibility. Rather than enforcing strict feasibility for every uncertainty realization, the operator specifies acceptable violation probabilities, leading to a more realistic and economically efficient operating point.

### 3.3.1 The Sigmoid Approximation

Conventionally, chance-constrained optimization problems are modeled using exact mathematical indicator functions or binary variables to flag whether a specific uncertainty scenario violates operational limits. While this approach provides a rigid, exact representation, the integration of discrete switches transforms the problem into a mixed-integer formulation (such as an MIQP). These combinatorial problems scale poorly and quickly become computationally intractable when applied to large-scale power networks evaluated across thousands of scenario samples.

To preserve computational tractability within a purely continuous optimization domain, literature frequently relies on smooth, continuous approximations to substitute these discrete binary indicators. Following this paradigm, this thesis proposes an NLP-based SCOPF formulation relying on slack-variable reformulations, and rectangular voltage representation. These slack variables quantify the magnitude of constraint violations and therefore provide a natural foundation for incorporating chance constraints. Inspired by the smooth step-function indicator $\theta(\tau, s)$ proposed in [8]:

$$\theta(\tau, s) = \frac{1 + m_1 \tau}{1 + m_2 \tau \exp\left(-\frac{s}{\tau}\right)} \tag{3.26}$$

As the parameter $\tau$ is reduced toward zero, the inner and outer solutions converge to the optimal AC-SCOPF solution. A key advantage of the approach is that it does not rely on restrictive distributional assumptions. Instead, uncertainty is represented through Monte Carlo sampling, allowing the framework to accommodate non-Gaussian distributions such as the Weibull distribution used to model wind power variability. Even so, the computational burden is significant, a 5-bus system required an average of 1247 seconds per run.

### 3.3.2 Rational Approximation Proposed

This work introduces a modified violation indicator tailored to the proposed formulation. The original step function acts as a binary violation detector, however, its discontinuous nature is unsuitable for gradient-based[1] nonlinear solvers, such as interior point methods. For these gradient-based algorithms, smooth, continuously differentiable approximations are always preferred to ensure reliable derivative evaluations and stable numerical convergence. For this reason, a rational violation flag, denoted by $Z$, is introduced. Generically, this function can be written as:

$$Z = \frac{\alpha \cdot s}{1 + \alpha \cdot s}$$

[1]A *gradient* tells the solver: *If I change this variable slightly, how will the objective or constraint change?*

where $s$ represents the slack variable associated with the constraint violation, and $\alpha$ is a parameter that controls how *sharp* the transition is. This function smoothly maps the magnitude of a slack variable into a bounded indicator such that:

- $Z \approx 0$ when no violation is present (slack $\rightarrow 0$);
- $Z \approx 1$ when a significant violation occurs.

The violation flag is defined for both voltage magnitude limits and branch flow limits, described in the following subsections.

#### 3.3.2.1 Voltage Violation Indicator

Voltage magnitude limits are among the primary security requirements in power system operation, as violations may lead to voltage instability, equipment stress, or cascading failures. Within the proposed framework, voltage constraint relaxations are captured through slack variables introduced in the network equations (subsection 3.2.3). To incorporate these deviations into the probabilistic assessment required by the chance-constrained formulation, a voltage violation indicator is defined:

$$Z^V_{i,o,t} = \frac{\alpha^V \cdot S^V_{i,o,t}}{1 + \alpha^V \cdot S^V_{i,o,t}}, \quad \forall i \in N, \ \forall o \in \Omega_o, \ \forall t \in T \tag{3.27}$$

where the aggregated voltage slack ($S^V_{i,o,t}$) is given by:

$$S^V_{i,o,t} = e^{Sl,up}_{i,o,t} + e^{Sl,dn}_{i,o,t} + f^{Sl,up}_{i,o,t} + f^{Sl,dn}_{i,o,t}. \tag{3.28}$$

This indicator translates the magnitude of aggregated voltage slack variables into a smooth probabilistic measure of constraint violation, ensuring that any deviation from admissible voltage limits contributes to the violation indicator.

#### 3.3.2.2 Branch Flow Violation Indicator

Thermal limits of transmission branches represent another critical operational constraint, ensuring safe power transfer and preventing line overloads. Similar to voltage constraints, branch flow limits may be temporarily relaxed through slack variables when strict feasibility cannot be achieved.

To quantify these violations within the chance-constrained framework, a branch flow violation indicator is introduced:

$$Z^B_{ij,o,t} = \frac{\alpha^B \cdot S^{SI}_{ij,o,t}}{1 + \alpha^B \cdot S^{SI}_{ij,o,t}}, \quad \forall ij \in B, \ \forall o \in \Omega_o, \ \forall t \in T \tag{3.29}$$

Similarly to the voltage magnitude violation indicator function, the rational structure of (3.29) provides a continuously differentiable approximation of a binary indicator while preserving numerical stability and compatibility with NLP solvers.

#### 3.3.2.3 Parameter Tuning

The parameter $\alpha$ controls the sharpness of the transition between non-violation and violation regions. To determine appropriate parameter values, several tests were conducted, as illustrated in Figure 3.1. The y-axis represents the violation indicator $Z$, while the x-axis represents the slack variable magnitude. The dotted curves show the exponential approximation proposed in [8], whereas the continuous curves correspond to the rational approximation adopted in this work.

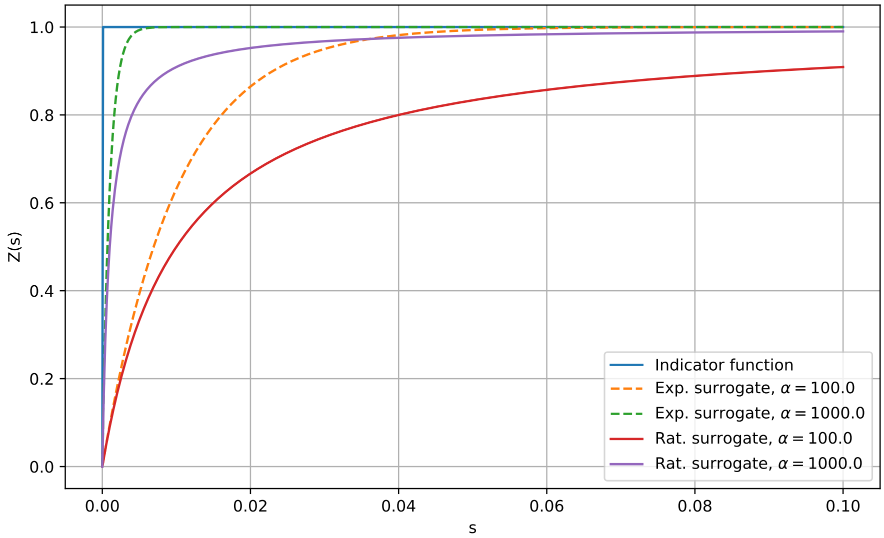


Figure 3.1: Effect of parameter $\alpha$ on sigmoid and rational approximations of the violation indicator function.

As it is possible to observe from Figure 3.1, large $\alpha$ values produce an almost discontinuous behavior, causing violations to be detected even for negligible slack values and degrading numerical conditioning. Conversely, very small values (e.g., 100) overly smooth the transition, reducing the sensitivity of the violation indicator.

Based on these experiments, the selected parameters were:

$$\alpha^V = 10\,000 \qquad \text{and} \qquad \alpha^B = 1\,000$$

which provided a suitable compromise between sensitivity to violations and numerical robustness.

### 3.3.3 Chance-Constraint Enforcement

Building upon the continuous violation indicators for voltage magnitudes and branch flows, the formulation enforces $N-1$ criteria within a probabilistic framework. Rather than demanding strict constraint satisfaction under every extreme scenario, which introduces severe over-conservatism, the chance-constrained approach restricts the probability of violations across the scenario space. This ensures that the system operates within a mathematically guaranteed confidence level while safely absorbing uncertainty.

The probabilistic security requirement is enforced by restricting the average value of the violation indicators across all operational realizations:

$$\frac{1}{\Omega_o}\sum_{o=1}^{\Omega_o} Z^V_{i,o,t} \leq \varepsilon^V, \quad \forall i \in N,\ \forall t \in T \tag{3.30}$$

$$\frac{1}{\Omega_o}\sum_{o=1}^{\Omega_o} Z^B_{ij,o,t} \leq \varepsilon^B, \quad \forall ij \in B,\ \forall t \in T \tag{3.31}$$

The parameters $\varepsilon^V$ and $\varepsilon^B$ represent the acceptable violation probabilities for voltage magnitudes and branch flow limits, respectively, while $\Omega_o$ represents the set of operational scenarios. In this manner, the proposed formulation transforms hard security limits into probabilistic guarantees.

## 3.4 SCOPF

The probabilistic multi-period SCOPF framework is obtained by extending the probabilistic multi-period OPF model to explicitly incorporate contingency analysis. All variables, equations, and constraints are therefore indexed by the contingency identifier $k$, representing pre-contingency ($k = 0$) and distinct post-contingency ($k \in K$) operating states. Furthermore, selected constraints are reformulated and additional security constraints are introduced to ensure that both pre- and post-contingency operational requirements are properly enforced.

### 3.4.1 Objective Function

As aforementioned, the main objective of the OPF algorithm proposed in this work is the minimization of the operating costs, as described in Subsection 3.2.1. To include security criteria directly into the NLP optimization problem, the original objective (3.1) is augmented with terms corresponding to the penalization of bus voltage magnitude and branch (lines and transformers) overload violations. The SCOPF objective function is therefore given by:

$$
\begin{aligned}
\min \quad & \sum_{o\in\Omega_o}\sum_{t\in T}\omega_o\cdot\Big( \\
& \sum_{g\in G}\sum_{k\in K} c_{g,t}\cdot\left(P_{g,o,k,t}\right) \\
& +\sum_{l\in L}\sum_{k\in K} c^{\text{Load, curt}}\cdot\left(P^{\text{curt,down}}_{l,k,o,t}+P^{\text{curt,up}}_{l,k,o,t}+Q^{\text{curt,down}}_{l,k,o,t}+Q^{\text{curt,up}}_{l,k,o,t}\right) \\
& +\sum_{g\in G^R}\sum_{k\in K} c^{\text{RES, curt}}\cdot P^{\text{curt}}_{g,k,o,t} \\
& +\sum_{l\in F^l}\sum_{k\in K} c^F_t\cdot\left(P^{\text{flex,down}}_{l,k,o,t}+Q^{\text{flex,down}}_{l,k,o,t}\right) \\
& +\sum_{e\in E}\sum_{k\in K} c^{\text{ESS}}\cdot\left(P^{ch}_{e,k,o,t}\cdot P^{dch}_{e,k,o,t}\right) \\
& +\sum_{i\in N} c^{V_0}\cdot\left(e^{\text{Sl,up}}_{i,0,o,t}+e^{\text{Sl,dn}}_{i,0,o,t}+f^{\text{Sl,up}}_{i,0,o,t}+f^{\text{Sl,dn}}_{i,0,o,t}\right) \\
& +\sum_{i\in N}\sum_{k\in K} c^{V_k}\cdot\left(e^{\text{Sl,up}}_{i,k,o,t}+e^{\text{Sl,dn}}_{i,k,o,t}+f^{\text{Sl,up}}_{i,k,o,t}+f^{\text{Sl,dn}}_{i,k,o,t}\right) \\
& +\sum_{ij\in B} c^{S_0}\cdot\left(S^{SI}_{ij,0,o,t}\right) \\
& +\sum_{ij\in B}\sum_{k\in K} c^{S_k}\cdot\left(S^{SI}_{ij,k,o,t}\right)\Big)
\end{aligned}
\tag{3.32}
$$

where:

- $K$ indicates the set of contingencies;
- $c^{V_0}$ and $c^{V_k}$ refer to the penalty associated with the use of voltage slack variables for the base and contingency cases, respectively;
- $c^{S_0}$ and $c^{S_k}$ denote penalty coefficients associated with apparent power flow slack variables for the base and contingency cases, respectively.

Through this comprehensive weighting scheme, the framework directly balances asset management costs against security limit violations. This unified objective function is subject to the network physics and technical operational constraints detailed in the following subsections.

### 3.4.2 Post-contingency Operating Constraints

To guarantee feasible post-contingency operation and prevent severe structural shocks to physical grid assets, the optimization model strictly constrains the allowable deviations between the pre-contingency base case ($k = 0$) and any active contingency state ($k \in K$).

#### 3.4.2.1 Generation Constraints

Following a contingency event, the variations in active and reactive power generation relative to the base case are physically bounded by the dynamic response capabilities of the generating units. These power adjustments are governed by constraints (3.33) and (3.34):

$$\left|P_{g,0,o,t} - P_{g,k,o,t}\right| \le \Delta P_g^{\max}, \quad \forall g \in G,\ \forall k \in K,\ \forall o \in \Omega_o,\ \forall t \in T \tag{3.33}$$

$$\left|Q_{g,0,o,t} - Q_{g,k,o,t}\right| \le \Delta Q_g^{\max}, \quad \forall g \in G,\ \forall k \in K,\ \forall o \in \Omega_o,\ \forall t \in T \tag{3.34}$$

Because absolute value functions exhibit non-differentiable boundaries at zero, their direct inclusion creates severe gradient discontinuities that impede interior-point solvers. To ensure compatibility with gradient-based NLP optimization, constraints (3.33) and (3.34) are immediately reformulated into equivalent pairs of smooth linear inequalities:

$$-\Delta P_g^{\max} \le P_{g,k,o,t} - P_{g,0,o,t} \le \Delta P_g^{\max} \tag{3.35}$$

$$-\Delta Q_g^{\max} \le Q_{g,k,o,t} - Q_{g,0,o,t} \le \Delta Q_g^{\max} \tag{3.36}$$

Constraints (3.35) and (3.36) physically enforce the operational ramp-rate limit of each generator during a disturbance. Consequently, they are tightly enforced only at the specific time instant when a contingency $k$ takes place ($t = t_{\text{cont},k}$). Structurally, if contingency $k$ represents a transmission line or transformer outage, the response limits are applied across all active system generators ($g \in G$). Conversely, if contingency $k$ denotes a generator outage, the constraint is applied globally to the surviving fleet, excluding the affected unit.

#### 3.4.2.2 Transmission Network Branches

To prevent systemic line damage and thermal stress on infrastructure during sudden topology shifts, the power flow bounds are adapted to reflect the expanded emergency limits allowed during contingencies. During standard time periods ($t \in T \setminus \{t = t_{\text{cont},k}\}$), branch flows are regulated by the baseline constraint (3.37). At the exact moment of a disturbance ($t = t_{\text{cont},k}$), the formulation dynamically shifts to constraint (3.38) to enforce these contingency-specific bounds:

$$S_{ij,k,o,t}^2 \le \left(S_{ij}^{\max}\right)^2 + S_{ij,k,o,t}^{SI}, \quad \forall ij \in B,\ \forall k \in K,\ \forall o \in \Omega_o,\ \forall t \in T \setminus \{t = t_{\text{cont},k}\} \tag{3.37}$$

$$S_{ij,k,o,t}^2 + S_{ij,k,o,t}^{SI} \le \Delta S_{ij}^2, \quad \forall ij \in B,\ \forall k \in K,\ \forall o \in \Omega_o,\ t = t_{\text{cont},k} \tag{3.38}$$

#### 3.4.2.3 Bus Voltage Magnitude Profiles

To protect the network from rapid voltage instability and cascading failures during contingencies, transient voltage step changes at every bus are strictly limited. This constraint is enforced at the exact moment of the contingency ($t = t_{\text{cont},k}$) through an explicit emergency tolerance envelope. By formulating it this way, we avoid non-differentiable absolute terms while allowing for controlled relaxation during high-stress operations:

$$\begin{gathered}\left(V_i^{\min} - CVL\right)^2 \le \left(e_{i,k,o,t}^2 + f_{i,k,o,t}^2\right) \le \left(V_i^{\max} + CVL\right)^2, \\ \forall i \in N,\ \forall k \in K,\ \forall o \in \Omega_o,\ t = t_{\text{cont},k}\end{gathered} \tag{3.39}$$

where $CVL$ represents the maximum allowable voltage variation limit associated with a contingent state.

#### 3.4.2.4 Regulatory Parameterization of Variation Limits

The maximum deviation thresholds utilized across this framework are parameterized in strict accordance with national grid codes and regulatory guidelines. Specifically, the Portuguese TSO defines the operational limits as follows:

$$\Delta P_g^{\max} = P_g^{\max}\,(\mathrm{MW}) \times \Delta t \times \Delta R_g, \qquad \forall g \in G \tag{3.40}$$

$$\Delta Q_g^{\max} = Q_g^{\max}\,(\mathrm{MVar}) \times \Delta t \times \Delta R_g, \qquad \forall g \in G \tag{3.41}$$

$$\Delta S_{ij} = S_{ij} \times (1 + \Delta R_{ij}), \qquad \forall ij \in B \tag{3.42}$$

As established by the Portuguese regulator, ERSE, the parameter $CVL$ in (3.39) is set to 0.05 p.u. (a 5% threshold) [44]. Furthermore, the quantities $\Delta P_g^{\max}$ and $\Delta Q_g^{\max}$ rely on a 15-minute time window ($\Delta t = 15$ minutes), reflecting the maximum period legally granted to a system operator to deploy corrective measures post-event. Individual unit ramp rates ($\Delta R_g$) are mapped directly from grid topology file (explained in Section 3.5). If omitted, the model applies regulatory defaults of 5% for conventional units and 10% for RESs assets. The admissible transient overload values ($\Delta R_{ij}$) used to establish $\Delta S_{ij}$ are detailed in Table 3.1.

Table 3.1: Ramp limits for lines and transformers under standard $N-1$ contingency states [44].

| **Contingency Type** | **Transient Overloads, $\Delta R_{ij}$, (%)** | | | |
|---|---|---|---|---|
| | $t < 2\,\mathrm{h}$ | | $t < 15\,\mathrm{min}$ | |
| | Lines | Transformers | Lines | Transformers |
| $N-1$ | 0 | 20 | 15 | 20 |

### 3.4.3 Energy Storage Systems Modeling

In the multi-period SCOPF formulation, the operational modeling of ESSs requires augmenting the energy balance equations to trace energy patterns continuously across all prospective contingency-indexed paths:

$$\mathrm{SoC}_{e,k,o,t} - \mathrm{SoC}_{e,k,o,t-1} = \left( P^{ch}_{e,k,o,t}\,\eta^{ch}_e - \frac{P^{dch}_{e,k,o,t}}{\eta^{dch}_e} \right) \times \frac{\Delta t}{60}, \qquad \forall e \in E,\ \forall k \in K,\ \forall o \in \Omega_o,\ \forall t \in T \tag{3.43}$$

For the initial boundary period ($t = 0$), the preceding historical charge is fixed to match $\mathrm{SoC}_{e,k,o,t-1} = \mathrm{SoC}^{\mathrm{init}}$, where $\mathrm{SoC}^{\mathrm{init}}$ represents a nominal baseline equal to 50% of the unit's total capacity.

Because this multi-period engine evaluates a vast scenario tree, an information structure problem regarding non-anticipativity arises. In the real world, system operators do not possess perfect foresight regarding which structural contingency will materialize. To preserve physical realism, the behavior of the ESSs must remain completely uniform across all contingency paths up until the exact moment a disturbance occurs. This tracking uniformity is strictly enforced through the following non-anticipativity rules:

$$P^{ch}_{e,k,o,t} = P^{ch}_{e,0,o,t}, \quad \forall e \in E,\ \forall k \in K,\ \forall o \in \Omega_o,\ \forall t < t_{\mathrm{cont},k} \tag{3.44}$$

$$P^{dch}_{e,k,o,t} = P^{dch}_{e,0,o,t}, \quad \forall e \in E,\ \forall k \in K,\ \forall o \in \Omega_o,\ \forall t < t_{\mathrm{cont},k} \tag{3.45}$$

By matching the charging and discharging decisions across all contingency threads to their base-case profiles ($k = 0$) for all time indices preceding the incident ($t < t_{\mathrm{cont},k}$), the model ensures storage assets operate independently of future scenario results. Post-contingency adjustments and resource differentiation are permitted exclusively for intervals following the event ($t \geq t_{\mathrm{cont},k}$).

### 3.4.4 Flexible Load Modeling

Analogous to storage systems, flexible loads are subject to strict non-anticipativity constraints to guarantee operational consistency across the time horizon. Demand-side management actions deployed before a disturbance occurs cannot exploit foreknowledge of a contingency. Consequently, active and reactive load modifications are locked across all scenarios until the event window opens:

$$P^{\mathrm{flex,up}}_{l,k,o,t} = P^{\mathrm{flex,up}}_{l,0,o,t}, \quad \forall l \in F^l,\ \forall k \in K,\ \forall o \in \Omega_o,\ \forall t < t_{\mathrm{cont},k} \tag{3.46}$$

$$P^{\mathrm{flex,down}}_{l,k,o,t} = P^{\mathrm{flex,down}}_{l,0,o,t}, \quad \forall l \in F^l,\ \forall k \in K,\ \forall o \in \Omega_o,\ \forall t < t_{\mathrm{cont},k} \tag{3.47}$$

$$Q^{\mathrm{flex,up}}_{l,k,o,t} = Q^{\mathrm{flex,up}}_{l,0,o,t}, \quad \forall l \in F^l,\ \forall k \in K,\ \forall o \in \Omega_o,\ \forall t < t_{\mathrm{cont},k} \tag{3.48}$$

$$Q^{\mathrm{flex,down}}_{l,k,o,t} = Q^{\mathrm{flex,down}}_{l,0,o,t}, \quad \forall l \in F^l,\ \forall k \in K,\ \forall o \in \Omega_o,\ \forall t < t_{\mathrm{cont},k} \tag{3.49}$$

These constraints prevent the optimization framework from creating unrealistic pre-contingency strategies based on future event data, aligning the model directly with the information horizons available to grid dispatchers.

### 3.4.5 Chance-Constrained Extension

The transition from a standard CC-OPF architecture to the comprehensive CC-SCOPF framework is achieved by expanding the probabilistic chance-constrained layers to structurally span contingency spaces. Accordingly, all continuous relaxation slacks and smooth rational violation flags are augmented with the contingency index $k$. This allows for continuous, differentiable risk tracking and constraint violation assessment across both steady-state and post-contingency states.

## 3.5 Python Implementation Framework

All optimization functions described in the previous sections were integrated into a unified Python package, providing users with the flexibility to explore, test, and extend the proposed methods.

Python was selected as the implementation language due to its extensive scientific ecosystem, readability, and ease of deployment. Crucially, the framework utilizes Pyomo [45] as its algebraic modeling language. Because Pyomo acts as a high-level abstraction layer between the mathematical formulation and the execution engine, the proposed framework is entirely solver-agnostic. This decoupling allows users to seamlessly switch between different open-source or commercial solvers (such as IPOPT for nonlinear problems or Gurobi for mixed-integer problems) depending on their specific computational needs, without requiring any modifications to the underlying code.

To support a clearer understanding of the proposed methodology, Figure 3.2 presents a simplified overview of the SCOPF process.

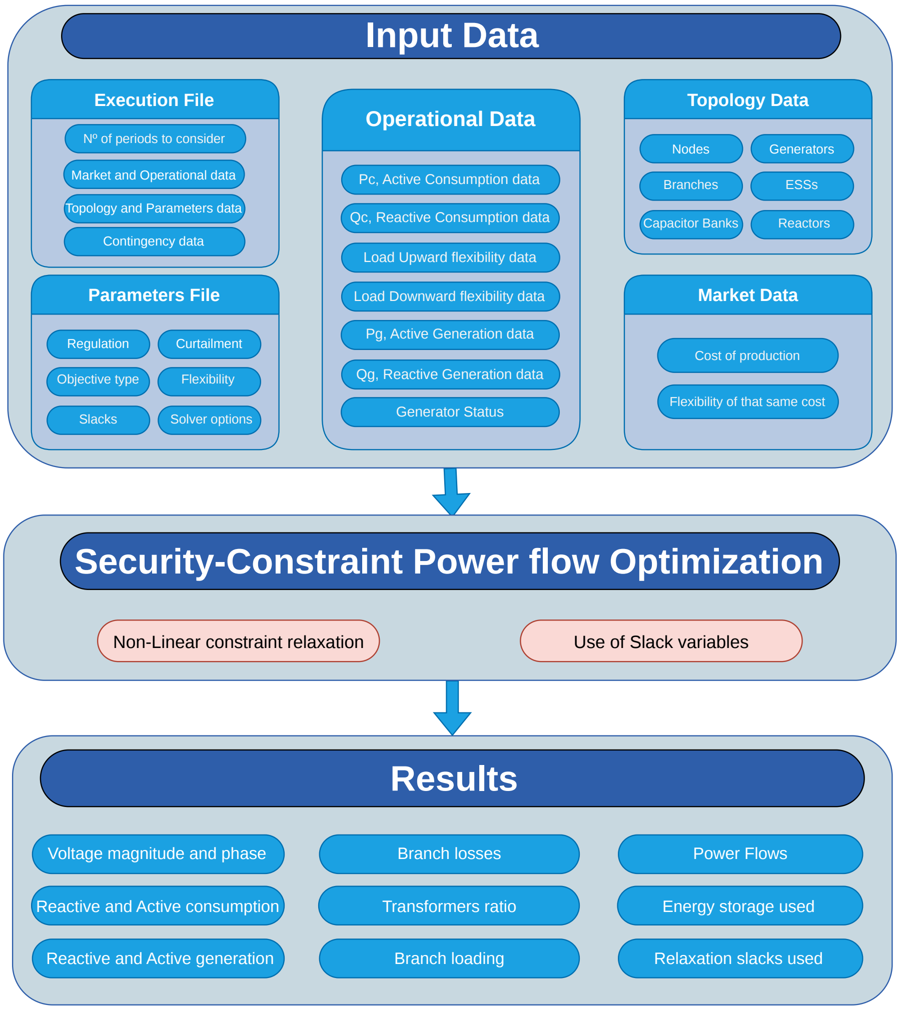


Figure 3.2: Python package methodology process mapping.

## 3.5.1 Input data

The proposed framework requires a structured set of input files to define the network topology and simulation parameters. These datasets are organized across complementary `.json` and `.xlsx` files, beginning with the primary execution master.

### 3.5.1.1 Execution File

This file serves as a central configuration file that defines the overall setup for solving a case. It specifies the number of time periods to be considered in the optimization and the duration of said periods. It provides the paths to all the necessary input files, including topology, parameters, production and consumption data, and market data. It also includes the contingencies to consider and the acceptable violation probabilities for voltage magnitudes and branch flow limits. It's defined by a `.json` file named after the case scenario, for example, `CS2.json`. To have a clearer image of how this file works, please check Figure 3.3.

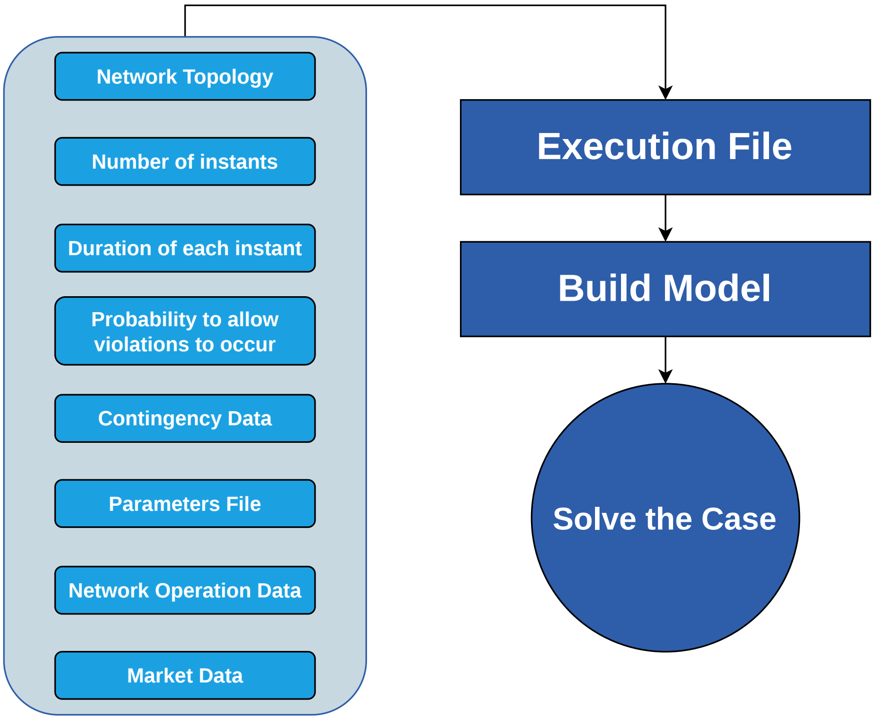


Figure 3.3: Data structures and parameter mapping within the centralized execution file.

In essence, the user provides several input files, namely: the grid topology and its operational data, the market values to be taken into account, and the parameters the user wishes to include. Then, through the execution file, the user specifies the number of periods and contingencies to be analysed. This execution file is the one that directs the SCOPF tool to the specific case that should be simulated.

#### 3.5.1.2 Topology of the Grid

This file defines the network topology of the electrical grid for a specific test case, describing the physical connectivity between buses, generators, loads, lines, transformers, ESSs, capacitor banks and reactors. The data is organized in a hierarchical `.json` format, where each component type is grouped into a dedicated array of objects containing the necessary operational parameters. The baseline system network for this framework is explicitly defined in the file `case9.json`.

#### 3.5.1.3 Configuration Parameters

This file defines the operational parameters and solver configurations required to execute a specific optimization case. It dictates how the SCOPF or multi-period OPF framework behaves by specifying execution settings such as the optimization model type, solver convergence tolerances, and objective function definitions. These parameters are structured within a complementary `.json` file, exemplified by `case9_params.json`.

#### 3.5.1.4 Production and Consumption data

This Excel file provides time-dependent data on both generation and consumption for the elements in the network. Each sheet represents a dataset for specific elements, such as generators or loads, and includes detailed profiles of power production, consumption, and availability. It's defined by a `.xlsx` file named after the case, for example, `case9.xlsx`.

#### 3.5.1.5 Market data

This Excel file contains a single sheet with market-related data necessary for running market-oriented optimizations. It provides cost curves, bids, offers, and other market-related parameters that define how generation and consumption units interact within the market framework. It's defined by a `.xlsx` file named after the case scenario, for example, `CS2_market_data.xlsx`.

### 3.5.2 Results Structure

The results of each OPF solution are saved as a Excel file named according to the case and the OPF type. For example: `CS2_opf_chance_constrained.xlsx` and `CS2_scopf_non_linear_chance_constrained.xlsx`. The structure of this excel file is illustrated in Table 3.2. These result files are stored in a "Results" folder located within the corresponding case scenario directory (e.g., within the `CS2` folder in this example).

Table 3.2: Results structure breakdown.

| **Sheet name** | **Explanation** |
| --- | --- |
| Main info | Summary of all results, including conventional generation and cost, renewable generation and curtailment, load flexibility and cost, losses, etc. |
| Market cost info | Information about the market per scenario and time period. |
| Voltage | Voltage results (magnitude and phase) per market, operational scenario, and time period. |
| Consumption | Consumption data (active and reactive power) per market, operational scenario, and time period. |
| Generation | Generation results (active and reactive power) per market, operational scenario, and time period. |
| Branch losses | Losses in each branch per market, operational scenario, and time period. |
| Transformers | Tap position and ratio of each transformer per market, operational scenario, and time period. |
| Capacitor Banks | Step settings and reactive power provided by each capacitor bank per market, operational scenario, and time period. |
| Reactors | Step settings and reactive power consumed by each reactor per market, operational scenario, and time period. |
| Branch loading | Utilization level of branch capacity in each direction per market, operational scenario, and time period. |
| Power flows | Power flow results in each branch per market, operational scenario, and time period. |
| Energy Storage | Energy storage results (e.g., $P$ [MW], $SoC$ [MWh], $SoC$ [%]) across all periods for each market and scenario. |
| Slacks | Slack variables used and their corresponding values per market, operational scenario, and time period. |

## 3.6 Concluding Remarks

This chapter has detailed the complete mathematical and architectural formulation of the proposed stochastic multi-period SCOPF framework. The core methodological contributions and design choices established in this framework are synthesized below:

- **Mathematical tractability and formulation design:** To mitigate the numerical challenges that non-convexities and non-differentiabilities present to gradient-based NLP solvers, non-differentiable absolute value operations and discontinuous step-function violation indicators were systematically reformulated into smooth, equivalent analytical structures. Furthermore, the selected voltage representation avoids trigonometric functions, casting the power flow equations as quadratic polynomials.

- **Slack-Based feasibility and violation modeling:** The integration of slack variables allows the framework to explicitly model and quantify operational constraint violations under highly stressed conditions. By softening hard operational boundaries through heavily penalized voltage and apparent power flow slacks, the formulation eliminates the risk of localized mathematical infeasibility. Post-convergence, these activated slacks transition from optimization relaxations to actionable physical metrics, providing system operators with interpretable diagnostic data regarding local flexibility deficits.

- **Non-Anticipative temporal modeling:** The multi-period modeling of ESSs and flexible loads explicitly accounts for temporal couplings without violating real-world operational boundaries. The enforcement of strict non-anticipativity constraints ensures that dispatch decisions remain identical across the scenario space prior to a contingency event, preserving operational realism by preventing the algorithm from exploiting foreknowledge.

- **Algorithmic modularity and portability:** By decoupling the network data ingestion layers from the core execution pipeline, the methodology can be systematically applied across arbitrary grid topologies, facilitating reproducible benchmarking and future framework extensions.

Chapter 4 presents a comprehensive numerical validation of this optimization framework across diverse grid topologies. Through various case studies, the subsequent chapter systematically evaluates the operational behavior, computational scalability, and physical reliability of the proposed models under high renewable penetration and severe contingency conditions.

# Chapter 4

# Case Studies and Results

This chapter evaluates the practical performance, computational efficiency, and operational robustness of the proposed optimization frameworks. By testing the formulations under high renewable penetration and multi-contingency conditions, this analysis validates the capabilities of the continuous NLP and alternative MIQP models developed in Chapter 3.

The chapter is organized as follows: Section 4.1 establishes the baseline operational setup, network parameters, and multi-scenario input datasets using a modified IEEE 5-Bus test network. Following this configuration, Section 4.2 contrasts the baseline OPF formulation against the CC-OPF model to isolate the exact impact of stochastic uncertainty tracking on grid variables. This security layer is expanded in Section 4.3, which evaluates the operational behavior and multi-period performance of the framework when $N-1$ contingency criteria are fully integrated into the probabilistic dispatch environment. Moving from modeling concepts to computational execution, Section 4.4 benchmarks the proposed continuous NLP formulation directly against the exact combinatorial MIQP baseline, highlighting the numerical advantages and convergence properties of the smooth relaxation approach. Finally, Section 4.5 provides a comprehensive scalability analysis utilizing a large-scale transmission system to determine the computational limits and performance scaling of the proposed optimization engines.

## 4.1 Test Case Description

This section outlines the benchmark framework used to evaluate the optimization engines. It details the topology of a modified IEEE 5-Bus transmission network, states the key intertemporal parameters governing energy storage, and establishes the multi-scenario profiles for renewable generation, market clearing prices, and system demands.

### 4.1.1 Network Configuration

The IEEE 5-Bus system [46] is originally composed of five buses, five conventional generators, three loads, and six transmission lines. In this work, the network is modified to reflect a high-renewable, low-inertia operating paradigm by adding a wind generator at bus 1 (designated as generator $G_6$) and a photovoltaic (PV) generator at bus 2 (designated as generator $G_7$). Additionally, two ESSs are integrated at buses 3 and 4, respectively. The complete modified grid layout is illustrated in Figure 4.1, and the technical capacities of the newly integrated components are summarized in Table 4.1.

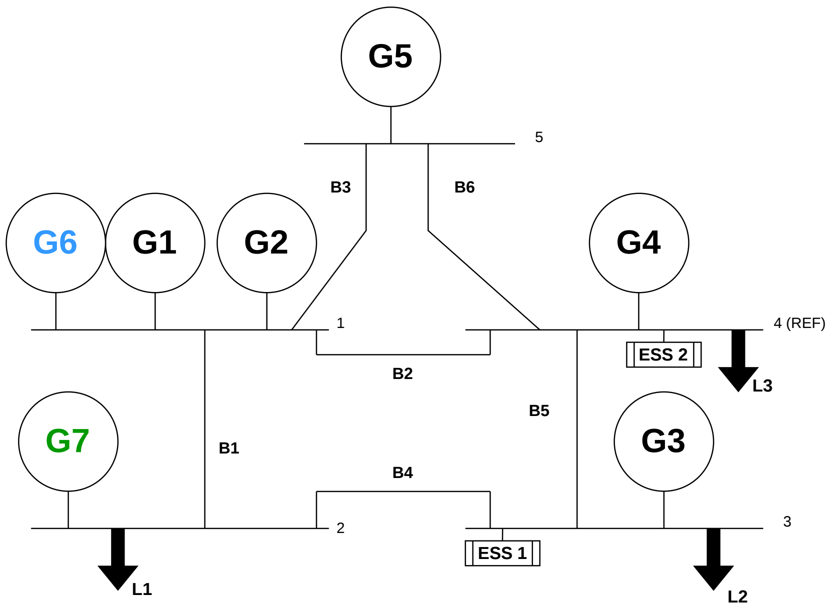


Figure 4.1: Modified IEEE 5-Bus transmission network topology incorporating co-located RES assets and distributed ESS units.

Table 4.1: Technical characteristics and node mapping of the supplementary renewable assets and ESS units in the modified IEEE 5-Bus system.

| **Network** | **PV Generator** | | **Wind Generator** | | **ESSs** | |
|---|---|---|---|---|---|---|
| | Bus | $P$ (MW) | Bus | $P$ (MW) | Bus | $P$ (MW) |
| IEEE-5 | 2 | 200 | 1 | 550 | 3 | 10 |
| | | | | | 4 | 10 |

While all three ESS mathematical representations detailed in Chapter 3 were implemented, the case studies in this chapter utilize the **RELAXED** model, which consistently provides the optimal trade-off between optimization accuracy and solver execution times. To protect battery asset longevity, the state-of-charge tracking variables are bounded between a lower limit of 10% and an upper limit of 90% of each unit's total nominal energy capacity.

### 4.1.2 Operational and Simulation Setup

To evaluate the multi-period capabilities of the framework, simulations are executed across a 24-hour planning horizon divided into 96 discrete, 15-minute intervals. This specific time-step aligns directly with ERSE regulatory guidelines [44], which grant the TSO a 15-minute window to implement corrective actions following a contingency event. Beyond regulatory compliance, this sub-hourly temporal granularity helps to mathematically capture the intertemporal SoC transitions of the ESSs and accurately track the continuous evolution of network variables. Simultaneously, to emulate future low-inertia grid dynamics, the network portfolio features a substantial share of non-synchronous renewable capacity, parameterized using the installed capacities detailed in Table 4.1. Displacing conventional synchronous dispatch with these stochastic renewable streams inherently reduces the natural inertial response of the system, pushing the network toward tightly binding security boundaries and increasing its overall exposure to contingency risks.

The baseline evaluation of the SCOPF and CC-SCOPF models integrates 20 distinct operational scenarios, 96 discrete time-steps, and 13 contingency conditions ($N-1$ states). To assess the framework under maximum operational stress, the contingency events are modeled to occur at the period exhibiting the lowest synchronous generation share (period 17). During this interval, high renewable output directly minimizes conventional online generation, creating a critical operating state characterized by minimal system inertia and elevated thermal vulnerability. The contingency set $K$ encompasses the intact pre-contingency state ($k = 0$), individual generation outages for units $G_1$–$G_7$ ($k = 1$ to 7), and single branch contingencies for transmission lines $B_1$–$B_6$ ($k = 8$ to 13), guaranteeing an exhaustive evaluation of $N-1$ supply and network failures.

### 4.1.3 Input Data and Operating Conditions

All raw datasets used to construct the case studies were sourced from the official planning archives of the ATTEST project [47]. The historical reference data is formatted over a 24-hour horizon with a coarse hourly resolution (24 intervals).

#### 4.1.3.1 Temporal Interpolation and Regulatory Alignment

To align the simulation framework with modern power market clearing rules and transmission regulatory requirements, such as the standard 15-minute imbalance settlement period enforced by the Portuguese TSO, a linear interpolation scheme was executed to upscale the hourly source records into a 96-period profile. The interpolated value for any sub-hourly interval $t \in T$ is calculated as:

$$f(t) = I + \frac{1}{4} \cdot (F - I), \quad \forall t \in T \tag{4.1}$$

where $I$ and $F$ correspond to consecutive hourly observations mapping the transition from hour $h$ to hour $h+1$. This yields three intermediate points equally spaced within each hour.

#### 4.1.3.2 Renewable Generation Profiles

The stochastic nature of the CC-SCOPF relies on historical uncertainty bounds mapped around the expected output profiles. Figure 4.2 illustrates the mean output curves paired with their respective standard deviation envelopes across the operational scenarios.

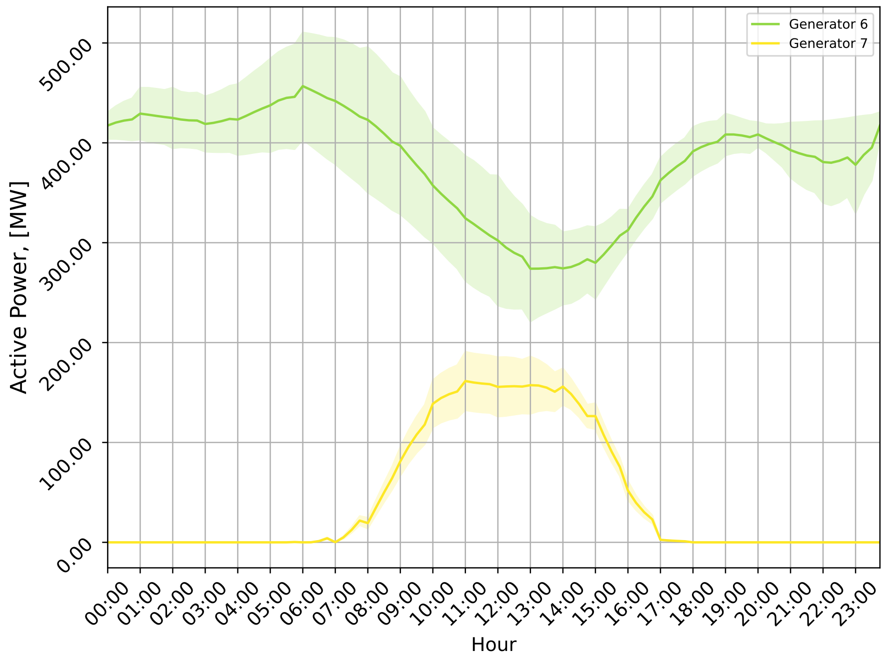


Figure 4.2: Stochastic renewable generation tracking profiles over the 24-hour horizon, displaying the expected output means and standard deviation uncertainty envelopes for the wind ($G_6$) and PV ($G_7$) assets.

The wind asset ($G_6$) provides a substantial share of total generation, maintaining a mean baseline shifting between 280 MW and 480 MW. The PV asset ($G_7$) complements this output by introducing a standard diurnal solar profile that peaks at approximately 160 MW between 11:00 and 13:00 h.

#### 4.1.3.3 Market Price Profiles

The financial optimization environment is structured around the time-varying market pricing paths shown in Figure 4.3.

The profiles demonstrate a significant divergence between active energy costs and flexibility market values. Energy prices present a clear ramp up to 130 €/MW at 19:00 h, tracking the evening net-load peak as solar generation drops. Flexibility costs remain stable through the early intervals but increase to 45 €/MW during peak net-demand windows, establishing the economic signal that dictates the storage dispatch strategy.

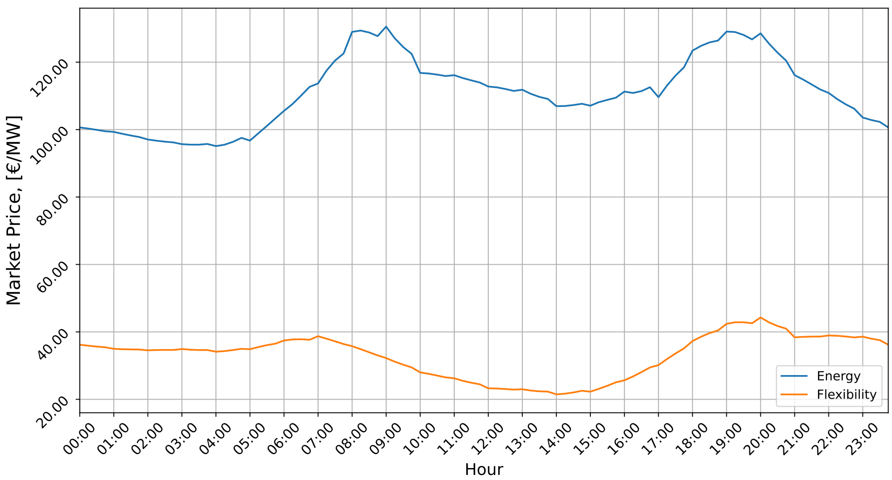


Figure 4.3: Temporal distribution of wholesale electricity market clearing prices and operational flexibility cost metrics over the 24-hour horizon.

#### 4.1.3.4 Load Profiles

The system demand profile aggregates three independent consumption paths tracking across the horizon, as shown in Figure 4.4.

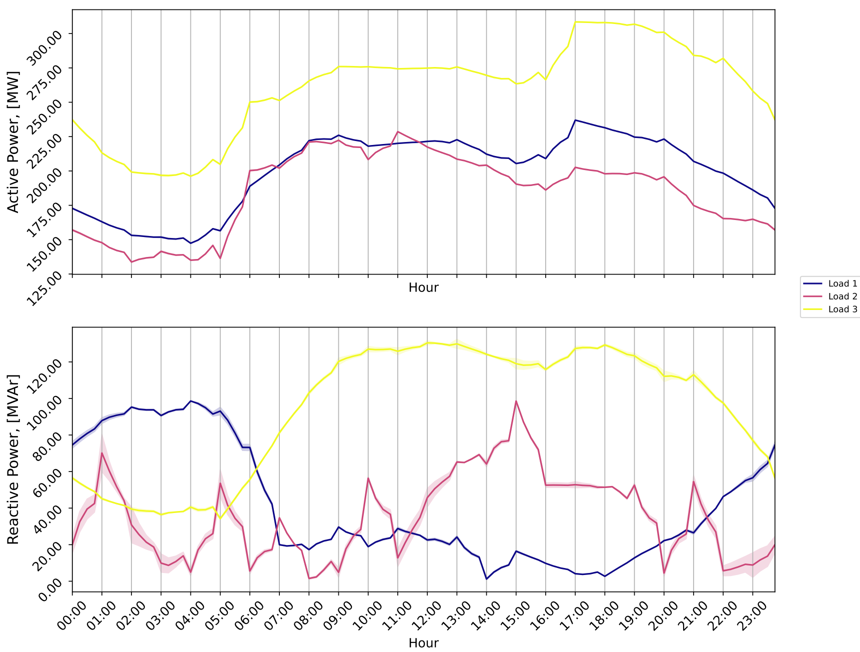


Figure 4.4: Nodal active and reactive power consumption profiles across the scenario space.

While Loads 1 and 3 present predictable, highly stable consumption baselines, Load 2 introduces significant volatility. Specifically, Load 2 exhibits sudden reactive power demand excursions approaching 100 MVAr alongside active power consumption peaks at 06:00 and 17:00 h. These synchronized peaks create a highly stressed operational environment designed to challenge transmission capacity boundaries and bus voltage stability margins.

## 4.2 Comparison Between Probabilistic OPF and CC-OPF

Table 4.2 presents a comparative assessment of the operational and computational performance obtained from the Probabilistic OPF and CC-OPF formulations. Both approaches were evaluated across 20 operational scenarios, with the CC-OPF having a 95% confidence level, which enforces that constraint violations are permitted in at most 5% of the cases. Accordingly, this probabilistic guarantee corresponds, in expectation, to at most one scenario with allowable violations in the considered sample set. Note that all NLP simulations were carried out using the IPOPT solver [43] with HSL-MA97 linear solver [48], while for MIQP simulations the Gurobi [49] solver was used. All simulations were conducted on a Mac studio equipped with an Apple M2 Max processor and 32 GB of RAM.

Table 4.2: Probabilistic and Chance-Constrained OPF results.

| **Metric / Operation** | **Probabilistic OPF** | **CC-OPF** |
|---|---|---|
| **Operational Results** | | |
| Conventional Generation Cost ($) | 2 435 731.64 | 2 435 731.45 |
| $E^{\text{conv}}$ (MWh) | 22 470.76 | 22 470.75 |
| $E^{\text{RES}}$ (MWh) | 39 589.50 | 39 589.65 |
| $E^{\text{RES, curt}}$ (MWh) | 5.35 | 5.20 |
| $E^{\text{losses}}$ (MWh) | 125.21 | 125.6 |
| **Computational Performance** | | |
| Iterations | 101 | 93 |
| Time (s) | 34.84 | 40.71 |

The results indicate that both approaches lead to nearly identical dispatch schedules, voltage profiles, and branch loading levels. The similarity of the operational outcomes suggests that the optimal operating point obtained with the Probabilistic OPF already satisfies the probabilistic security margins enforced by the CC-OPF formulation. Consequently, the introduction of chance constraints does not significantly alter generator dispatch, renewable utilization, or system losses. This behavior indicates that the CC-OPF framework achieves risk-aware operation without introducing excessive conservatism or unnecessary operational costs.

Regarding computational performance, the CC-OPF formulation converged in 93 interior-point iterations of the NLP solver IPOPT, compared to 101 iterations required by the Probabilistic

OPF. Although the CC-OPF exhibits a slightly higher computational time per iteration, resulting in a total execution time of 40.71 s versus 34.84 s, this increase is primarily attributed to the additional evaluations of inverse cumulative distribution functions associated with the chance constraints. Despite this added computational burden, the overall performance of both approaches remains comparable. The modest increase in execution time represents a reasonable trade-off for incorporating explicit probabilistic security guarantees. Furthermore, the observed convergence behavior indicates that the inclusion of chance constraints does not significantly worsen the problem's nonlinearity or numerical conditioning. This stability stems directly from the smooth, continuously differentiable nature of the adopted analytical reformulations, which avoid sharp gradient discontinuities and maintain well-behaved Jacobian and Hessian matrices throughout the optimization process. These results confirm the practical suitability of the proposed framework for multi-period dispatch with 15-minute resolution over a 24-hour operational horizon.

### 4.2.1 Impact of High Renewable Penetration

To further challenge the system and evaluate robustness under extreme renewable operating conditions, an additional high-penetration scenario was considered. This experiment aims to investigate the impact of increased renewable integration on the relative performance of the Probabilistic OPF and CC-OPF formulations. In this scenario, renewable generation levels were increased by 20%, thereby intensifying system variability and further reducing the contribution of conventional synchronous generation. Table 4.3 presents a comparative assessment of the operational and computational performance for the case of high RES generation.

Table 4.3: Probabilistic and Chance-Constrained OPF results and computational performance comparison for higher renewable penetration.

| **Metric / Operation** | **Probabilistic OPF** | **CC-OPF** |
|---|---|---|
| **Operational Results** | | |
| Conventional Generation Cost ($) | 1 592 264.86 | 1 592 264.77 |
| $E^{\text{conv}}$ (MWh) | 14 581.74 | 14 581.74 |
| $E^{\text{RES}}$ (MWh) | 47 621.48 | 47 598.66 |
| $E^{\text{RES, curt}}$ (MWh) | 234.55 | 257.37 |
| $E^{\text{losses}}$ (MWh) | 245.42 | 222.43 |
| **Computational Performance** | | |
| Iterations | 2454 | 2148 |
| Time (s) | 535.43 | 561.36 |

As seen in Table 4.3, despite the higher renewable penetration, both formulations produced comparable results. The conventional generation output, and operating costs remained nearly identical, indicating that the optimal economic dispatch is largely preserved. A slight increase in renewable curtailment was observed in the CC-OPF solution. This increase in renewable curtailment reflects the enforcement of probabilistic security margins. By slightly reducing renewable dispatch, the optimization model compensates for elevated uncertainty levels, ensuring that operational constraints remain satisfied with the prescribed confidence level. This behavior demonstrates that the CC-OPF internalizes uncertainty directly within the dispatch decisions.

Figures 4.5 and 4.6 present the voltage magnitude and branch loading profiles obtained with both formulations.

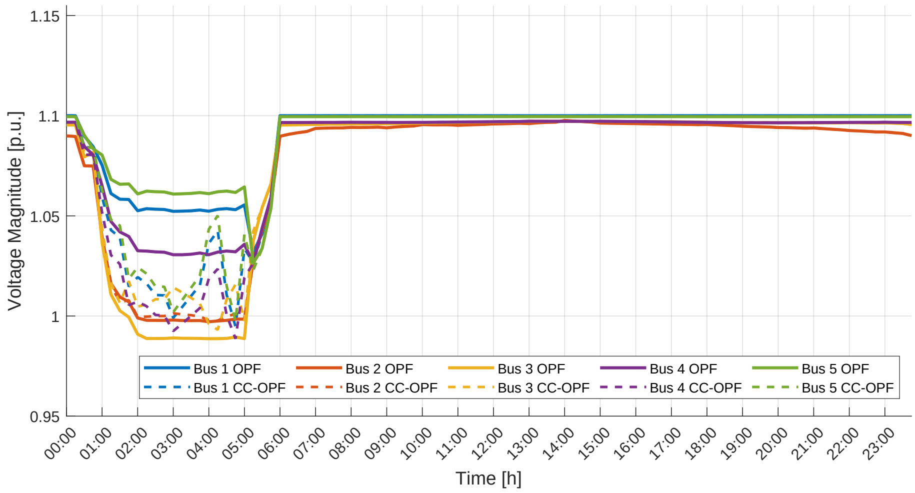


Figure 4.5: Comparison of Voltage Magnitude in each node between Probabilistic and Chance-Constrained OPF.

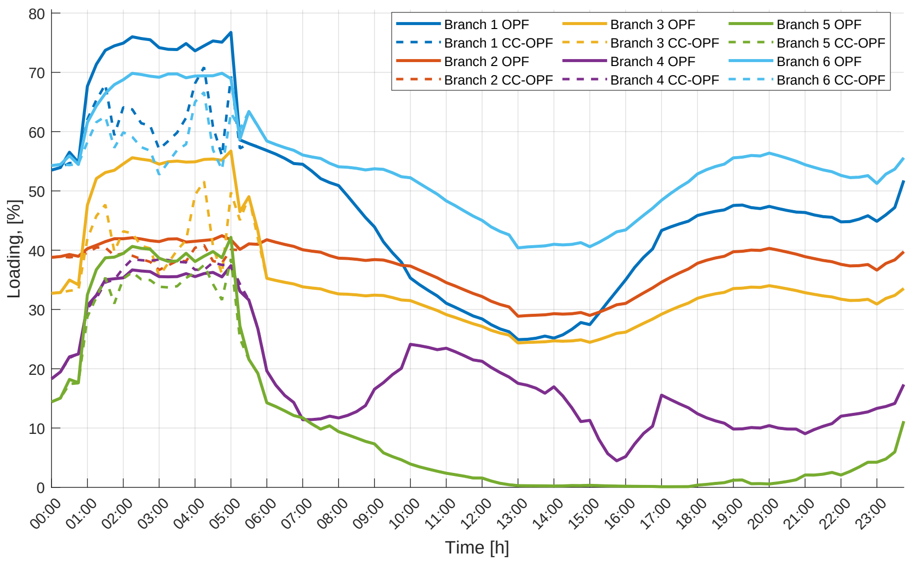


Figure 4.6: Comparison of Branch loading in each branch between Probabilistic and Chance-Constrained OPF.

The Probabilistic OPF exhibits smooth voltage trajectories and stable branch loading patterns, consistent with optimization around a single expected operating condition. In contrast, the CC-OPF solution displays increased temporal fluctuations in both voltage magnitudes and line loadings. This behavior is inherent to chance-constrained optimization. Rather than enforcing feasibility for a single deterministic trajectory, the CC-OPF continuously adjusts operating points to satisfy probabilistic limits across multiple uncertainty realizations. As a result, the system operates closer to security boundaries while maintaining predefined reliability levels. Therefore, the observed fluctuations represent adaptive preventive control actions and should be interpreted as evidence of risk-aware operation rather than degraded system performance.

From a computational perspective, higher renewable penetration significantly intensifies the numerical complexity of both formulations. The CC-OPF converged in 2148 interior-point iterations with a total execution time of 561.36 s, whereas the Probabilistic OPF required 2454 iterations and completed in 535.43 s. Although the CC-OPF requires fewer total solver iterations, each individual step demands a higher computational effort to evaluate the analytical expressions of the chance constraints. As renewable variability scales, the optimization engine must execute more intensive numerical updates to safely navigate the tightly bound boundaries of the feasible region.

Overall, the results demonstrate that higher renewable penetration does not significantly alter economic dispatch decisions but fundamentally changes how network security is managed. The proposed CC-OPF formulation preserves economic optimality while explicitly accounting for uncertainty, leading to a more adaptive operating regime that maintains reliable operation under stochastic renewable generation.

## 4.3 Comparison Between CC-OPF and CC-SCOPF

This section presents a comparative assessment of the proposed CCO frameworks applied to the modified IEEE 5-Bus system detailed in Section 4.1. The analysis aims to quantify the exact effects of integrating security criteria and probabilistic uncertainty boundaries on operational decisions and overall system robustness.

The evaluation is structured across three distinct analytical dimensions. First, in Section 4.3.1, the global operational and computational results are benchmarked under different confidence thresholds to map the core trade-offs between financial economy and probabilistic safety. In Section 4.3.2, the steady-state pre-contingency operating configurations ($k = 0$) are examined to isolate changes in generation dispatch patterns, battery energy management, and voltage regulation profiles. Finally, in Section 4.3.3, the post-contingency behavior of the grid ($k \in K$) is evaluated across the entire scenario space to demonstrate how the security-constrained engine proactively handles unexpected equipment failures and preserves network stability.

### 4.3.1 Global Results

The systemic impact of varying user risk aversion is analyzed under two discrete confidence thresholds: $p = 90\%$ and $p = 95\%$. Given the 20-scenario uncertainty distribution considered, these thresholds restrict constraint violations to a maximum of two operational scenarios and one operational scenario, respectively. Transitioning from $p = 90\%$ to $p = 95\%$ thus represents an explicit shift toward a highly risk-averse dispatch strategy. Table 4.4 summarizes the system operational data alongside the execution parameters of the formulations, where the column $\Delta$ traces the mathematical variation induced by tightening the chance constraints.

Table 4.4: Global operational and computational results under varying probabilistic confidence levels.

| **Operational Variable** | $p = 90\%$ | $p = 95\%$ | $\Delta$ |
|---|---|---|---|
| **Operational Results** | | | |
| Conventional Generation Cost ($) | 2 151 085.48 | 2 293 843.90 | 6.22% |
| $E^{\text{conv}}$ (MWh) | 19 868.47 | 21 059.82 | 5.66% |
| $E^{\text{RES}}$ (MWh) | 42 215.96 | 41 017.19 | -2.92% |
| $E^{\text{RES, curt}}$ (MWh) | 0.15 | 0.18 | 14.39% |
| $E^{\text{losses}}$ (MWh) | 139.83 | 130.82 | -6.89% |
| **Computational Performance** | | | |
| CC-OPF (Interior-Point Iterations) | 160 | 49 | -69.38% |
| CC-OPF (Total Solution Time [s]) | 78.75 | 15.79 | -79.95% |
| CC-SCOPF (NLP) (Interior-Point Iterations) | 112 | 75 | -33.04% |
| CC-SCOPF (NLP) (Total Solution Time [s]) | 530.30 | 360.36 | -32.05% |

#### 4.3.1.1 Economic Costs and Transmission Losses

The global results in Table 4.4 reveal a direct relationship between increased risk aversion and grid economic efficiency. Restricting the admissible violation space ($p = 95\%$) forces total dispatched conventional generation ($E^{\text{conv}}$) to rise by 5.66%, causing a 6.22% increase in conventional operating costs. Concurrently, renewable energy dispatched ($E^{\text{RES}}$) falls by 2.92%, driving a 14.39% increase in renewable energy curtailment ($E^{\text{RES, curt}}$).

This behavior highlights how chance constraints structurally alter the dispatch landscape. Restricting the risk parameter shrinks the valid inner boundaries of the feasible region, forcing the optimizer to establish larger protective margins relative to safe-operating thresholds before stochastic uncertainty materializes. Consequently, the optimization engine displaces volatile, non-dispatchable renewable streams with firm, controllable conventional units, effectively procuring implicit operating reserves to hedge against forecast errors. Stricter risk bounds also lower allowable transmission loading limits. Under high renewable volatility, the optimization curtails renewable output to ensure post-contingency security margins remain intact. Under this framework, renewable curtailment functions as a deliberate preventive security measure rather than a systemic operational flaw.

Conversely, despite the growth in total generation, active network transmission losses ($E^{\text{losses}}$) decrease by 6.89% under the $p = 95\%$ case. The conservative dispatch strategy automatically redistributes power flows away from heavily loaded, high-impedance paths, reducing long-distance, high-current power transfers from remote renewable generation units and significantly lowering total thermal losses.

#### 4.3.1.2 Solver Convergence and Execution Times

The performance values in Table 4.4 indicate that tightening the chance-constrained confidence level improves the convergence behavior of the mathematical solver. Mathematically, increasing $p$ requires a proportional decrease in the admissible risk allocation variable $\varepsilon$. Under a constant scenario space size $\Omega_o$, this tighter bound forces the optimization framework to minimize the continuous violation indicator variables $Z$. To satisfy this condition, the model minimizes continuous relaxation slacks across the scenario tree, shifting the nominal operating point deeper inside the interior of the safe admissible space. By navigating regions of the feasible domain where fewer constraints are binding, the solver avoids numerical oscillations near the operational thresholds. This reduction preserves highly stable, well-conditioned Jacobian and Hessian matrices within the gradient-based solver. The reduction in active constraints at optimality enables the interior-point NLP engine to resolve the problem in fewer total iterations, yielding lower execution times despite the conservative formulation.

Resorting from the baseline CC-OPF model to the full CC-SCOPF architecture creates a significant computational penalty. At $p = 95\%$, the CC-OPF converges in 49 iterations requiring 15.79 s, whereas the integration of contingency security layers increases the execution time to 360.36 s across 75 iterations. This computational expansion is driven by three main factors: i) the explicit replication of the full AC network constraints across each post-contingency state $k \in K$, ii) the dense intertemporal temporal coupling introduced by multi-period storage tracking, and iii) the inclusion of complex, nonlinear analytical approximations for scenario aggregation. Nevertheless, the framework consistently converges without numerical stagnation, validating the practical tractability of the smooth relaxation approach for sub-hourly operational environments.

### 4.3.2 Base Case Operational Analysis

The comparative analysis between the CC-OPF and CC-SCOPF formulations under the conservative risk threshold ($p = 95\%$) highlights the operational differences between standard economic dispatch and security-constrained optimization. While both frameworks integrate a significant share of renewable generation, achieving a net renewable penetration of approximately 66%, the inclusion of post-contingency security layers forces a more preventive baseline strategy.

#### 4.3.2.1 Generation Dispatch and Losses

Table 4.5 outlines the core pre-contingency energy data obtained for both optimization models.

Table 4.5: Pre-contingency ($k = 0$) system energy allocation and network loss results under the $p = 95\%$ confidence level.

| Optimization | $E^{\text{Conv}}$ (MWh) | $E^{\text{RES}}$ (MWh) | $E^{\text{RES, curt}}$ (MWh) | $E^{\text{losses}}$ (MWh) |
|---|---|---|---|---|
| CC-OPF | 21 048.07 | 41 016.53 | – | 130.67 |
| CC-SCOPF (NLP) | 21 059.82 | 41 017.19 | 0.18 | 130.82 |

This data indicates that enforcing the full $N-1$ constraint layer causes minor deviations from the unconstrained economic dispatch point. Total conventional energy dispatch increases by 11.75 MWh, while a minimal renewable curtailment of 0.18 MWh appears exclusively in the CC-SCOPF case to satisfy binding thermal limits under contingency paths. Additionally, system losses increase by 0.11% (0.15 MWh) under the security-constrained framework. This marginal efficiency loss represents the physical cost of preventive redispatch. To guarantee that subsequent asset outages do not cause thermal overload violations, power flows are routed through electrically longer or more resistive pathways, increasing baseline network transmission losses.

Figures 4.7 and 4.8 display the time-varying generation dispatch schedules, showing that both models maintain highly aligned profiles due to the close proximity of the unconstrained base case to the secure operating region.

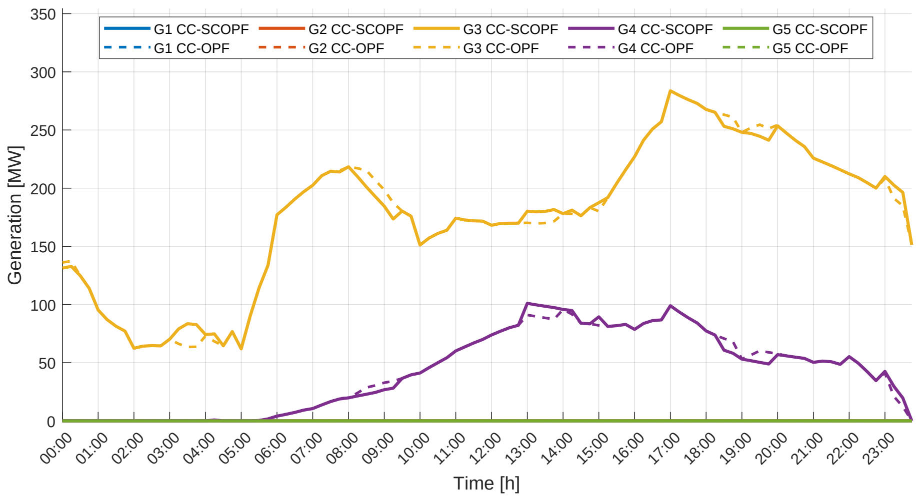


Figure 4.7: Temporal comparison of conventional generator active power dispatch schedules between the pre-contingency base cases of CC-OPF and CC-SCOPF.

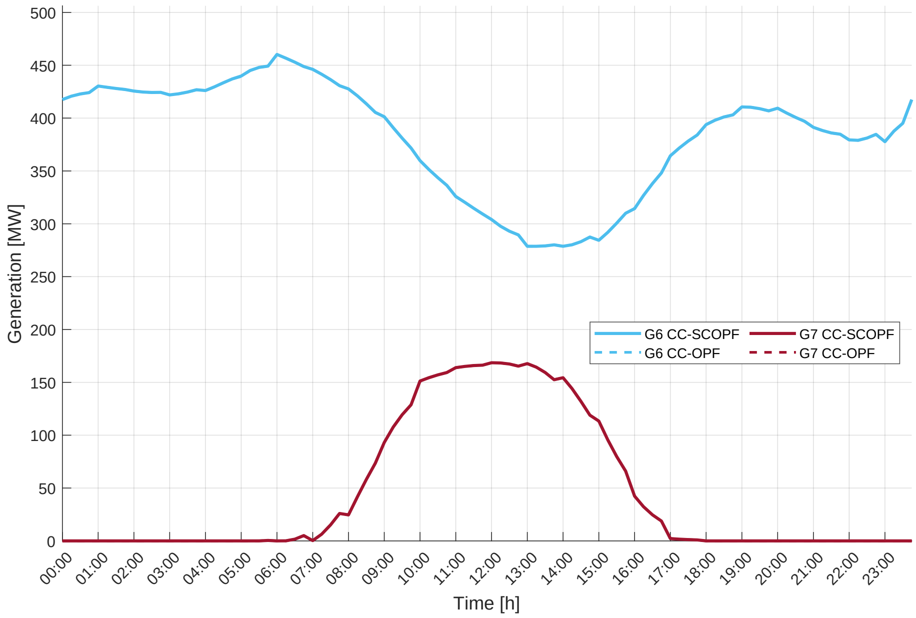


Figure 4.8: Temporal comparison of renewable generator active power output profiles between the pre-contingency base cases of CC-OPF and CC-SCOPF.

#### 4.3.2.2 Energy Storage Operation

The most significant operational distinction between the two frameworks appears in the intertemporal SoC trajectories of the distributed ESS units, as illustrated in Figure 4.9.

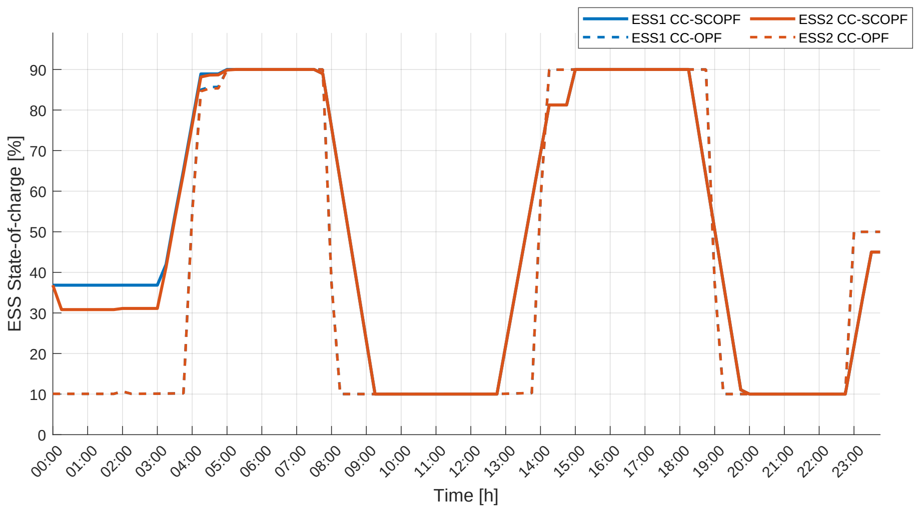


Figure 4.9: Intertemporal comparison of state-of-charge tracking profiles of the ESSs between the CC-OPF and CC-SCOPF frameworks.

Under the baseline CC-OPF model, the storage units operate entirely to maximize financial arbitrage, cycling down to their lower structural bound of 10%. Conversely, the CC-SCOPF engine maintains a highly conservative lower storage bound tracking near 30%. This remaining 20% energy margin serves as a localized, preventive security reserve. By avoiding full battery depletion, the security-constrained formulation preserves upward active power flexibility to respond to equipment contingencies. This strategy is highlighted during the early discharge window (08:00–09:00 h). While the purely economic CC-OPF depletes its storage energy at the maximum rate to capture price spreads, the CC-SCOPF enforces a gradual, restricted discharge rate. A portion of the stored energy is withheld from standard market operation to provide a protective layer of operational resilience.

#### 4.3.2.3 Voltage Profiles

The preventive nature of the security-constrained framework is also evident in the nodal voltage magnitude profiles, mapped across the network buses in Figure 4.10.

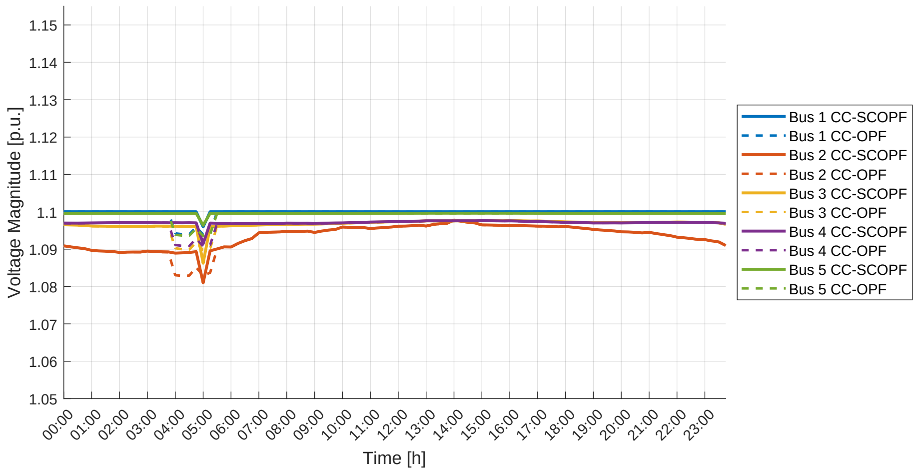


Figure 4.10: Nodal voltage magnitude profiles across the network buses, demonstrating the enhanced voltage stabilization achieved by the CC-SCOPF framework.

Under the CC-OPF dispatch, the bus voltage magnitudes exhibit wide temporal fluctuations, dropping toward 1.08 p.u. during periods of intense system stress. These drops correspond to maximum storage charging phases (04:00–05:30 h), where localized active power surges draw down node voltage magnitudes and compromise voltage security margins. Conversely, the CC-SCOPF model maintains a highly stable voltage profile across the planning horizon, with deviations occurring exclusively during the contingency interval. Keeping nodal voltages close to the upper operational limit of 1.10 p.u. establishes an elevated baseline that serves as a critical reactive power buffer, enhancing network robustness against voltage instability during prospective $N-1$ contingency states. This proactive voltage regulation explains the slight increase in conventional baseline dispatch, demonstrating that the framework accepts a marginal reduction in economic efficiency to guarantee global voltage security.

### 4.3.3 Contingency Scenarios Analysis

This subsection evaluates the post-contingency behavior of the network assets to demonstrate the corrective mechanisms embedded within the multi-period CC-SCOPF engine.

#### 4.3.3.1 Generator Re-Dispatch

Figure 4.11 tracks the active power response of conventional generator $G_3$ across the entire contingency set.

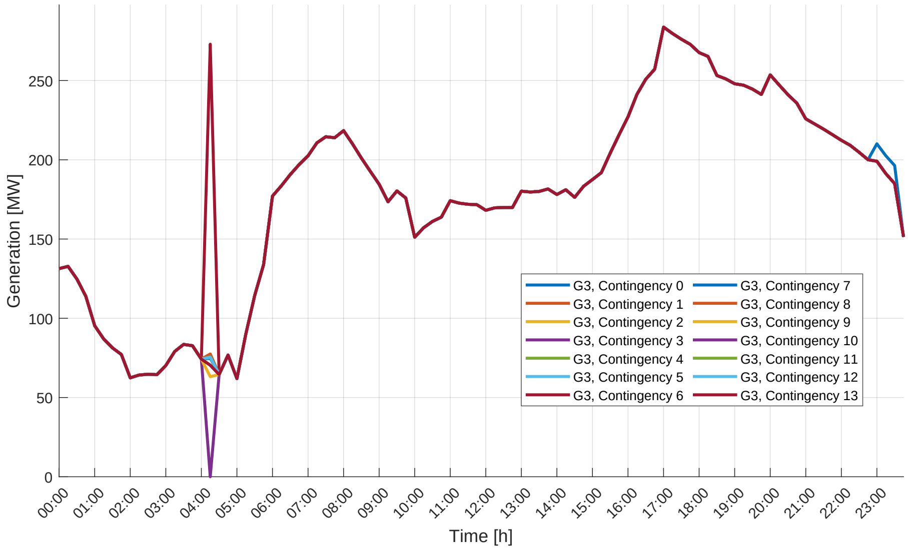


Figure 4.11: Active power dispatch of Generator 3 across all evaluated contingency states.

Under its own outage state ($k = 3$), the generator's active output drops to zero at the contingency event period ($t = 17$: 04:15 h), confirming the strict enforcement of the physical disconnection constraint. The unit's output under alternative contingency states illustrates the automated redispatch mechanism. The most prominent case appears under contingency $k = 6$, which represents the unexpected loss of wind asset $G_6$ during a high-output interval. To compensate for the resulting power deficit, generator $G_3$ executes a sharp upward step change at 04:15 h. This corrective step validates the model's ability to coordinate surviving conventional units to restore system balance following a major renewable generation failure.

#### 4.3.3.2 Nodal Voltages

Figure 4.12 maps the voltage magnitude profile at Bus 1 across the contingency space.

The trajectories remain tightly clustered near 1.10 p.u. across the 24-hour horizon, indicating that the model preserves strong nominal voltage setpoint control during standard operations. At the contingency instant (04:15 h), several failure states push the post-contingency voltage toward the upper limit, reaching approximately 1.15 p.u. This behavior demonstrates that the optimization framework utilizes the emergency voltage tolerance envelope ($\pm 5\%$) as a source of operational flexibility. Rather than maintaining an overly conservative and economically inefficient pre-contingency dispatch, the chance-constrained approach allocates security margins probabilistically, allowing the system state to approach outer physical boundaries during temporary fault conditions without risking cascading failures. The rapid return of the voltage profiles to nominal values after the event confirms the availability of adequate reactive power control reserves.

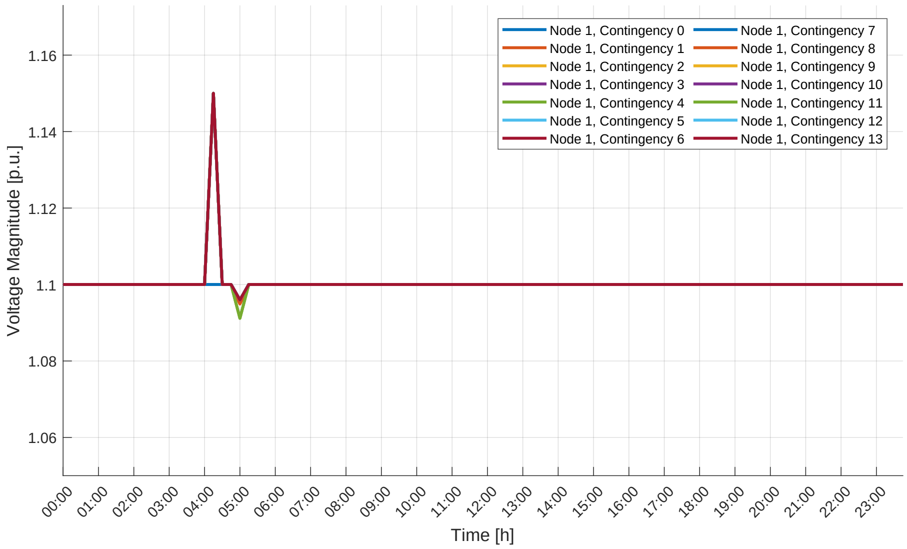


Figure 4.12: Nodal voltage magnitude at Bus 1 across the contingency space.

#### 4.3.3.3 Branch Power Flows

Figure 4.13 traces the apparent power loading profile of Branch 2 across all contingency scenarios.

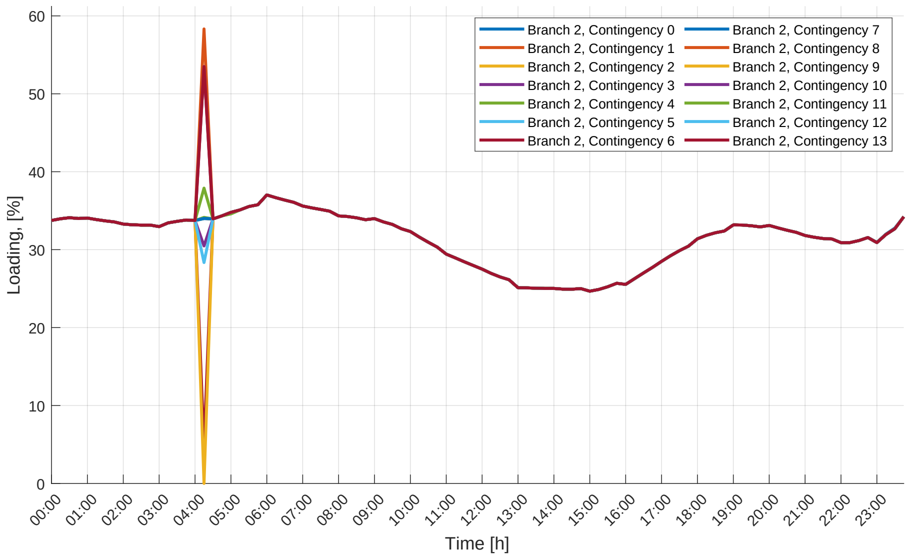


Figure 4.13: Apparent power loading percentage profiles on Branch 2 across all contingencies.

Branch utilization remains well below its thermal limits, peaking within the 50%–60% range during contingency scenario $k = 8$, which corresponds to the outage of parallel Branch 1 and the subsequent redirection of power flows. The narrow dispersion between the post-contingency loading paths indicates that transmission power flow redistributions are anticipated by the optimization engine. Because the CC-SCOPF explicitly optimizes pre-contingency scheduling alongside corrective capabilities, it ensures that alternative network corridors retain sufficient transmission headroom prior to any disturbance. This preventively manages thermal stress and prevents overloading during topology changes. Furthermore, the absence of capacity saturation during peak demand intervals confirms that the network operates with a robust safety margin, avoiding congestion-driven vulnerabilities.

In summary, the nonlinear CC-SCOPF changes how uncertainty is handled by optimizing preventive positioning and corrective deployment simultaneously. This optimization minimizes post-contingency risk while preserving high economic efficiency across the scenario space.

## 4.4 Comparison Between NLP and MIQP CC-SCOPF

To evaluate the computational efficiency of the proposed NLP-based CC-SCOPF formulation, a comparative study with a classical MIQP implementation was conducted. Due to the large number of binary variables introduced by the Big-$M$ formulation, solving the MIQP model at the full problem scale would result in excessive computational burden. Therefore, a reduced test setting was adopted to enable a fair and tractable comparison.

### 4.4.1 Mixed-Integer Benchmark Formulation

To verify the precision of the smooth, continuous NLP surrogate approximations against exact combinatorial solution methods, the classical MIQP variant is applied here as the baseline verification framework. Rather than utilizing continuous algebraic tracking functions, this formulation models risk-bounded violation events through exact logical rules via the Big-$M$ method, creating a discrete, binary mapping of security violations.

In this benchmark application, the discrete binary variables $Z$ operate as absolute mathematical switches that explicitly govern the behavior of the network relaxation slacks. When a binary indicator resolves to zero, its associated constraint is strictly enforced, forcing the corresponding voltage or branch flow slack variable to zero. Conversely, when a binary variable evaluates to one, the underlying operational constraint is relaxed, allowing a controlled physical violation bounded by a sufficiently large numerical constant $M$:

$$Slack^{V}_{i,k,o,t} \leq Z^{V}_{i,k,o,t} M^{V}, \quad \forall i \in N, k \in K, o \in \Omega_o, t \in T \tag{4.2}$$

$$S^{Sl}_{ij,k,o,t} \leq Z^{B}_{ij,k,o,t} M^{B}, \quad \forall ij \in B, k \in K, o \in \Omega_o, t \in T \tag{4.3}$$

By casting risk tracking as a combinatorial counting problem, this framework provides an exact baseline for evaluating permitted violation frequencies. The resulting mixed-integer structure balances the operational dispatch selection against the specific subset of scenarios and contingencies where boundary violations are allowed to clear, resolved via the Gurobi optimization engine [49]. The global security requirements are bounded by identical risk thresholds ($\varepsilon$) across both models, ensuring a perfectly consistent probabilistic limit for verification.

### 4.4.2 Computational Performance and Scalability

The comparative evaluation was conducted on the modified IEEE 5-Bus network considering a condensed temporal horizon of 4 time periods, 11 contingency states and a target confidence level of 95% ($p = 95\%$). To ensure a highly demanding test environment, all asset outages were modeled to occur during Period 1, representing a critical low-inertia operating condition characterized by high renewable penetration and low synchronous generation availability. The active contingency set $K$ encompasses the intact base case ($k = 0$), individual generator outages for units $G_1$–$G_5$ ($k = 1$ to 5), and branch outages for transmission lines $B_1$–$B_6$ ($k = 6$ to 11). To test scalability, the benchmarks were solved across two independent scenario dimensions containing 5 and 10 operational scenarios, respectively.

Table 4.6 summarizes the computational performance of the proposed formulations for a confidence level of $p = 95\%$.

Table 4.6: Performance results comparison, NLP vs MIQP.

| **Set of Operational Scenarios ($\Omega_o$)** | **Time (s)** | |
|---|---|---|
| | CC-SCOPF (**NLP**) | CC-SCOPF (**MIQP**) |
| $\Omega_o = 5$ | 3.09 | 97.42 |
| $\Omega_o = 10$ | 5.13 | 226.33 |

The computational runtimes demonstrate a substantial performance advantage for the proposed continuous NLP formulation over the combinatorial mixed-integer approach. The interior-point solver exhibits highly favorable scalability characteristics. Doubling the active scenario space from 5 to 10 instances results in a moderate runtime increase of approximately 66.02%. In contrast, the MIQP formulation resolved via Gurobi experiences a severe computational penalty, with execution times expanding by 132.32% under identical conditions. At the 10-scenario scale, the MIQP model requires approximately 3.77 minutes (226.33 s) to achieve convergence, which severely restricts its applicability for time-critical or online grid dispatch environments. By comparison, the proposed continuous NLP framework resolves the identical problem in just 5.13 s while strictly satisfying the same probabilistic risk boundaries. This speedup represents a 97.73% reduction in total execution time, highlighting the superior numerical scalability of the smooth relaxation approach.

### 4.4.3 Solution Accuracy

To verify that the computational speedup achieved by the NLP approach does not introduce suboptimality or mathematical inaccuracies, the resulting operational schedules were cross-examined. All subsequent comparative analyses correspond to the 10-scenario configuration ($\Omega_o = 10$).

Both formulations converged to identical active power generation schedules for all conventional and renewable assets across the network. The only detectable variation appears as a marginal numerical deviation in the final objective function values, as summarized in Table 4.7.

Table 4.7: Total objective function cost comparison under the 10-scenario optimization horizon.

| **Optimization Framework** | **Total Objective Cost ($)** |
|---|---|
| CC-SCOPF (NLP) | 1 457 095.94 |
| CC-SCOPF (MIQP) | 1 457 011.97 |

The objective values confirm the numerical accuracy and robustness of the continuous relaxation technique. While the exact combinatorial MIQP model achieves a lower total operating cost of $1 457 011.97, the continuous NLP solution yields a value of $1 457 095.94. The resulting economic gap is practically negligible, representing an operational cost difference of only 0.0058%. Because both approaches yield mathematically identical asset dispatch schedules, this minor discrepancy functions purely as a minor numerical artifact originating from the continuous scaling of the rational surrogate function ($\alpha$-parameter tuning) rather than an actual operational suboptimality. Furthermore, both formulations produce identical pre-contingency base case profiles ($k = 0$), matching exactly across all bus voltage magnitudes, generator output levels, storage state-of-charge trajectories, and branch flow capacity values. This high numerical agreement extends completely into the post-contingency domain ($k \in K$). Across all evaluation states from Contingency 1 through 11, the post-disturbance line loading profiles and corrective generator re-dispatch steps remain perfectly aligned, showing complete graphical and numerical overlap.

In conclusion, these benchmarking investigations verify that NLP, when unified with a smooth, continuous rational surrogate function, serves as a highly effective and mathematically sound alternative to traditional mixed-integer frameworks for solving complex CC-SCOPF problems. By eliminating binary switching variables, the proposed framework removes the combinatorial branch-and-bound bottlenecks that slow down mixed-integer engines. This allows transmission system operators to safely manage high-renewable, low-inertia networks with high computational speed and operational confidence, ensuring that thermal asset limits and voltage stability thresholds are strictly maintained across prospective $N-1$ contingency states.

## 4.5 Scalability Analysis

To evaluate the scalability of the proposed CC-SCOPF formulation, computational experiments were conducted using four widely adopted benchmark networks: the IEEE 9-bus, IEEE 30-bus, IEEE 118-bus, and IEEE 300-bus systems [46]. These test systems represent progressively increasing network sizes and operational complexity, enabling a systematic assessment of the computational performance and robustness of the proposed approach under diverse operating conditions.

### 4.5.1 Market Context and Simulation Design

Conducting a full multi-period stochastic simulation, such as an entire 24-hour horizon discretized into 96 periods with 20 scenarios, is computationally prohibitive for large-scale networks. For a nonlinear solver, optimizing a fully coupled time horizon generates a constraint matrix with millions of nonlinear state variables, leading to the curse of dimensionality. Furthermore, evaluating the algorithm during non-critical, low-stress hours provides limited scientific value regarding its computational boundaries.

To overcome this constraint and provide a mathematically rigorous validation, this study adopts a representative critical snapshot methodology. Instead of simulating a full day, the algorithm's performance is isolated and tested during the most severe and highly congested operational window. Specifically, the scalability tests are executed for the 09:00 – 10:00 h window, which coincides with the third session of the Iberian Intraday Market (MIBEL), integrated into the pan-European Single Intraday Coupling as Intraday Auction 3 (IDA3), as outlined in Table 4.8 [50].

Table 4.8: Pan-European Intraday Auction (IDA) session schedule [50].

| **Pan-European Intraday Auctions** | **IDA 1 Session** | **IDA 2 Session** | **IDA 3 Session** |
|---|---:|---:|---:|
| Session Overture | 14:00 | 21:00 | 09:00 |
| Session Closure | 15:00 | 22:00 | 10:00 |
| Matching and Publication | <15:20 | <22:00 | <10:20 |
| Programming Horizon Schedule | | | |
| (Quarter-hour Periods) | 96 periods | 96 periods | 48 periods |

The selection of this specific hour is strategically justified by both market operations and extreme physical stress on the grid. From a market perspective, the 10:00 h gate closure time for IDA3 requires operators to rapidly manage heavy forecasting errors realized during the early morning. From a physical grid perspective, the 09:00 – 10:00 h window captures an aggressive solar ramp. During this period, a massive influx of solar photovoltaic generation forces the sudden disconnection of conventional synchronous thermal generators, drastically reducing the system's dynamic voltage support.

The operational vulnerability of transmission networks during this specific window was notably demonstrated by the Iberian blackout on April 28, 2025, where unexpected solar ramps and high voltage variability starting at 09:00 h initiated the instability that ultimately led to a massive system collapse [51, 52]. Successfully resolving this maximum-stress scenario provides strong evidence that the formulation can seamlessly manage the remaining, less volatile periods of the day.

### 4.5.2 Network Configurations and Asset Parameters

To reflect modern power system characteristics, all benchmark networks were extended to include renewable energy sources, specifically photovoltaic and wind generation, as well as distributed ESSs:

- **IEEE 9-bus system:** Expanded with six renewable generators (three PV and three wind units) and three ESSs.
- **IEEE 30-bus system:** Expanded with two renewable generators (one PV and one wind unit) and three ESSs.
- **IEEE 118-bus system:** Expanded with four renewable generators (two PV and two wind units) and three ESSs.
- **IEEE 300-bus system:** Expanded with five renewable generators (three PV and two wind units) along with five ESSs.

The technical characteristics of each modified test system are summarized in Table 4.9.

Table 4.9: Technical characteristics and bus allocation of the supplementary renewable assets and ESS units.

| Network | PV Generator | | Wind Generator | | ESSs | |
|---|---|---|---|---|---|---|
| | Bus | $P$ (MW) | Bus | $P$ (MW) | Bus | $P$ (MW) |
| IEEE-9 | 4 | 10 | 4 | 30 | 4 | 10 |
| | 6 | 17 | 6 | 60 | 6 | 10 |
| | 8 | 13 | 8 | 40 | 8 | 10 |
| IEEE-30 | 21 | 13 | 30 | 50 | 1 | 10 |
| | | | | | 13 | 10 |
| | | | | | 22 | 10 |
| IEEE-118 | 13 | 70 | 82 | 260 | 1 | 15 |
| | 14 | 120 | 106 | 210 | 8 | 15 |
| | | | | | 27 | 15 |
| IEEE-300 | 13 | 75 | 228 | 450 | 10 | 15 |
| | 38 | 125 | 562 | 285 | 98 | 15 |
| | 199 | 100 | | | 138 | 15 |
| | | | | | 186 | 15 |
| | | | | | 7130 | 15 |

The one-hour scheduling horizon within the IDA3 session (09:00–10:00 h) was modeled using five discrete time points. The first four periods correspond to the quarter-hour operating intervals of the session, while the fifth period represents the terminal system state. For all network applications, the contingency event was modeled to occur during the second time period. To capture operational uncertainty, 10 operational scenarios ($\Omega_o = 10$) were considered, along with a 90% confidence level ($\varepsilon = 10\%$). Additionally, four contingency states were defined for each network to evaluate robustness under adverse conditions, consisting of two generator outages and two network element outages (branches or transformers). Specifically, the IEEE-9 system considered outages of Generators 1 and 3 and Branches 5 and 6. The IEEE-30 system considered outages of Generators 2 and 5 and Branches 5 and 8. The IEEE-118 system considered outages of Generators 9 and 13, Branch 9, and Transformer 95. And the IEEE-300 system considered outages of Generators 1 and 5, Transformer 5, and Branch 69.

### 4.5.3 Problem Scale Expansion

To understand the computational behavior of the framework, it is necessary to analyze the mathematical expansion of the problem size as the network scales. Figure 4.14 illustrates the evolution of the total number of decision variables and constraints across the test systems, where the values represented on the vertical axis are expressed in millions.

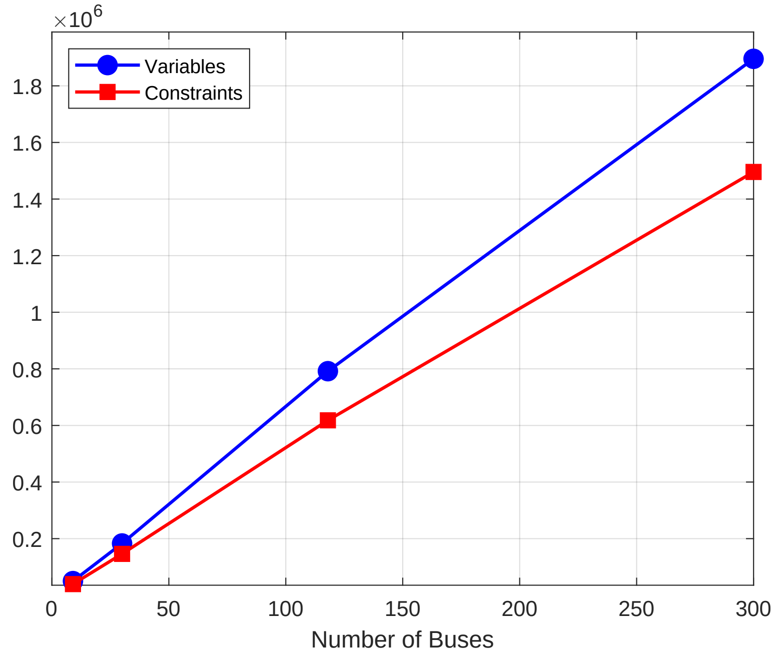


Figure 4.14: Problem size growth across the evaluated network systems.

As observed, both the number of variables and the number of constraints increase significantly with the grid size, reaching values on the order of millions for the IEEE-300 system. In particular, the largest test case comprises approximately 1.9 million decision variables and 1.5 million constraints, highlighting the large-scale nature of the resulting nonlinear optimization problem. This combinatorial expansion in problem dimensions directly impacts the structural complexity of the underlying matrices explored by the solver.

### 4.5.4 Computational Performance

This growth in problem dimensions is directly reflected in the final computational performance of the algorithm. Table 4.10 summarizes the solution parameters obtained for a confidence level of $p = 90\%$, mapping the relationship between system size, required iterations, and total runtime.

Table 4.10: Computational performance results for the CC-SCOPF framework with a 90% confidence level.

| **Test Case** | **Interior-Point Iterations** | **Total Time (s)** |
|---|---|---|
| IEEE-9 | 33 | 1.34 |
| IEEE-30 | 109 | 70.08 |
| IEEE-118 | 85 | 381.52 |
| IEEE-300 | 204 | 2955.11 |

These results provide insight into the numerical burden associated with larger networks and enable an assessment of the scalability characteristics of the proposed solution methodology. To visualize this scaling trend, Figure 4.15 highlights the mathematical trajectory of execution times in relation to the network size.

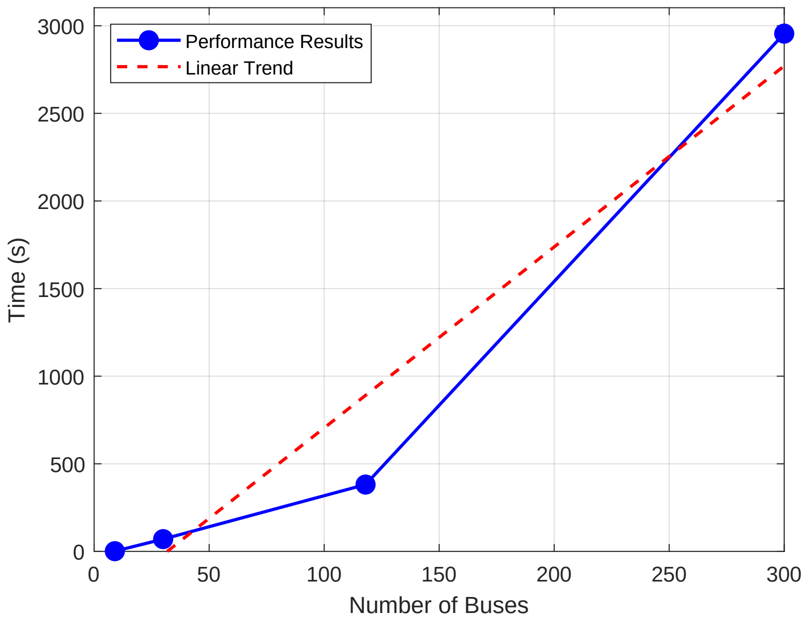


Figure 4.15: Scalability behavior of the continuous CC-SCOPF algorithm as network size increases.

As shown in Figure 4.15, the computational trajectory exhibits a distinct nonlinear evolution that deviates meaningfully from the linear reference baseline. For small- to medium-scale networks (spanning from the 9-bus up to the 118-bus configurations), the actual execution times remain noticeably below the linear trend line. This sub-linear scaling behavior indicates that the continuous NLP framework maintains high numerical tractability over this size range. Within these dimensions, the sparse network matrix structures remain highly decoupled, allowing the interior-point algorithm to calculate updates with minimal computational friction per step. However, as the network scales up to the IEEE-300 bus system, the execution time curve experiences a sharp upward inflection, crossing above the linear baseline to reach a final solution time of 2955.11 s. This super-linear progression is characteristic of centralized nonlinear optimization frameworks applied to large-scale grids. Crucially, this sudden rise in execution time cannot be solely attributed to the number of solver iterations required for convergence. For instance, the IEEE-118 system requires fewer total iterations (85) than the smaller IEEE-30 system (109), yet its total runtime increases more than fivefold.

This behavior confirms that the overall computational runtime is primarily driven by the internal mathematical complexity of the optimization subproblems rather than by the absolute iteration count alone. As the physical network layout expands into millions of coupled variables and constraints, the processing effort required to factorize the underlying sparse linear equations and update the large Jacobian and Hessian matrices at each individual interior-point step grows at a super-linear, polynomial rate.

## 4.6 Summary and Concluding Remarks

The comprehensive numerical evaluations conducted throughout this chapter deliver clear experimental proof regarding the operational effectiveness, accuracy, and performance boundaries of the proposed optimization engines. By systematically benchmarking the continuous NLP framework against classical probabilistic formulations and mixed-integer models, several fundamental insights are established:

- **Operational paradigm shift:** Transitioning from standard probabilistic setups to the full security-constrained architecture (CC-SCOPF) radically alters how grid security margins are held. The framework successfully internalizes uncertainty and contingency tracking simultaneously. Instead of scheduling resources solely for baseline cost minimization, the engine proactively secures higher SoC buffer margins in distributed energy storage devices, flattens spatial voltage profiles near their upper operating limits, and pre-positions transmission capacity line headroom. This coordinated strategy ensures that alternate network corridors possess adequate spare capacity to seamlessly absorb sudden, post-disturbance power flow redirections without triggering emergency cascading overloads.

- **Mathematical tractability:** The algorithmic comparison between the continuous NLP relaxation and the exact MIQP baseline verifies that substituting discrete binary switches with smooth, rational surrogate functions eliminates the severe combinatorial bottlenecks of branch-and-bound searches. On the benchmark environments evaluated, the proposed NLP framework reproduces identical asset dispatch schedules and matching power-flow configurations while achieving an extraordinary 97.73% reduction in execution times. The total objective function cost mismatch rests at a negligible 0.0058%, validating that the continuous formulation identifies high-quality operating points at a fraction of the computational cost, making it highly appropriate for sub-hourly operational scheduling.

- **Dimensionality and memory limitations:** While the smooth relaxation strategy exhibits exceptional stability, the scalability investigations expose a clear computational bottleneck rooted in physical hardware requirements. As the grid size expands toward large-scale configurations like the IEEE-300 bus system, the coupling of intertemporal multi-period profiles and multi-scenario uncertainty sets creates a massive growth in problem size, with decision variables and constraints crossing into the millions.

Under these massive dimensions, a centralized continuous execution requires significant memory allocation to construct and invert the underlying Jacobian and Hessian matrices during the interior-point update steps. When uncertainty trees scale tightly, the required data structures can exceed standard physical RAM limits, forcing the operating system to offload computations to disk-based SWAP memory. Because disk access overheads drastically stall solver progression, these findings demonstrate that physical memory capability, rather than pure CPU processing speed, represents the primary operational threshold for centralized stochastic grid optimization. Managing this hardware constraint constitutes a core requirement for scaling continuous nonlinear optimization structures to utility-scale, pan-European transmission topologies.

# Chapter 5

# Conclusions and Future Work

This dissertation investigated the formulation and solution of a multi-period, chance-constrained AC-SCOPF problem capable of addressing the operational challenges associated with modern power systems characterized by increasing renewable energy penetration, growing uncertainty, and reduced conventional generation. The research focused on developing a computationally tractable optimization framework that preserves the physical fidelity of AC network models while maintaining scalability for realistic transmission system applications.

This final chapter synthesizes the outcomes of the research and places them within the broader context of power system operation and planning. It begins by reviewing the principal contributions of the proposed methodology, highlighting the theoretical and practical advances achieved throughout the dissertation. Subsequently, the main limitations and challenges encountered during the development and validation of the framework are discussed. Finally, several directions for future research are identified, with the objective of further enhancing the methodology and facilitating its application to increasingly complex and large-scale power system environments.

## 5.1 Main contributions

This dissertation successfully addresses a persistent mathematical and operational bottleneck in power system engineering: the development of a MP-AC-SCOPF framework that pragmatically balances physical modeling accuracy with computational tractability. By directly confronting the optimization trilemma, this work demonstrates that the full nonlinear AC power flow equations can be retained in large-scale stochastic planning while achieving reliable convergence on the benchmark systems considered.

The primary methodological contribution of this research is the systematic formulation of the network equations in rectangular coordinates, which structures the AC power flow framework as a system of pure quadratic polynomials. When paired with continuous rational violation indicators within a pure NLP environment, this algebraic design yields significant computational advantages. Rather than utilizing linearizations (DC-OPF) that overlook reactive power physics and voltage stability margins, or convex approximations (SDP/SOCP) that inherently sacrifice exactness, the proposed methodology actively smooths the non-convex boundaries of the solution space. This formulation is designed to improve the numerical conditioning of the optimization problem, making it highly suitable for gradient-based NLP solvers such as IPOPT. By maintaining well-behaved KKT matrices even under the severe mathematical stress of overlapping $N-1$ contingencies and probabilistic renewable energy variations, the framework preserves the full fidelity of the AC network representation without numerical stagnation. Furthermore, the explicit integration of a sub-hourly temporal resolution, specifically 15-minute operational intervals, and ESSs SoC dynamics proved highly effective for modern grid scenarios. The case studies demonstrated that the CC-SCOPF formulation successfully internalized uncertainty, forcing a preventive, risk-aware dispatch strategy. Notably, the model secures expanded SoC margins within the storage assets compared to standard deterministic formulations, thereby safeguarding the upward flexibility required to withstand sudden drops in generation.

The development of a fully functional, open-source Python implementation validates the practical viability of this approach, providing a highly scalable foundation for modern transmission system operators navigating the complexities of the energy transition.

## 5.2 Limitations

Despite the demonstrable successes of the methodology, certain limitations regarding extreme scalability and parameter sensitivity must be acknowledged.

First, although the slack-variable reformulations significantly improved numerical robustness and enabled reliable convergence across the benchmark systems considered, the dimensionality of the optimization problem remains a major challenge. As detailed in the scalability analysis (Section 4.5), attempting to solve the IEEE-300 bus system over a continuous multi-period horizon with extensive stochastic scenarios resulted in hardware limitations. The combinatorial growth in decision variables and contingency constraints caused severe memory overflow, forcing the computing environment to rely on physical SWAP memory, which drastically increases computational time. These results indicate that:

1. Although the proposed continuous NLP formulation remains computationally tractable, its centralized implementation becomes increasingly memory-intensive as the number of buses, contingency cases, time periods, and uncertainty scenarios grows

2. Because the proposed formulation is solved using the gradient-based IPOPT solver, the obtained solutions correspond to locally optimal operating points. Owing to the non-convex nature of the MP-AC-SCOPF problem, global optimality cannot generally be guaranteed, although the numerical results consistently converged to high-quality solutions across the benchmark systems considered

3. The chance-constrained enforcement relies heavily on a continuously differentiable rational violation indicator. The accuracy and gradient stability of this surrogate function are highly

sensitive to the scalar tuning parameter $\alpha$. Selecting an appropriate value for $\alpha$ currently relies on tailored tuning and may require recalibration for different network sizes, operating conditions, or uncertainty levels.

Finally, the proposed methodology was validated using standardized IEEE benchmark systems. Although these test cases are widely accepted for evaluating optimization algorithms, further validation using real transmission network models and operational datasets would be required before practical deployment in transmission system operator environments.

## 5.3 Future Work

The limitations identified in Section 5.2 open several promising avenues for future research. To transition the proposed framework toward operational deployment in real-world grid environments, subsequent developments should focus on the following directions, ordered by operational priority:

1. **Decomposition and parallelization:** To directly address the memory limitations observed in the IEEE-300 test case, the immediate next step must focus on integrating the NLP formulation into a distributed optimization framework. Utilizing techniques such as the ADMM or Benders Decomposition would allow individual $N-1$ contingencies or stochastic scenarios to be isolated as distinct, parallel sub-problems solved across high-performance computing environments, effectively bypassing centralized memory constraints.

2. **Automated parameter tuning framework:** To resolve the sensitivities surrounding the manual calibration of the $\alpha$ parameter, future work should develop an adaptive, automated parameter selection framework.

3. **Corrective control of grid assets:** The current multi-period formulation focuses heavily on preventive dispatch scheduling. Future work should integrate explicit variables for continuous corrective control, such as dynamic set-point adjustments for high-voltage direct current lines and phase-shifting transformers.

4. **Validation on real-world utility networks:** To bridge the gap between academic benchmarks and industrial deployment, the framework should be stress-tested using large-scale, real-world utility networks and empirical operational datasets. This expansion will validate the model's performance against practical telemetry errors, complex network topologies, and authentic market environment behaviors.

## 5.4 Final Remarks

As modern electrical grids continue to displace synchronous, dispatchable generation with volatile, inverter-based renewable resources, traditional deterministic optimization paradigms become structurally insufficient.

The mathematical frameworks developed in this dissertation prove that retaining full, non-convex AC physics within an uncertainty-aware, security-constrained environment is computationally achievable. By combining a rectangular voltage formulation with smooth probabilistic approximations, this work provides a robust algorithmic foundation for securing future transmission networks under high operational uncertainty.

# References

[1] Eurostat. *Share of energy from renewable sources*. Dataset, European Commission, 2025. DOI: 10.2908/NRG_IND_REN.

[2] Eurostat. *Batteries power capacities and energy storage*. Dataset, European Commission, 2025. DOI: 10.2908/nrg_inf_bt.

[3] ENTSO-E. *Costs of Congestion Management [13.1.C] – ENTSO-E Transparency Platform*. European Network of Transmission System Operators for Electricity (ENTSO-E), 2020. URL: https://transparency.entsoe.eu/transmission/congestionCost.

[4] Micael Simões Diogo Pereira Diogo Reis and Tiago Soares. "Nonlinear Programming-Based Multi-Period Approach for Security Constrained Optimal Power Flow". In: *Smart Grids and Sustainable Energy* 11.2 (2026), p. 41. ISSN: 2731-8087. DOI: 10.1007/s40866-026-00355-8.

[5] Nan Yang et al. "A Comprehensive Review of Security-constrained Unit Commitment". In: *Journal of Modern Power Systems and Clean Energy* 10.3 (2022), pp. 562–576. DOI: 10.35833/MPCE.2021.000255.

[6] Vahid Askari Ghourttapeh, Reza Ghanizadeh, and Mojtaba Beiraghi. "Probabilistic Security-Constrained Optimal Power Flow (PSCOPF) Considering a Wide Range of Uncertainties Based on Data Clustering". In: *IET Renewable Power Generation* 19.1 (2025), e70065. DOI: https://doi.org/10.1049/rpg2.70065.

[7] Ashley M. Hou and Line A. Roald. "Chance Constraint Tuning for Optimal Power Flow". In: *2020 International Conference on Probabilistic Methods Applied to Power Systems (PMAPS)*. 2020, pp. 1–6. DOI: 10.1109/PMAPS47429.2020.9183552.

[8] Keerthi Chacko et al. "Chance Constrained Framework for AC Security Constrained Optimal Power Flow". In: *2024 International Conference on Smart Energy Systems and Technologies (SEST)*. 2024, pp. 1–6. DOI: 10.1109/SEST61601.2024.10694549.

[9] Mohammad Iman Alizadeh, Muhammad Usman, and Florin Capitanescu. "Toward Stochastic Multi-period AC Security Constrained Optimal Power Flow to Procure Flexibility for Managing Congestion and Voltages". In: *2021 International Conference on Smart Energy Systems and Technologies (SEST)*. 2021, pp. 1–6. DOI: 10.1109/SEST50973.2021.9543107.

[10] Mohammad Iman Alizadeh, Muhammad Usman, and Florin Capitanescu. "Envisioning security control in renewable dominated power systems through stochastic multi-period AC security constrained optimal power flow". In: *International Journal of Electrical Power and Energy Systems* 139 (2022), p. 107992. ISSN: 0142-0615. DOI: https://doi.org/10.1016/j.ijepes.2022.107992.

[11] Hui Cai, Chunke Hu, and Xi Wu. "Preventive-Security-Constrained Optimal Power Flow Model Considering IPFC Control Modes". In: *Energies* 17.7 (2024). ISSN: 1996-1073. DOI: 10.3390/en17071660.

[12] Florin Capitanescu et al. "Contingency Filtering Techniques for Preventive Security-Constrained Optimal Power Flow". In: *IEEE Transactions on Power Systems* 22.4 (2007), pp. 1690–1697. DOI: 10.1109/TPWRS.2007.907528.

[13] Arman Zarrin et al. "Model Predictive Control of Security in Real-Time via AC Security Constrained Optimal Power Flow". In: *2024 International Conference on Smart Energy Systems and Technologies (SEST)*. 2024, pp. 1–6. DOI: 10.1109/SEST61601.2024.10694494.

[14] Javad Mohammadi, Gabriela Hug, and Soummya Kar. "Agent-Based Distributed Security Constrained Optimal Power Flow". In: *IEEE Transactions on Smart Grid* 9.2 (2018), pp. 1118–1130. DOI: 10.1109/TSG.2016.2577684.

[15] Mohammad Iman Alizadeh and Florin Capitanescu. "A Tractable Linearization-Based Approximated Solution Methodology to Stochastic Multi-Period AC Security-Constrained Optimal Power Flow". In: *IEEE Transactions on Power Systems* 38.6 (2023), pp. 5896–5908. DOI: 10.1109/TPWRS.2022.3220283.

[16] James Jamal Thomas and Santiago Grijalva. "Flexible Security-Constrained Optimal Power Flow". In: *IEEE Transactions on Power Systems* 30.3 (2015), pp. 1195–1202. DOI: 10.1109/TPWRS.2014.2345753.

[17] Arman Zarrin et al. "Sensitivity-Based Sequential Linear Approximation for Solving Multi-Period Security-Constrained Optimal Power Flow in Real-Time". In: *2025 IEEE Kiel PowerTech*. 2025, pp. 1–8. DOI: 10.1109/PowerTech59965.2025.11180461.

[18] Juan S. Guzmán-Feria et al. "Security constrained OPF for AC/DC systems with power rescheduling by power plants and VSC stations". In: *Sustainable Energy, Grids and Networks* 27 (2021), p. 100517. ISSN: 2352-4677. DOI: https://doi.org/10.1016/j.segan.2021.100517.

[19] Mohammad Iman Alizadeh and Florin Capitanescu. "Affinely Adjustable Robust Optimization for Constraint Filtering in AC Security Constrained Optimal Power Flow Under Uncertainties". In: *IEEE Transactions on Power Systems* 40.1 (2025), pp. 1118–1129. DOI: 10.1109/TPWRS.2024.3406784.

[20] Rony Seto Wibowo et al. "Security constrained optimal power flow incorporating preventive and corrective control". In: *2014 Electrical Power, Electronics, Communicatons, Control and Informatics Seminar (EECCIS)*. 2014, pp. 29–34. DOI: 10.1109/EECCIS.2014.7003714.

[21] Wang Zhang et al. "Robust Security Constrained-Optimal Power Flow Using Multiple Microgrids for Corrective Control of Power Systems Under Uncertainty". In: *IEEE Transactions on Industrial Informatics* 13.4 (2017), pp. 1704–1713. DOI: 10.1109/TII.2016.2644738.

[22] María del Pilar Buitrago-Villada and Carlos E. Murillo-Sánchez. "A stabilized Benders decomposition approach for solving the multi-period secure stochastic AC optimal power flow for energy, reserves, and storage scheduling". In: *e-Prime - Advances in Electrical Engineering, Electronics and Energy* 14 (2025), p. 101134. ISSN: 2772-6711. DOI: https://doi.org/10.1016/j.prime.2025.101134.

[23] Micael Simoes et al. “TSO-DSO Coordinated Operational Planning in the Presence of Shared Resources $i,m,o,t$”. In: *2023 IEEE Belgrade PowerTech*. 2023, pp. 01–08. DOI: 10.1109/PowerTech55446.2023.10202840.

[24] Dzung Phan and Jayant Kalagnanam. “Some Efficient Optimization Methods for Solving the Security-Constrained Optimal Power Flow Problem”. In: *IEEE Transactions on Power Systems* 29.2 (2014), pp. 863–872. DOI: 10.1109/TPWRS.2013.2283175.

[25] Tomás Valencia-Zuluaga et al. “A Fast Decomposition Method to Solve a Security-Constrained Optimal Power Flow (SCOPF) Problem Through Constraint Handling”. In: *IEEE Access* 9 (2021), pp. 52812–52824. DOI: 10.1109/ACCESS.2021.3067206.

[26] Hussein Sharadga et al. “Scalable Solutions for Security-Constrained Optimal Power Flow With Multiple Time Steps”. In: *IEEE Transactions on Industry Applications* 61.3 (2025), pp. 4812–4821. DOI: 10.1109/TIA.2025.3532927.

[27] A. Attarha and N. Amjady. “Solution of security constrained optimal power flow for large-scale power systems by convex transformation techniques and taylor series”. In: *IET Generation, Transmission and Distribution* 10 (4 2016), pp. 889–896. DOI: 10.1049/iet-gtd.2015.0494.

[28] Si Lv et al. “Security-Constrained Optimal Traffic-Power Flow With Adaptive Convex Relaxation and Contingency Filtering”. In: *IEEE Transactions on Transportation Electrification* 9.1 (2023), pp. 1605–1617. DOI: 10.1109/TTE.2022.3175499.

[29] Parikshit Pareek and Hung D. Nguyen. “A Convexification Approach for Small-Signal Stability Constrained Optimal Power Flow”. In: *IEEE Transactions on Control of Network Systems* 8.4 (2021), pp. 1930–1941. DOI: 10.1109/TCNS.2021.3090205.

[30] Leonel de Magalhães Carvalho, Armando Martins Leite da Silva, and Vladimiro Miranda. “Security-Constrained Optimal Power Flow via Cross-Entropy Method”. In: *IEEE Transactions on Power Systems* 33.6 (2018), pp. 6621–6629. DOI: 10.1109/TPWRS.2018.2847766.

[31] Zwe-Lee Gaing and Rung-Fang Chang. “Security-constrained optimal power flow by mixed-integer genetic algorithm with arithmetic operators”. In: *2006 IEEE Power Engineering Society General Meeting*. 8 pages. 2006. DOI: 10.1109/PES.2006.1709334.

[32] Jubeyer Rahman, Cong Feng, and Jie Zhang. “Machine Learning-Aided Security Constrained Optimal Power Flow”. In: *2020 IEEE Power and Energy Society General Meeting (PESGM)*. 2020, pp. 1–5. DOI: 10.1109/PESGM41954.2020.9281941.

[33] Ziming Yan and Yan Xu. “A Hybrid Data-Driven Method for Fast Solution of Security-Constrained Optimal Power Flow”. In: *IEEE Transactions on Power Systems* 37.6 (2022), pp. 4365–4374. DOI: 10.1109/TPWRS.2022.3150023.

[34] A. Berizzi et al. “Enhanced security-constrained OPF with FACTS devices”. In: *IEEE Transactions on Power Systems* 20.3 (2005), pp. 1597–1605. DOI: 10.1109/TPWRS.2005.852125.

[35] Line A Roald. “Optimization methods to manage uncertainty and risk in power systems operation”. PhD thesis. ETH Zurich, 2016.

[36] Line Roald et al. “Security constrained optimal power flow with distributionally robust chance constraints”. In: *arXiv preprint arXiv:1508.06061* (2015). URL: https://arxiv.org/abs/1508.06061.

[37] Line Roald et al. "Analytical reformulation of security constrained optimal power flow with probabilistic constraints". In: *2013 IEEE Grenoble Conference*. 2013, pp. 1–6. DOI: 10.1109/PTC.2013.6652224.

[38] Line Roald et al. "Risk-based optimal power flow with probabilistic guarantees". In: *International Journal of Electrical Power & Energy Systems* 72 (2015). The Special Issue for 18th Power Systems Computation Conference., pp. 66–74. ISSN: 0142-0615. DOI: https://doi.org/10.1016/j.ijepes.2015.02.012.

[39] Florin Capitanescu. "Approaches to Obtain Usable Solutions for Infeasible Security-Constrained Optimal Power Flow Problems Due to Conflicting Contingencies". In: *2019 IEEE Milan PowerTech*. 2019, pp. 1–6. DOI: 10.1109/PTC.2019.8810962.

[40] Subhonmesh Bose et al. "Equivalent Relaxations of Optimal Power Flow". In: *IEEE Transactions on Automatic Control* 60.3 (2015), pp. 729–742. DOI: 10.1109/TAC.2014.2357112.

[41] Daniel K. Molzahn and Ian A. Hiskens. "Moment-based relaxation of the optimal power flow problem". In: *2014 Power Systems Computation Conference*. 2014, pp. 1–7. DOI: 10.1109/PSCC.2014.7038397.

[42] J. Carpentier. "Contribution to the economic dispatch problem". In: *Bulletin de la Société Française des Electriciens* 3.8 (1962), pp. 431–447.

[43] Andreas Wächter and Lorenz T. Biegler. "On the Implementation of a Primal-Dual Interior Point Filter Line Search Algorithm for Large-Scale Nonlinear Programming". In: *Mathematical Programming* 106.1 (2006), pp. 25–57. DOI: 10.1007/s10107-004-0559-y.

[44] ERSE – Entidade Reguladora dos Serviços Energéticos. *Diretiva n.º 7/2025: Aprova o Manual de Procedimentos da Gestão Global do Sistema do Setor Elétrico (MPGGS)*. 2025. URL: https://www.erse.pt/media/jedd1fqg/cp127_mpggs_vs-pext.pdf.

[45] Michael L. Bynum et al. *Pyomo–Optimization Modeling in Python*. Third. Vol. 67. Springer, 2021.

[46] MATPOWER Team. *Example Matpower Cases*. MATPOWER User's Manual — Seção D.3. 2025. URL: https://matpower.app/manual/matpower/ExamplematpowerCases.html.

[47] ATTEST Project Consortium. *ATTEST Project: Advanced Tools Towards cost-efficient decarbonisation of future reliable Energy Systems*. https://github.com/ATTEST-project. 2020.

[48] HSL Mathematical Software Library. *HSL: A Collection of Fortran Codes for Large-Scale Scientific Computation*. Science and Technology Facilities Council, 2024. URL: https://www.hsl.rl.ac.uk/.

[49] Gurobi Optimization, LLC. *Gurobi vs. Other Solvers: How to Benchmark Optimization Solutions the Right Way*. https://www.gurobi.com/misc/lp/all/gurobi-vs-other-solvers-how-to-benchmark-optimization-solutions-the-right-way. 2026.

[50] OMIE. *Electricity Market*. https://www.omie.es/en/mercado-de-electricidad. 2026.

[51] Red Eléctrica de España. *Blackout in the Spanish Peninsular Electrical System the 28th of April 2025*. Technical Report. System Operation Division, Red Eléctrica de España, June 18, 2025. URL: https://d1n1o4zeyfu21r.cloudfront.net/WEB_Incident_%2028A_SpanishPeninsularElectricalSystem_18june25.pdf.

[52] ENTSO-E Expert Panel. *Final Report on the Grid Incident in Spain and Portugal on 28 April 2025*. Technical Report. European Network of Transmission System Operators for Electricity (ENTSO-E), Oct. 3, 2025. URL: https://eepublicdownloads.blob.core.windows.net/public-cdn-container/clean-documents/Publications/2025/iberian-blackout/Final%20Report%20on%20the%20Grid%20Incident%20in%20Spain%20and%20Portugal%20on%2028%20April%202025.pdf.